The behaviour of steel bonded joints under hygrothermal and creep loadings

Chantal de Zeeuw

Master of Science

TU Delft Delft University of Technology

Aerospace Structures and Materials

The behaviour of steel bonded joints under hygrothermal and creep loadings

Chantal de Zeeuw

18-01-2018

A thesis
submitted in partial fulfillment of the
requirements for the degree of

Master of Science

in

Aerospace Engineering

Faculty of Aerospace Engineering · Delft University of Technology

Delft University of Technology
Faculty of Aerospace Engineering
Department of Structural Integrity and Composites

GRADUATION COMMITTEE

Dated: 18-01-2018

Chair holder:

Prof. dr. ir. Rinze Benedictus

Committee members:

Dr. Sofia Teixeira de Freitas

Dr. Dimitrios Zarouchas

Dr. Marko Pavlović

Dr.-Ing. Pedro Dolabella Portella

Abstract

Hybrid structures consisting of steel and Glass Fiber Reinforced Polymer [GFRP] parts with adhesive bonds are a potential solution for the desire to improve the performance of marine vehicles. These bonds will however be subjected to moisture and potential creep loading, which are two of the main causes for damage development in polymers. It is therefore important to get a good understanding of the behaviour of adhesively bonded composite-to-metal joints that are subjected to combined moisture and loading. In this thesis an initial step is made in the research on the long-term behaviour of composite-to-metal bonds that are loaded under hygrothermal conditions. In this initial step the GFRP adherend will be substituted with a metal one to focus on the response and behaviour of the adhesive in these bonds under moisture and loading.

This thesis is mostly based on experimental work that has been carried out to determine the water uptake, creep strain and residual strength of metal-to-metal bonds under different conditions. Where appropriate this experimental work is supported by a Finite Element Method [FEM] model. The experimental work was inconclusive on the effect of loading on the water uptake. The load level and environment were however found to have a significant influence on the creep behaviour and residual strength of the bonds.

An increase in load level resulted in a larger elastic portion of the creep strain and a higher strain rate. Specimens loaded in air experienced a lower creep strain than specimens loaded in water. It was found that at the initial stages of water absorption creep is suppressed while at later stages creep is promoted. This can possibly be explained by two different processes being at play when water is absorbed. The creep strain is initially lowered due to bonding of the water molecules to the macromolecules and thereby decreasing relaxations. As the water continues to diffuse the plasticizing effect becomes stronger and the creep strain becomes larger.

Low load levels were found to have a positive effect on the residual lap shear strength. This can be attributed to orienting of the molecular chains in the direction of the loading due to the creep deformation. This results in some kind of strain hardening of the epoxy. At higher load levels the residual strength is decreased: the loading no longer has a strain hardening effect and instead damages the adhesive. Immersion of the specimens in water results in swelling and plasticisation of the adhesive, resulting in a reduced residual lap shear strength. The experimental results also suggest that Araldite 2015 might be affected by ambient humidity.

Preface

Before you lies the Master thesis "The behaviour of steel bonded joints under hygrothermal and creep loadings", the basis of which is experimental work on metal-to-metal bonds performed at the Delft Aerospace Structures and Materials Laboratory [DASML] in Delft and the Bundesanstalt für Materialforschung und -prüfung [BAM] in Berlin. This thesis has been written to fulfill the graduation requirements for the degree of Master of Science Aerospace Engineering at the Delft University of Technology [TU Delft] Faculty of Aerospace Engineering.

The initial reason this Master thesis topic stood out to me came from a desire to retain a bit of a Maritime focus after making the unusual switch from a Maritime Engineering Bachelor to an Aerospace Engineering Master. At the start of my Master studies I thought this Master would merely be a stepping stone towards designing better ships. Over the course of the past two years I did however come to realize there is so much more to love about structural design and that research is the direction I want to go. There are still so many unknowns and so many exciting possibilities to study. I hope my Master thesis helps to set a small step in furthering our knowledge on the behaviour of adhesive bonds.

I am grateful to all people from DASML, TU Delft and BAM that were involved in this thesis. First of all I would like to thank my supervisors Dr. Sofia Teixeira De Freitas and Dr. Dimitrios Zarouchas for their guidance and support but most of all for believing in me even when I did not, it really means a lot to me. Your kind words, encouragement and advice have helped me to grow a lot in the past months. I thank Dr.-Ing. Pedro Dolabella Portella for the opportunity to perform the experiments for this thesis at the BAM and for his support during my stay in Berlin. I am also grateful for the company and support of Dr.-Ing. Ute Niebergall, Dr. rer. nat. Martin Böhning, Markus Schilling, MSc and Maren Erdmann, MSc during this period. I would like to thank Debbie de Zeeuw, Emiel Lorist and Liza van Kempen for proofreading parts of this thesis.Finally, I would like to thank my parents for their unconditional love and support. I am forever grateful that they gave me the opportunity to study at the TU Delft.

I hope you enjoy your reading.

Chantal de Zeeuw

Delft, December 20, 2017

"It is not the mountain we conquer, but ourselves."

— *Sir Edmund Hillary*

Table of Contents

Glossary

List of Symbols

Latin Symbols

Symbol	Description	Unit
C_t	Moisture Concentration at time t	$[-]$
C	Moisture concentration	$[kg \cdot m^{-3}/\%]$
$\dot{C}$	Mass flux	$[kg \cdot m^{-2} \cdot s^{-1}]$
c_p	Specific heat	$[J \cdot kg^{-1} \cdot K^{-1}]$
D	Diffusion coefficient	$[m^2/s]$
D	Moisture diffusivity coefficient	$[m^2 \cdot s^{-1}]$
$D(t)$	Creep compliance	$[MPa^{-1}]$
E	Linear spring constant or Young's modulus	$[N/m^2]$
k	Thermal conductivity	$[W \cdot m^{-1} \cdot K^{-1}]$
S	Sample surface area	$[mm^2]$
k_t	Stiffness at time t	$[N/mm]$
k_{t0}	Stiffness at time t = 0	$[N/mm]$
$\dot{T}$	Heat flux	$[W \cdot m^{-2}]$
T	Temperature	$[K]$
t	Time	$[h/days]$
T_g	Glass transition temperature	$[K]$
V	Sample volume	$[mm^3]$
w_0	Initial weight at start	$[g]$
w_t	Initial weight at time t	$[g]$
x	Depth of water penetration	$[m]$

Greek Symbols

Symbol	Description	Unit

α	Thermal diffusivity	$[m^2 \cdot s^{-1}]$
ε_0	Instantaneous strain	$[-]$
ε_c	Creep strain	$[-]$
$\dot{\varepsilon}$	Creep strain rate	$[-]$
ε_{0_e}	Elastic instantaneous strain	$[-]$
ε_{0_p}	Plastic instantaneous strain	$[-]$
ε_{ve}	Viscoelastic strain	$[-]$
ε_{ve}	Viscoplastic strain	$[-]$
η	Coefficient of viscosity	$[(N \cdot s)/m^2]$
ρ	Density	$[kg \cdot m^{-3}]$
σ_0	Applied stress	$[MPa]$
σ_c	Linear-nonlinear stress threshold	$[-]$
σ_{pre}	Pre-stress	$[MPa]$
σ_t	Lap shear strength at time t	$[MPa]$
σ_{t0}	Lap shear strength at time t = 0	$[MPa]$

Abbreviations

Symbol	Description
BAM	Bundesanstalt für Materialforschung und -prüfung
DASML	Delft Aerospace Structures and Materials Laboratory
FEM	Glass Finite Element Method
FEM	Glass Finite Element Method
FNCT	Full Notch Creep Test
GFRP	Glass Fiber Reinforced Polymer
RSI$_1$	Residual Strength Index
RSI$_2$	Residual Stiffness Index
SOLAS	International Convention for the Safety of Life at Sea
TU Delft	Delft University of Technology

List of Figures

List of Tables

Chapter 1

Introduction

In 2002 the International Convention for the Safety of Life at Sea [SOLAS] has updated their regulations to allow the approval of materials other than steel for load-bearing parts as long as the safety level and non-combustibility is preserved [1]. This update makes the use of Glass Fiber Reinforced Polymer [GFRP], with their low weight, high strength to weight ratio and corrosion resistance, an interesting possible solution to the desire to improve the performance of marine vehicles that are traditionally made of steel and aluminum [1, 2]. The use of GFRP substructures will lead to a reduction in the structural weight. This reduction can result in an increase in the payload and the speed of the vessel and/or in a decrease in fuel consumption [2]. On top of that, composites allow designs that cannot be made using metal. It can also decrease the labour and time involved in shipbuilding since they can be molded in large sections [3]. Using GFRP for the whole vessel will however often be too complex, expensive or unfeasible. A hybrid structure can be used to get the benefits of both the traditional materials and GFRP [4]. The joining of composite substructures to the metal ship is most commonly done using adhesive, bolts or a combination of the two [1]. Adhesive bonds have large advantages over bolts, including the minimization of stress concentrations, the distribution of stresses over a larger area and reducing the overall weight and manufacturing cost [5].

Adhesives and GFRP do however exhibit viscoelastic behaviour, which means that their response to loads or deformation will be time dependent. This results in creep, an increasing deformation under constant load, and relaxation, a decrease in stress under constant deformation [5]. Creep is among the main causes for damage development in polymers [6] and for most structures creep loading will be present in its load spectra [7]. Another important factor in damage development in polymers is water absorption or moisture. The absorbance of water will result in a stiffness and strength decrease and will also cause an increase in the creep strain [6]. This results in a combined creep and moisture effect damaging the polymer material. It is therefore important to get a good understanding of the behaviour of adhesively bonded composite-to-metal joints under combined moisture and loading conditions.

This thesis aims to provide an initial step in the research on the long term behaviour of composite-to-metal bonds that are loaded under environmental conditions. In this initial step the GFRP adherend will be substituted with a metal one in order to focus on the response and behaviour of the adhesive in these bonds under moisture and loading. This will be done by trying to answer the following research question:

RQ: How do hygrothermal and creep loadings influence the water uptake, creep and residual strength of steel bonded joints?

This research question can be split up in the following sub-research questions:

How does the load level influence the water uptake of steel bonded joints subjected to hygrothermal and creep loadings?

How do load level and (hygro)thermal conditions influence the creep behaviour of loaded steel bonded joints?

How do the creep and (hygro)thermal loadings influence the residual strength and stiffness of steel bonded joints?

The thesis will start by presenting a state of the art literature review in which the following will be discussed: water absorption in polymers, the influence of water absorption on the viscoelastic response of polymers and the modeling of creep behaviour. This will be followed by the experimental procedure used during the experimental work. The next chapter will present and discuss the results for the water uptake, creep and residual strength of the steel bonded joints and answer the sub-research questions. Finally, the thesis will conclude with the conclusions and a future perspective.

Chapter 2

Literature Review

In this chapter a state of the art literature review will be presented on the water absorption in polymers, the influence of water absorption on the viscoelastic response of polymers and modeling of creep behaviour.

2.1 Water absorption in polymers

Many polymers will absorb moisture when they are exposed to humid air or water. Moisture is absorbed in polymers through diffusion. The simplest diffusion model is given by Fick's law [8]. If water absorption follows Fickian behaviour the first part of water uptake will be linearly increasing, followed by a nonlinear increase for the second part up to a plateau. This behaviour is illustrated in Figure 2.1. The moisture absorption of polymers and composites has often been found to follow Fickian behaviour [9–13].

When absorption data is available Fick's second law can be used to calculate the diffusion coefficient of water in the resin using the data from the initial linear region of the Fickian diffusion process [14]:

$$\frac{\mathrm{d}C}{\mathrm{d}t} = D\frac{\mathrm{d}^2C}{\mathrm{d}x^2} \tag{2-1}$$

where C is the concentration of seawater absorbed (%), t is the immersion time in seconds, D is the diffusion coefficient of water in the adhesive (m^2/s) and x is the depth of water penetration in meters [14].

For some polymers Fick's law gives an inaccurate representation of moisture diffusion, for example because the model does not take the cumulative moisture-induced damage in the material into account [10]. Cases in which Fick's law does not represent the absorption process are called non-Fickian or anomalous [8]. This non-Fickian behaviour can manifest itself in a lot of different ways. Some examples are a continuing uptake instead of a plateau at long immersion times [11], weight losses [14–17] and a two-step absorption process [18,19]. Figure 2.1 shows schematic representations for these different types of non-Fickian moisture diffusion.

The non-Fickian behaviour is attributed to supplementary absorption mechanics [11] or degradation phenomena in the polymer due to the water [14, 19]. For the two-step absorption process some other explanations have been found. One explanation is that part of the fluid is entrapped and immobile in the polymer while the remaining fluid continues to diffuse into the materia. A second explanation is a changing viscoelastic

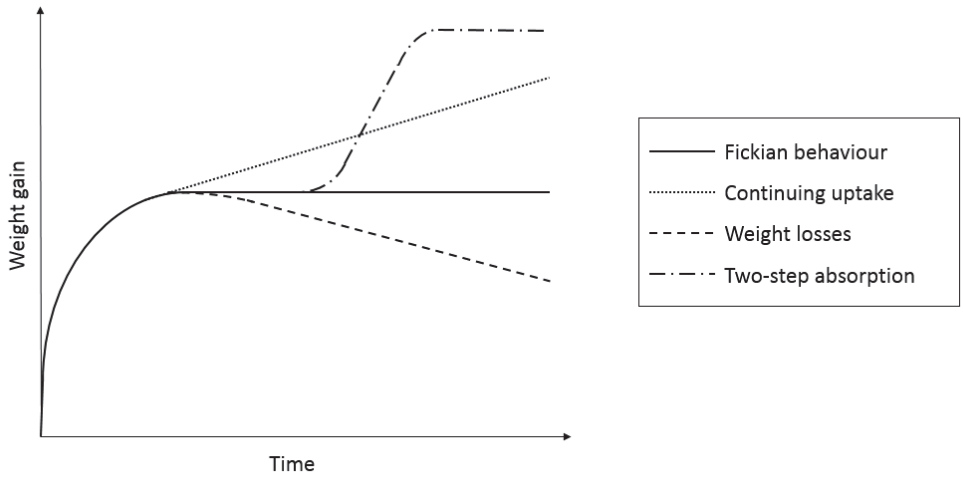

Figure 2.1: Schematic representations for Fickian and non-Fickian moisture diffusion

response over time, which results in changing of the the boundary conditions for moisture transport [18]. Karbhari & Zhang [18] trace the two-step absorption process to a combination of factors. The first part of their explanation is that the initial moisture gain will result in relaxation of elastic forces exerted by the cross-linked network. The second part of the explanation is for composites and deals with the damage occurring at the fiber-matrix interphase and fiber levels. This damage not only results in a reduction in mechanical properties but will also allow an increase in moisture absorption after the initial plateau.

The moisture absorption of a polymer is influenced by a wide range of factors, some of which are detailed below.

Temperature The behaviour of the diffusion process is highly dependent on the T_g of the polymer. Immersion in water with temperatures above T_g will result in a higher diffusion rate and a higher plateau. This has been explained by immersion in water above T_g being more damaging to the matrix material resulting in a higher water uptake [20].

Loading Loading enhances the water uptake of polymers and polymer based composites [11, 17, 21, 22]. A tensile stress will result in a larger increase in moisture absorption than a three point bending stress [11, 21]. An increase in the level of stress will result in an increase in the moisture uptake for specimens loaded under tension or three point bending [21]. The effect of a load increase on the water uptake of specimens loaded in shear seems to be variable, with a higher load not necessarily resulting in a higher water uptake [17].

The effect of loading on the diffusion coefficient is variable. For polyesters and phenolics loading increases the diffusion coefficient [11, 21] while for vinylesters a decrease was observed [11]. For polyesters loaded in tension the diffusion coefficient

was found to increase with an increasing load while specimens loaded under three point bending showed a decrease at higher load levels [21].

Degree and type of crosslinking Partially cured composites have been found to gain less mass when immersed in water than fully cured composites [16]. This has been attributed to a residual curing reaction in the partially cured resin. Visco et al. [23] speculate that the cross-linking reaction that occurs in the matrix repels the water molecules.

Void content A larger void content resulting in an increase in both the rate of moisture uptake and the peak uptake [11, 13, 24].

Pressure A higher pressure will result in a greater weight gain and is attributed to more water being pushed into the pores [13].

Medium Epoxy based composites and epoxy adhesives immersed in distilled water have been found to have a higher moisture content than the same specimens immersed in seawater or a NaCl solution [9, 25, 26]. This has been explained by an osmotic pressure that is created by the concentration of salt particles in the specimen being less than the concentration in the seawater. This osmotic pressure then acts against the water absorption resulting in a lower equilibrium moisture content for the specimens immersed in seawater [9]. Another explanation is that the cross-linked network of the polymer behaves as a semi-permeable membrane when immersed in water. Water will be able to permeate while the large inorganic ions in the NaCl solution will be obstructed. This way the chlorides in the water slow the degradation process. A similar explanation is that local salt deposits will form once the solubility of dissolved salts in seawater has been reached. These salt deposits will then form a physical barrier to the entrance of water [14]. Several studies [15, 27] observed small white spots on their samples after immersion in water and attributed this to the extraction of some soluble compound in the samples. These white spots could perhaps also (partially) be explained by these salt deposits.

The absorbtion of water by an adhesive will lead to swelling and plasticisation of the polymer network [8]. With longer periods of exposure the diffused water will cause hydrolysis. This is a chemical reaction at the molecular level that results in a permanent change in the mechanical behaviour [25].

Both plasticisation and hydrolysis will result in higher levels of molecular mobility and result in a decrease in the glass transition temperature, T_g [18, 19]. The glass transition temperature is the temperature at which the polymer material transforms from a glassy (hard) to a rubbery (soft) state. Below T_g the polymer chains are 'frozen' into position and cannot move, T_g marks the onset of chain motion [28]. With the decrease in T_g there will also be a considerable reduction in the strength and stiffness of the polymer [25]. The decrease in properties might be partially offset by a reactivation of the curing reaction of the immersed polymer. This reactivation of curing has been observed by various studies [6, 18, 23] and might lead to an improvement or regain of the T_g, strength and stiffness of the polymer. Curing is the process by which polymer chains are linked together via so-called cross-links. A material with a low cross-link density, so which has

few junction points per unit volume, will be flexible while a material with a high cross-link density will be rigid [28]. Increased cross-linking will result in a higher strength, modulus and also in an increase in the glass transition temperature, T_g. After longer immersion times the T_g, strength and stiffness will however decrease again due to the plasticising effect of the absorbed water becoming stronger [6].

The swelling of the polymer will cause mechanical forces on the material which can result in degradation. Moisture cycling will lead to mechanical stress cycling of the material and can lead to fatigue damage in the inter- and intralaminar region of composite laminates, hereby influencing the long term durability and performance [6].

The process of moisture absorption and its damaging effects can be reversed by drying but this may not result in complete recovery of the original properties [24]. This partial recovery is dependent on whether permanent reactions have taken place. The water that is chemically linked is responsible for the long-term degradation of the chemical properties of the adhesive while the water that is not chemically linked will only temporarily affect the polymer properties. The moisture concentration at which irreversible damage starts to take place is called the critical moisture concentration [14, 24].

Conclusion

The literature review on moisture absorption in polymers showed that the water uptake of the metal-to-metal bonds might follow Fickian or non-Fickian diffusion and will depend on factors such as (glass transition) temperature, loading, degree and type of crosslinking and void content. Water uptake seems to be unpredictable, to determine what it looks like for metal-to-metal bonds water uptake experiments will need to be carried out. Water absorption by the adhesive will lead to degradation of the polymer through plasticisation, swelling and, for long exposure times, hydrolysis.

Loading has been found to influence the water uptake of polymers and might in some cases lead to a significant increase in the uptake. This would lead to faster degradation of the polymer then expected based on unloaded water uptake tests. No research has been found on the influence of loading on the water uptake and strength of thick(er) (2 mm) epoxy adhesives. This thesis will study the water uptake of metal-to-metal bonds in unloaded and different loaded conditions. After the water uptake experiments the residual strength of the joints will be determined to find whether the joints degraded differently in the varying conditions.

2.2 The influence of water absorption on the viscoelastic response of polymers

The response of a viscoelastic material subjected to a load or deformation is to a large extent time dependent and might also depend on any previous load, deformation or temperature history. Two ways in which this time dependence manifests itself are creep and relaxation. Creep is the time dependent deformation of the material under constant load, while relaxation is the gradual decrease in stress under constant deformation. Removing the load on a viscoelastic material that has experienced creep will result in a process called recovery, during which the material will (partly) return to the original state. The time-dependent properties of polymers influence and limit their use in structural and load-bearing applications. The behaviour is caused by the material trying to minimize localised stresses by undergoing molecular rearrangement when it is under a load. This results in the strain/modulus being respectively higher/lower for long-term measurements than for short-term measurements [5].

Applying a constant and uniform load on a viscoelastic polymer under constant temperature and humidity will result in the creep curve that is given by the solid line in Figure 2.2. First there will be an instantaneous strain ε_0 which will, depending on the magnitude of the stress, either be elastic, where $\varepsilon_0 = \varepsilon_{0_e}$ or elastic-plastic, where $\varepsilon_0 = \varepsilon_{0_e} + \varepsilon_{0_p}$. Here ε_{0_e} is the elastic instantaneous strain and ε_{0_p} the plastic instantaneous strain. After this initial response three different creep stages can be distinguished. The first stage is characterized by a decreasing rate of deformation and is also called primary or transient creep. In the second stage the material will experience a nearly constant rate of deformation. This second stage is also called secondary or steady state creep. After the second stage the rate of deformation will increase again, this final creep stage is called tertiary creep. The third stage will end with fracture of the material [5,7]. Creep failure can either be widespread or localised. In the case of uniform loading the whole part will creep and fail by creep rupture. When stresses are localised, a localised crack will form and failure will be characterised by the propagation of this crack in the creeping material [7].

The dashed line in Figure 2.2 is the recovery curve. Removing the load before creep rupture will result in an instantaneous decrease in the strain. This instantaneous decrease is equal to the elastic portion of the instantaneous strain, ε_{0_e}. This will be followed by a process called recovery in which the material will exhibit a time-dependent decrease in strain. The degree of recovery is dependent on the material and creep mechanisms. Some polymers may fully recover after a sufficiently long recovery period [5,7]. In many polymers the creep strains will however not be entirely recovered, resulting in permanent strains. The total creep strain can thus be decomposed in a viscoelastic part, (ε_{ve}), that will be recovered when the load is removed, and a viscoplastic part, (ε_{ve}), that will be permanent. This results in $\varepsilon(t) = \varepsilon_{ve} + \varepsilon_{vp}$ [30].

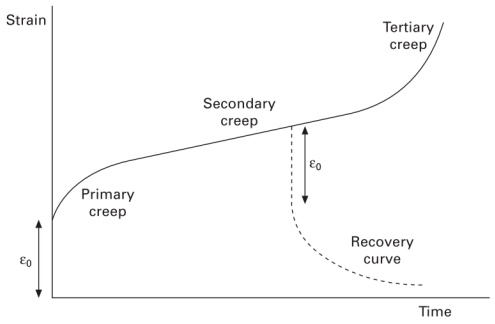

Figure 2.2: Creep curve for a viscoelastic polymer under constant stress and temperature. From: Ashcroft & Briskham [7]

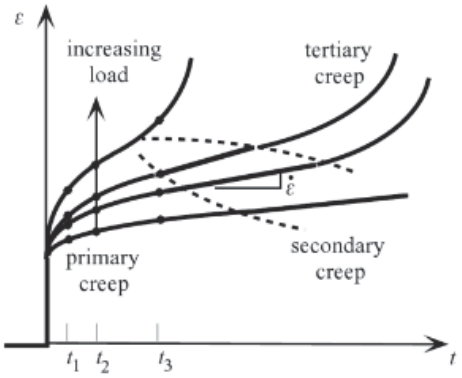

Figure 2.3: The influence of load level on the creep curve. From: Lakes [29]

It is well documented that an increase in the load will result in an increase in the creep strain, ε_c and creep strain rate, $\dot{\varepsilon}$, eg. [17, 30–44]. A higher strain rate will result in the same strain being reached in a shorter time, as illustrated in Figure 2.3. The viscoelastic behaviour of polymers has also been found to be largely dependent on the environment: an increase in temperature will result in an increase in the creep strain, eg. [12,17,33,42–50], and specimens exposed to water will generally experience a larger creep strain than dry specimens, eg. [11,17,40,46,50–52]. Feng et al. [46] and Yao & Ziegmann [50] have established that there is an equivalence between the effects of moisture and temperature on the viscoelastic response for respectively epoxy adhesive specimens and GFRP epoxy pipe specimens. It is suggested that the presence of absorbed moisture can result in the same creep response as a higher temperature in the dry condition [46].

The effect of the easier relaxation of matrix macromolecules at higher moisture contents [6] (see Section 2.1) can be so large that immersed specimens experience up to double the creep strain of their atmospherically aged counterparts [11]. The creep strain will already be influenced by a small amount of absorbed water, as shown by Dean [40] by comparing the creep behaviour of epoxy adhesive specimens stored in a desiccator with specimens stored under ambient conditions. If the polymer has not yet been fully cured before immersion the water exposure can lead to a reactivation of the curing reactions. The resulting increase in T_g, strength and stiffness of the polymer can result in an increase in the modulus and tensile strength [18, 23] and a decrease in the creep response [6]. After longer exposure times the mechanical properties of the polymer will decrease again because the damaging effect of the water becomes stronger [18]

The studies that have looked at the influence of (sea)water or humidity on the creep behaviour of composite (pipe) specimens, adhesives, resins and joints have done this in one of two ways. The first approach is to precondition the specimen in (sea)water or humidity and then test them in a dry environment [6,17,40,50,51] . The second approach is to subject the specimens to combined moisture and loading with [17, 46, 52–54] or

without [11, 53, 54] preconditioning.

Conclusion

The literature review on the influence of water absorption on the viscoelastic response of polymers started by presenting the basic creep and recovery response. This was followed by a discussion of the influence of load level, temperature and water absorption on the viscoelastic response. It was found that water absorption by fully cured polymers will result in a more pronounced viscoelastic response.

Studies looking at the influence of water absorption on creep behaviour have done so by either preconditioning specimens in (sea)water or humidity and testing them in a dry environment or by subjecting them to combined moisture and loading with or without preconditioning. In this thesis specimens will be creep tested in air and under combined moisture and loading without preconditioning to determine the differences in the creep response.

2.3 Modeling of creep behaviour

Determination of the (non)linear region of the viscoelastic response

The first step in modeling the viscoelastic behaviour of a material is to determine whether its measured response is linear or nonlinear. This is done by conducting creep (and recovery) experiments and analysing the result. Based on whether the response is linear or nonlinear an appropriate (non)linear model can be chosen to model the viscoelastic behaviour.

A viscoelastic material is said to behave linear if the stress and strain are proportional and the linear superposition principle holds. The behaviour is nonlinear if any of these conditions is no longer satisfied. The degree of nonlinearity will depend on factors such as temperature and applied stress level.

The stress-strain proportionality means that the creep compliance is independent of the stress levels. The creep compliance $D(t)$ is the ratio of the total strain, $\varepsilon(t)$, to the applied constant stress, σ_0 [5]:

$$D(t) = \frac{\varepsilon(t)}{\sigma_0} \tag{2-2}$$

The linear superposition principle means that the strain or recovery as a result from a currently applied or removed load is independent from any previously applied load. If this holds each loading step makes an independent contribution to the final deformation and the final deformation does not change with the order of the applied loads [5].

One way of determining whether the viscoelastic response is linear is to use the creep portion of the experiment to develop a suitable model for the compliance. This model is then used to predict the recovery strains. The behaviour is linear if the experimental

recovery strains match these predicted recovery strains because this means that the linear superposition principle holds [5].

Papanicolaou et al. [37, 55] have described a different approach that looks at stress versus creep strain curves at different times to determine whether the response is linear or nonlinear. These curves, also called isochronals, will be linear for linear viscoelastic materials [7] while for nonlinear materials the isochronals will be curved [56]. The difference in isochronals for linear and nonlinear materials is shown in Figure 2.4.

a) *Linear behaving material* **b)** *Nonlinear behaving material*

Figure 2.4: Stress-strain curves at constant time (isochronals) for linear and nonlinear behaving materials. From: Lakes [56]

Isochronals are constructed from creep curves by using the stresses and strains at different times, as shown in Figure 2.5. The linear-nonlinear stress threshold, σ_c σ_c, can be determined by plotting the isochronous data from the experiments [37] and looking where the isochronals deviate from linearity. A schematic representation of the determination of the linear-nonlinear stress threshold from an isochronal can be found in Figure 2.6. By doing this for multiple times, as shown in Figure 2.4 and Figure 2.5, it is possible to see the change in (non)linearity over time.

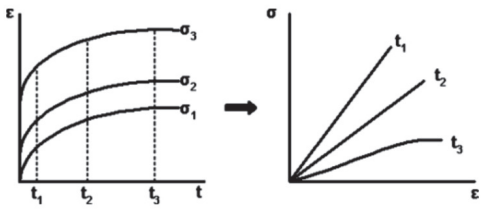

Figure 2.5: Construction of isochronous stress-strain curves from creep curves. From: Papanicolaou et al. [55]

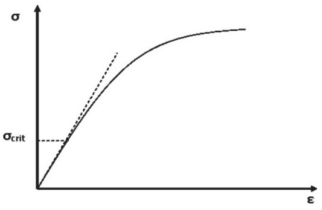

Figure 2.6: Determination of σ_c from an isochronous stress-strain curve. From: Papanicolaou et al. [55]

Mechanical models

The focus for this part of the literature review will be on the mechanical models that can be used to simulate creep behaviour. These models are made up of linear/Hookean springs and linear/Newtonian viscous dashpots in series and/or parallel. The stress-strain relationships of spring and dashpot are respectively $\sigma = E \cdot \varepsilon_1$ and $\sigma = \eta \cdot \dot{\varepsilon_2}$, where E can be interpreted as a linear spring constant or a Young's modulus and η η is the coefficient of viscosity [5, 7].

The parallel and series combinations of these two basic elements have been found to adequately fit experimental creep data, even for complicated composite materials. In general, adding more elements to the viscoelastic model will improve its accuracy in describing viscoelastic behaviour [46]. The mechanical models are however all empirical models. The values of the elastic modulus and coefficient of viscosity are determined by varying them until the analytical curve closely matches the experimental curve. Since the deformation processes in viscoelastic materials are quite complex it might be necessary to use different models for different loading conditions [57].

Nonlinear viscoelasticity can be represented by substituting the linear elements with nonlinear elements. This approach has for example been used by Majda & Skrodzewicz [31] and Zehsaz et al. [41,42]. A drawback of this method is however that the models will be complex and difficult to implement. On top of that they also have many parameters that require data [5, 7].

Various commonly used mechanical models will be presented, starting with the simple two element Maxwell and Kelvin-Voigt models. These simple models will be followed by the more complicated three-element solid and Burgers' fluid model.

Maxwell model Figure 2.7a shows the Maxwell model. The constitutive equation of this model is as follows [5]:

$$\dot{\varepsilon} = \frac{\dot{\sigma}}{E} + \frac{\sigma}{\eta}. \tag{2-3}$$

For creep under constant stress, $\sigma = \sigma_0$, applied at t = 0, the Maxwell model will give the following response, the graphic representation of which can be found in Figure 2.7b [5]:

$$\varepsilon(t) = \frac{\sigma_0}{E} + \frac{\sigma_0}{\eta}t. \tag{2-4}$$

This is generally a poor representation of creep and recovery in polymers. The response of the model can be improved by using a generalized Maxwell model with several Maxwell units in parallel with varying spring and dashpot constants. By doing this it can model instantaneous elasticity, viscous flow, creep with various retardation times and relaxation with various relaxation times. The model is however more convenient when the strain history is known, so for stress relaxation. The other variation of the generalized Maxwell model is several Maxwell models in series. This model will however give a response that is not much different from a single Maxwell model and is therefore not significant [5, 7].

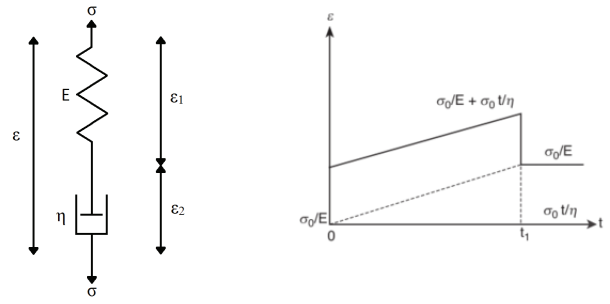

a) *Maxwell model*

b) *Response to loading and unloading of a constant load. From: Papanicolaou & Zaoutsos [5]*

Figure 2.7: The Maxwell model and its response to a constant load σ_0 and its removal

Figure 2.8: Wiechert model

A finite number of Maxwell elements in parallel with a linear spring element is also known as a Wiechert model. Figure 2.8 shows a graphical representation of this model. The Wiechert model has been used by Nciri et al. [58] to model the viscoelastic part of a coupled viscoelastic-viscoplastic scheme used to model the response of a polypropylene reinforced with short-glass fibres. The Wiechert model with an infinite number of Maxwell elements is used by Zobeiry et al. [59] as a mechanical representation for a differential formulation of viscoelasticity. This model is then used for the finite element modelling of the three-dimensional behaviour of isotropic and transverse isotropic viscoelastic materials.

Kelvin-Voigt model Figure 2.9a shows the Kelvin-Voigt model. The constitutive equation for the Kelvin-Voigt model is as follows [5]:

$$\dot{\varepsilon} + \frac{E\varepsilon}{\eta} = \frac{\sigma}{\eta}. \tag{2-5}$$

For creep under constant stress, $\sigma = \sigma_0$, applied at t = 0, the Kelvin-Voigt model gives the following response which can also be found in Figure 2.9b [5]:

$$\varepsilon(t) = \frac{\sigma_0}{E}[1 - e^{-Et/\eta}]. \tag{2-6}$$

Where t is the time and η/E is the retardation time t_c which is a measure of the rate at which deformation occurs. This equation gives a reasonable approximation of transient/primary creep. The representation of recovery is however poor since the instantaneous recovery and permanent strain after unloading are unaccounted for. The model shows a finite initial strain rate whereas the apparent initial strain rate for many materials is very rapid. It also only indicates a single retardation time while there will be a range of retardation times in a real polymer [5, 7].

The range of retardation times that is observed in real polymers be modelled using a generalized Kelvin-Voigt model with Kelvin-Voigt units in series with varying spring

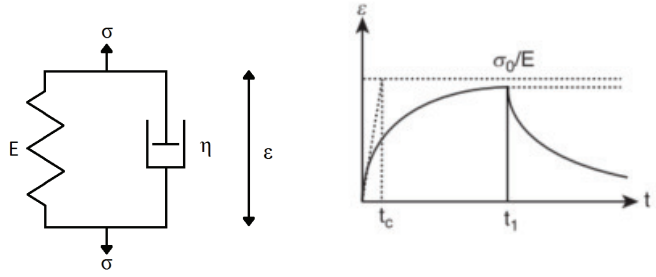

a) *Kelvin-Voigt model*

b) *Response to loading and unloading of a constant load. From: Papanicolaou & Zaoutsos [5]*

Figure 2.9: The Kelvin-Voigt model and its response to a constant load σ_0 and its removal

and dashpot constants. The creep response of this model to a constant stress, σ_0 is as follows [5]:

$$\varepsilon(t) = \sigma_0 \sum_{i=1}^{N} D_i \left(1 - e^{-t/t_c^i}\right),$$

Roseley et al. [44] used two Kelvin-Voigt units in series to model the creep response of epoxy adhesives over a wide range of temperatures.
The other generalized Kelvin-Voigt model consists of Kelvin-Voigt units in parallel with varying spring and dashpot constants. Since the response of many Kelvin-Voigt models in parallel does not differ from the response of a single Kelvin-Voigt element this model is not significant.

Three-element solid The three-element solid model, also called three-parameter solid or standard linear solid, is the simplest model that provides a satisfactory simulation of the viscoelastic response to both loading and unloading. The model either consists of a spring in series with a Kelvin-Voigt model as shown in Figure 2.10a or of a spring in parallel with a Maxwell model as shown in Figure 2.10b. The first model makes instantaneous elongation possible while the second gives bounded creep.

Both models will lead to the same form of constitutive equation [60]. The constitutive equations can be found by using the constitutive equations of the spring and of respectively the Kelvin-Voigt model (2-5) and the Maxwell model (2-3).

The constitutive equation for the first model (Figure 2.10a) will be as follows [5]:

$$\sigma + \frac{\eta_2}{E_1 + E_2}\dot{\sigma} = \frac{E_1 E_2}{E_1 + E_2}\varepsilon + \frac{E_1 \eta_2}{E_1 + E_2}\dot{\varepsilon} \tag{2-7}$$

This model has been used to model the viscoelastic behaviour of single lap joints [61,62] and epoxy adhesives [40]. Dean [40] used exponential models based on the model to create a two-process model that can simulate both the short-term and the long-term

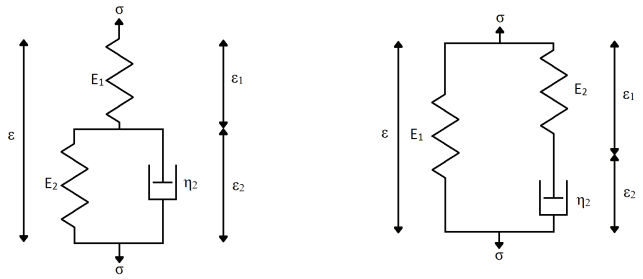

a) *Spring in series with a Kelvin-Voigt model* **b)** *Spring in parallel with a Maxwell model*

Figure 2.10: Three-element solid model

creep process. These two processes have different relaxation processes and thus different relaxation times. Feng et al. [46] used a coupling model similar to Dean's two-process model to model structural epoxy adhesives that were exposed to combined moisture and loading. The model was found to be capable of describing the long-term creep behaviour in both the wet and dry conditions.

For the second model (Figure 2.10b) the following constitutive equation can be found [60]:

$$\sigma + \frac{\eta_2}{E_2}\dot{\sigma} = E_1\varepsilon + \frac{\eta_2(E_1 + E_2)}{E_2}\dot{\varepsilon} \tag{2-8}$$

Ferrier et al. [47] used two Maxwell three-element-solid model in series to model composite to concrete adhesive joints subjected to shear loading. Zehsaz et al. [41, 42] used two models and a spring in series with nonlinear functions of temperature and stress for the parameters to model the viscoelastic behaviour of a structural epoxy adhesive.

Burgers' fluid model The Burgers' fluid model is shown in Figure 2.11a. It is a four element-model consisting of a Kelvin-Voigt model and a Maxwell model in series. The model assumes linear viscoelastic behaviour of the polymer and will exhibit both transient (primary) and steady state (secondary) creep as well as partial recovery [5, 7].

The constitutive equation for the Burgers' fluid model is as follows [5]:

$$\sigma + \left(\frac{\eta_3}{E_1} + \frac{\eta_3}{E_2} + \frac{\eta_2}{E_2}\right)\dot{\sigma} + \frac{\eta_2\eta_3}{E_1E_2}\ddot{\sigma} = \eta_3\dot{\varepsilon} + \frac{\eta_2\eta_3}{E_2}\ddot{\varepsilon} \tag{2-9}$$

The creep behaviour for the Burgers' fluid model is characterized by the following equation and can also be found by combining (2-4) and (2-6) [5]:

$$\varepsilon(t) = \frac{\sigma}{E_1} + \frac{\sigma}{E_2}[1 - e^{-E_2t/\eta_2}] + \frac{\sigma}{\eta_3}t. \tag{2-10}$$

The Burgers' fluid model has been successfully used to model glass-epoxy composites exposed to water [6], double lap shear joints [63] and the epoxy adhesive in a single lap joint [32]. Majde & Skrodzewicz [31] replaced the constant parameters η_1, η_2 and E_2 in (2-10) by stress dependent functions and assumed a constant value for E_1 to model the nonlinear viscoelastic behaviour of an epoxy adhesive.

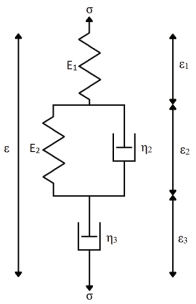

a) *Burgers' fluid model*

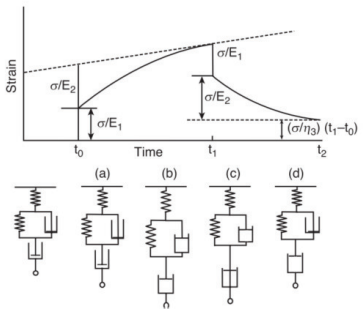

b) *Response to loading and unloading of a constant load. From: Papanicolaou & Zaoutsos [5]*

Figure 2.11: The Burgers' model and its response to a constant load σ_0 and its removal

Conclusion

The literature review on the modeling of creep behaviour found that the first step to modeling viscoelastic behaviour is to determine whether the viscoelastic response is linear or nonlinear. This can be determined by conducting creep experiments and analysing the results.

Once it is known whether the viscoelastic response is linear or nonlinear an appropriate linear or nonlinear viscoelastic model can be chosen. The modeling of creep behaviour in this thesis will be done using mechanical models. These models are made up of linear springs and dashpots in series or parallel. In general, the accuracy of the model will be improved by adding more elements. These mechanical models can be used to model nonlinear behaviour by using nonlinear springs and dashpots. All viscoelastic models are empirical in that their parameters are fitted to experimental results. The final model that is to be used to simulate the creep response of the metal-to-metal bonds will be the simplest model that gives a good fit.

Chapter 3

Experimental procedure

During the experiments single lap joint specimens will be subjected to one of three loading and/or ageing conditions for a predefined period of time before being tensile tested to determine the residual lap shear strength. These three loading and/or ageing conditions are as follows:

Condition 1: Ageing at elevated temperatures in water without loading.
Condition 2: Ageing at elevated temperatures in water with loading.
Condition 3: Ageing at elevated temperatures in air with loading.

The testing conditions were chosen as follows:

Experiment duration: 14 days 14 days was the maximum amount of time available for a single experiment to ensure it was possible to test specimens at at least two different load levels in both water and air.

Testing temperature: 40^{o}C The choice of testing temperatures was limited by the diffusion data and moisture dependent mechanical properties found in literature [26]: 20^{o}C, 40^{o}C and 60^{o}C. The final choice for 40^{o}C was based on a trade-off between accelerating the water absorption process by increasing the temperature and ensuring the specimen could still withstand the load for two weeks.

Testing environment: distilled water and air The creep testing equipment available at the moment of testing was not suitable for the use of salt water. Moreover, literature shows that distilled water results in worse ageing conditions in terms of water uptake than salt water. No special actions were taken for the testing in air.

Loading conditions: 1 MPa, 3 MPa, 6 MPa and 9 MPa The 1 MPa and 3 MPa load levels were chosen to avoid failure of the specimens during the 14 days of loading. Failure of the specimen while creep loading would make it impossible to determine the effect of creep loading and ageing on the residual strength. Moreover, it would also result in the crack surface being exposed to the distilled water which would lead to additional water absorption by the adhesive, thereby making the specimen unsuitable for determining the effect of creep loading on the water uptake. The 6 MPa and 9 MPa load levels were later added to observe the creep behaviour at higher load levels.

Section 3.1 will start by describing the materials and fabrication process of the single lap shear joints used during the experimental work. This is followed by Section 3.2 in which the experiments for condition 1 are outlined. Section 3.3 will describe the procedure for condition 2 and condition 3. Finally, the chapter will conclude with a description of the tensile testing in Section 3.4.

3.1 Materials and specimens

This section will describe the materials and fabrication process of the single lap shear joints used during the experimental work. Figure 3.1 shows the shape and dimensions of the final joint.

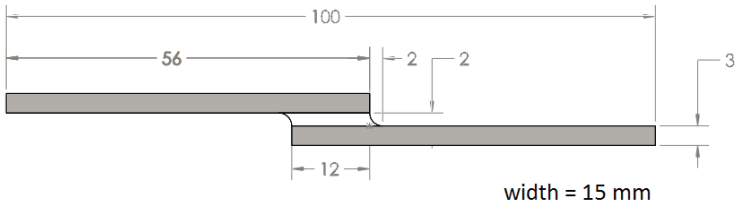

Figure 3.1: Dimensions in mm of the single lap joints

The substrate material used is S700MC steel. Table 3.1 lists the chemical composition of this steel. The adhesive is Araldite 2015, a two component epoxy paste adhesive by Huntsman. For the surface treatment Silquest A-187 epoxy silane (γ-glycidoxypropyltrimethoxysilane [γ-GPS]) from Momentive was used as a silane coupling agent.

C	SI	MN	P	S	AL	NB	V	TI	CU	CR	NI	MO	B	ZR
0.056	0.18	1.78	0.012	0.004	0.04	0.061	0.012	0.114	0.015	0.05	0.03	0.006	0.0001	0.003

Table 3.1: Chemical composition % of S700MC steel [64].

After milling S700MC steel plates with a thickness of 3 mm to the desired dimensions (see Figure 3.2) the edges were deburred using sandpaper and the bond area was sand-blasted. After sand blasting the bond area was wiped clean in a single direction using a clean cloth with acetone. The bond areas were then tested for water breaks using distilled water. If water breaks were detected the surface was further cleaned using acetone before application of the silane solution.

The silane pretreatment used is based on [65–68] and is a 1% solution of silane with distilled water. The silane solution was hydrolyzed for one hour under continuous stirring in distilled water with a natural pH of 5-6 and was then applied within 15 minutes to the bond area using a clean brush. To ensure the adsorption equilibrium of silane with the steel surface was reached, care was taken that the surface remained wet for ten minutes [66]. The substrates were placed vertically on a paper towel to allow the absorption of excess silane solution by the paper and were then left to dry at room temperature for an hour. Room temperature drying was chosen because the current body of research is inconclusive on the effect of elevated temperature drying [65] and the work of Gledhill, Shaw & Tod [68], one of the few that studied (mild) steel joints, shows that room temperature curing resulted in greater durability than elevated temperature drying.

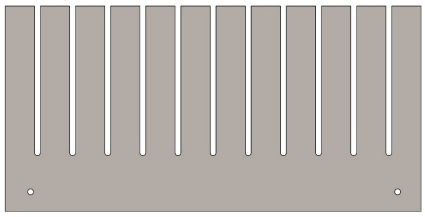

Figure 3.2: Steel substrates

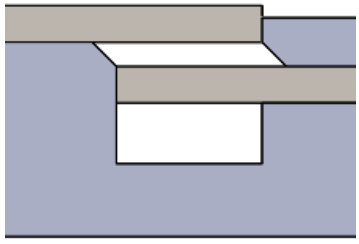

Figure 3.3: Detail of the mould

Once the silane solution had dried for one hour, substrates were bonded using an alignment mould. To ensure the mould and substrates would not be bonded together, four layers of Marbocote were applied to the mould. The use of the mould ensures that specimens are always properly aligned and helps to achieve a consistent bond line thickness. The way the mould was designed also results in consistent 2 by 2 mm 45^o fillets on the lap joints, as shown in Figure 3.3. Figure 3.4a - 3.4d shows how the alignment mould is used. Pressure is applied to the bond line via a weight placed on the second substrate.

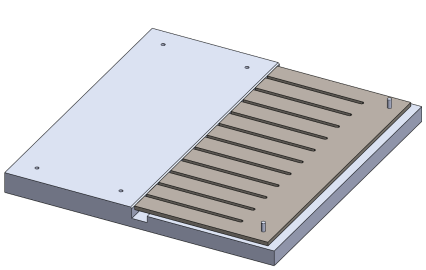

a) *Step 1: Assembly of the first plate*

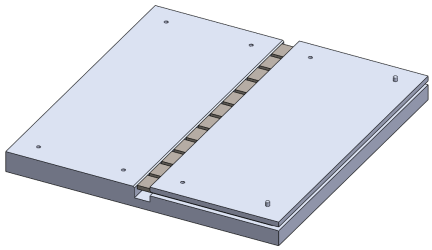

b) *Step 2: Assembly of second part of the mould*

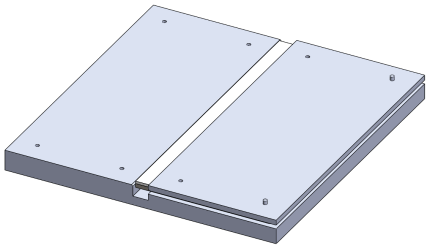

c) *Step 3: Application of adhesive*

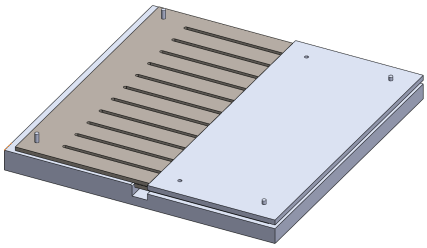

d) *Step 4: Assembly of the second plate*

Figure 3.4: Bonding of the steel substrates using the alignment mould

The assembled plates were put in a 80^oC oven for 2 hours. Since Araldite 2015 has a pot life of 30-40 minutes [69], the bonded substrates were placed in a preheated oven within 20 minutes of initial application. A thermocouple was used to determine the temperature of the adhesive during curing. Since the intended curing period and temperature of the adhesive of 1 hour at 80^oC was not reached specimens were later post-cured in a 90^oC oven for three hours. This was done to ensure the specimens were fully cured and there

would not be a reactivation of curing caused by the ingress of water as observed by several studies, e.g. [5, 18, 23].

After curing the steel plates were cut, resulting in twelve single lap joints. The outer two specimens and all other specimens with imperfections in the bond line and/or fillets were discarded. Excess adhesive was removed and sandpaper was used to create fillets with a radius of 2 mm as shown in Figure 3.1. When all excess adhesive was removed specimens were weighed and measured. Finally, the steel adherends were cleaned using a generic paint cleaner from GAMMA and coated using two layers of "Hammerite No.1 Rust Beater" to protect them against rust while immersed in the water. This was later followed by four layers of "Hammerite Direct to Rust Metal Paint" once it was found that the coating was affected by the water during experiments. In this thesis the coating with "Hammerite No.1 Rust Beater" is referred to as "coating 1". The coating consisting of both "Hammerite No.1 Rust Beater" and "Hammerite Direct to Rust Metal Paint" is referred to as "coating 2".

3.2 Ageing at elevated temperatures in water without loading

Specimens were exposed to 40^{o}C distilled water by placing them in a glass pot filled with distilled water and placing this pot in a 40^{o}C water bath, as shown in Figure 3.5. The temperature of the water is controlled using a sensor, a heating element and a pump.

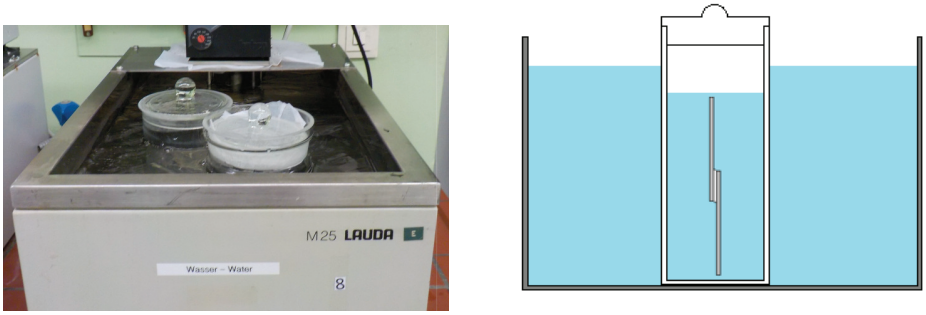

a) *Picture* **b)** *Schematic cross-section*

Figure 3.5: Water bath

The water uptake of the specimens is determined by weighing the specimens before and after exposure to the distilled water and calculating the difference. Specimens weighed after exposure are first wiped dry using a paper towel to remove excess moisture. The specimens are removed from the water bath and weighed at least once a day.

After the initial experiments the coating applied to the adherends ("Hammerite No.1 Rust Beater") was found to absorb water and thereby influence the weight measurements. In an attempt to prevent this, an extra (different) coating ("Hammerite Direct to Rust

Metal Paint") was applied to the rest of the specimens. In order to determine the water uptake of the coatings, plain steel adherend specimens were coated and immersed in water alongside the bonded joints. The water uptake of the coatings was then compared with the water uptake of the metal-to-metal bonds to obtain the water uptake of the adhesive.

Table 3.2 summarizes the experiments performed under accelerated ageing in water with loading (condition 1).

Test series	Specimen	Coating	Duration	Environment	Load	Sample size
SLJ1_W_0MPa - Exp	SLJ	Coating 1	14 days	40^{o}C distilled water	-	3
SLJ2_W_0MPa - Exp	SLJ	Coating 2	14 days	40^{o}C distilled water	-	4
Steel1_W_0MPa - Exp	Steel	Coating 1	14 days	40^{o}C distilled water	-	4
Steel2_W_0MPa - Exp	Steel	Coating 2	14 days	40^{o}C distilled water	-	4

Table 3.2: Test matrix for experiments with accelerated ageing without loading in water

3.3 Ageing at elevated temperatures in water and air with loading

Specimens were tested under accelerated ageing with loading using custom environmental chambers in a Full Notch Creep Test [FNCT] machine at the BAM. This machine can control the applied load and temperature during testing and automatically records the creep strain. During the experiments the load was applied with an accuracy of ± 1 N and the temperature was controlled with an accuracy of ± 0.5^{o}C. Figure 3.6 summarizes the loading sequence consisting of a pre-stress σ_{pre} and an applied stress σ_0.

Figure 3.6: Schematic view of the applied loading during the creep experiments

Ageing at elevated temperatures in water with loading

Specimens subjected to ageing in water under creep loading were placed in the custom environmental chambers shown in Figure 3.7. The chambers are placed on a heating element and the temperature is controlled using a sensor in the chamber. Figure 3.8 shows clamped specimens with coating 1 before just before insertion in the environmental chamber. The specimens are weighed twice: once before the start of the experiment and once after 14 days of combined moisture and loading.

a) *Picture* **b)** *Schematic cross-section*

Figure 3.7: FNCT Environmental chamber for fluids.

Figure 3.8: FNCT machine with environmental chambers for fluids and clamped specimens.

Table 3.3 summarizes the accelerated ageing with loading in water experiments that have been conducted for the thesis. Two different types of specimens were tested: Single lap joints with coating 1 and single lap joints with coating 2.

Test series	Specimen	Coating	Duration	Environment	Load	Sample size
SLJ1_W_1MPa - Exp	SLJ	Coating 1	14 days	40°C distilled water	1 MPa	2
SLJ2_W_1MPa - Exp	SLJ	Coating 2	14 days	40°C distilled water	1 MPa	2
SLJ2_W_3MPa - Exp	SLJ	Coating 2	14 days	40°C distilled water	3 MPa	2
SLJ2_W_6MPa - Exp	SLJ	Coating 2	Until failure	40°C distilled water	6 MPa	1
SLJ2_W_9MPa - Exp	SLJ	Coating 2	Until failure	40°C distilled water	9 MPa	2

Table 3.3: Test matrix for experiments with accelerated ageing with loading in water

Ageing at elevated temperatures in air with loading

Specimens subjected to ageing with loading in air were placed in the custom environmental chambers shown in Figure 3.9. The chambers are placed on a heating element and the temperature is controlled using a sensor in the chamber. The environmental chamber is double walled, as shown in the schematic sketch in Figure 3.9b. The outer portion of the chamber is filled with water. This water will be heated by the heating element and result in heating of the air in the inner portion.

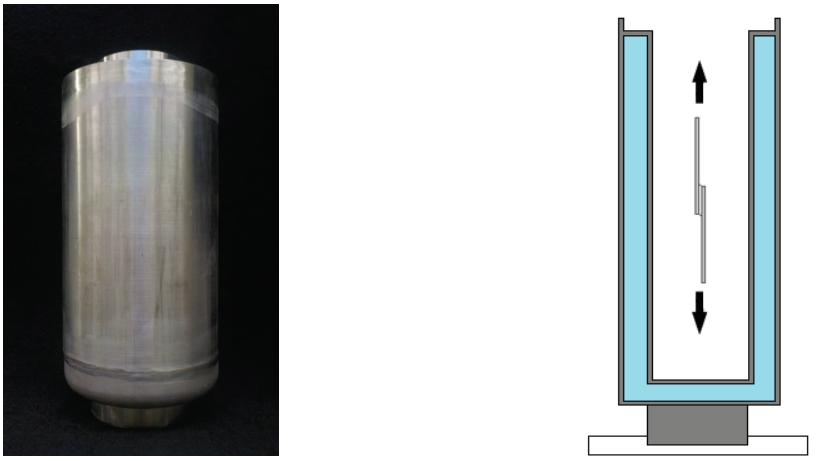

a) *Picture* **b)** *Schematic cross-section*

Figure 3.9: FNCT Environmental chamber for air

Table 3.4 summarizes the experiments performed with ageing in air under creep loading.

Test series	Specimen	Coating	Duration	Environment	Load	Sample size
SLJ2_A_1MPa - Exp	SLJ	Coating 2	14 days	40°C air	1 MPa	2
SLJ2_A_3MPa - Exp	SLJ	Coating 2	14 days	40°C air	3 MPa	2
SLJ2_A_6MPa - Exp	SLJ	Coating 2	4 days	40°C air	6 MPa	1
SLJ2_A_9MPa - Exp	SLJ	Coating 2	Until failure	40°C air	9 MPa	2

Table 3.4: Test matrix for experiments with accelerated ageing with loading in air

3.4 Tensile testing

Tensile testing has been used to determine the initial and the residual lap shear strength of the single lap shear joints. The initial lap shear strength is defined as the lap shear strength of the specimens as manufactured. The residual lap shear strength refers to the lap shear strength of specimens after accelerated ageing and loading conditions as described in Section 3.2 and Section 3.3.

First, the initial lap shear strength of specimens has been determined at the DASML using a Zwick 250 kN tensile testing machine. This was later repeated at the BAM using a Zwick 1454 20 kN testing machine. The tensile tests for the residual lap shear strength have all been performed using the Zwick 1454 at the BAM. All tests were executed with a cross-head speed of 1.3 mm/min. The testing machines at the DASML and the BAM had different clamping mechanisms. The Zwick 250kN at the DASML was fitted with hydraulic grips that could be adjusted to fit the single lap shear joints. The Zwick 1454 20 kN at the BAM did not have this option and therefore aluminum spacers were manufactured to ensure proper loading of the specimens and the specimens needed to be fastened by hand. Figure 3.10 gives a schematic representation of the clamps used in both the Zwick 250 kN and the Zwick 1454 20 kN.

Table 3.5 summarizes the tensile tests that have been conducted.

a) *Clamps Zwick 250 kN* **b)** *Clamps Zwick 1454 20 kN*

Figure 3.10: Schematic representation of the clamps used during tensile testing

Test series	Specimen	Coating	Environment (Preconditioning)	Load (Preconditioning)	Sample size (Preconditioning)	
SLJ_A_0MPa - Exp	SLJ	No Coating	-	-	-	5
SLJ1_A_0MPa - Exp	SLJ	Coating 1	-	-	-	5
SLJ1_W_0MPa - Exp	SLJ	Coating 1	14 days	40^{o}C distilled water	-	3
SLJ1_W_1MPa - Exp	SLJ	Coating 1	14 days	40^{o}C distilled water	1 MPa	2
SLJ2_W_0MPa - Exp	SLJ	Coating 2	14 days	40^{o}C distilled water	-	4
SLJ2_A_1MPa - Exp	SLJ	Coating 2	14 days	40^{o}C air	1 MPa	2
SLJ2_W_1MPa - Exp	SLJ	Coating 2	14 days	40^{o}C distilled water	1 MPa	2
SLJ2_A_3MPa - Exp	SLJ	Coating 2	14 days	40^{o}C air	3 MPa	2
SLJ2_W_3MPa - Exp	SLJ	Coating 2	14 days	40^{o}C distilled water	3 MPa	2

Table 3.5: Test matrix for residual strength experiments

Chapter 4

Results and Discussion

This chapter will present and discuss the results for the experiments described in Chapter 3. First, the water uptake results that followed from condition 1 and condition 2 will be discussed, followed by the creep result from condition 2 and condition 3. The chapter will end with the strength and stiffness results from the tensile testing.

4.1 Water uptake

This section will present and discuss the water uptake results for the ageing of single lap joint specimens in water at elevated temperatures with and without loading as described in Chapter 3. It will also present numerical results for the unloaded case. The work has been carried out with the aim of answering the following sub-research question:

> *How does the load level influence the water uptake of steel bonded joints subjected to hygrothermal and creep loadings?*

First the Finite Element Method [FEM] model and the numerical results will be presented. This will be followed by the experimental results. Finally, the sub-reseach question will be answered and some recommendations will be given.

4.1.1 FEM model

Figure 4.1 shows an illustration of the adhesive to be modelled. The dimensions of the single lap joint are shown in Figure 3.1 in Chapter 3.1. Table 4.1 lists the mechanical properties of the steel and adhesive. Figure 4.2 shows the evolution of the Young's modulus and yield stress versus the moisture concentration as found by Bordes et al. [26].

Property	S700MC Steel	Araldite 2015 Adhesive
Poisson's ratio	0.3 [-]	0.33 [70] [-]
Young's Modulus	210 [GPa]	see Figure 4.2a [GPa]
Yield Strength	770 [MPa] [64]	see Figure 4.2b [MPa]
Diffusion Coefficient	0 [m^2s^{-1}]	2.20×10^{-13} [26] [m^2s^{-1}]

Table 4.1: Material mechanical properties for S700MC steel and Araldite 2015 adhesive for 40^{o}C distilled water.

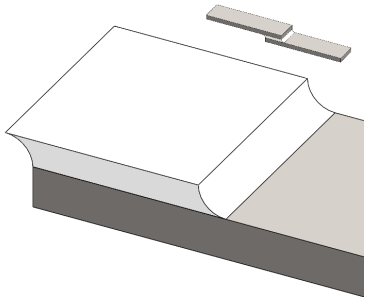

Figure 4.1: Illustration of adhesive (white) with adherend(s) (grey)..

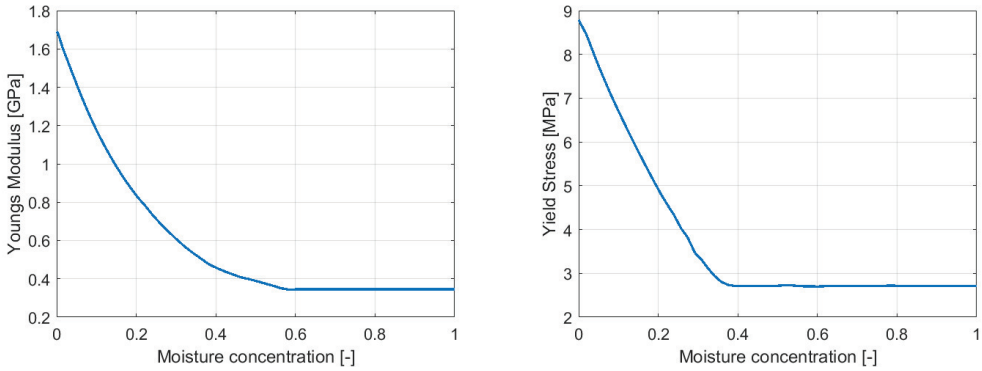

a) *Young's Modulus* **b)** *Yield Stress*

Figure 4.2: Young's modulus and yield stress evolution versus the moisture concentration obtained by numerical simulation. Based on Bordes et al. [26]

The model has been created using Abaqus Software version 6.14 from Dassault Systèmes. The model will only include the adhesive layer. The steel adherends will not absorb moisture when immersed in water. It is therefore not necessary to include them in the model since the goal of the simulation is to simulate the water uptake of the joint.

To minimize the computational time needed for the simulation only a quarter of the adhesive layer is modeled and Symmetry (Figure 4.3a) and Anti-Symmetry (Figure 4.3b) boundary conditions are applied. The water immersion of the adhesive is simulated by assigning an initial normalised moisture concentration (temperature in Abaqus) boundary condition of 1 at the surfaces exposed to water [22, 26], see Figure 4.3c. The application of a moisture concentration boundary condition via a temperature boundary condition is possible by using a heat transfer analogy. This heat transfer analogy is detailed in Appendix A.1. For the simulation it has been assumed that the adhesive layer is homogeneous and that the temperature field is uniform at a given time, thereby conforming to the assumption of uniform conductivity and diffusivity required for the use of the heat transfer analogy [71].

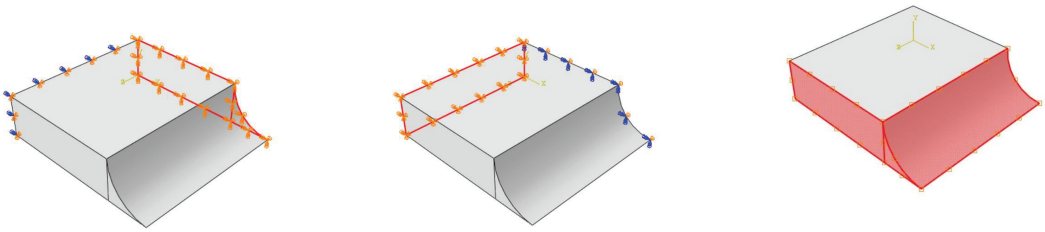

a) *Symmetry* **b)** *Anti-Symmetry* **c)** *Normalised moisture concentration*

Figure 4.3: Applied boundary conditions.

The model is meshed using heat transfer (DC3D8). The step size used during the analyses is controlled by setting the maximum allowable temperature change per increment to 0.1. When compared to an increment size of 0.01, the 0.1 increment gives less than a 1% overestimate of the water absorption in the adhesive.

A mesh convergence study has been conducted to find the optimal mesh. This has been done by comparing the water profile along half the overlap length for different mesh sizes. The study has been carried out at different locations in the adhesive with the same results, the results presented here correspond to the location indicated by the black line in Figure 4.4a and the dotted lines in Figure 4.4b. The analyses were run for periods of one hour, one day, one week and two weeks to ensure the mesh will be able to represent the behaviour of the adhesive over the experimental period of two weeks.

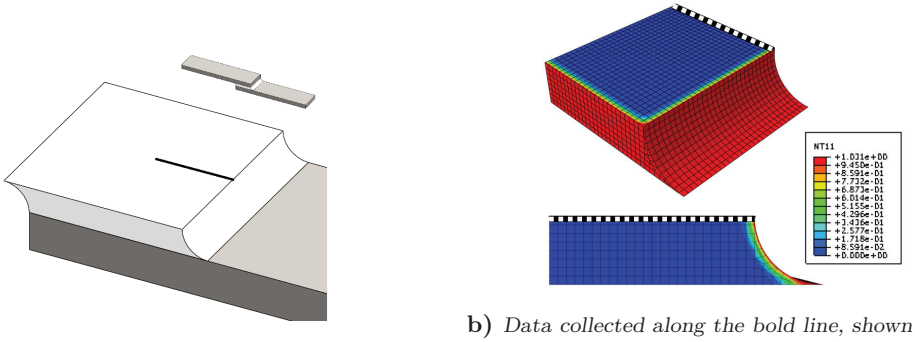

a) *Half the overlap length of single lap joint* **b)** *Data collected along the bold line, shown for a mesh size of 0.25 mm at one day*

Figure 4.4: Data collected along half the overlap length.

The results for the mesh convergence study are shown in Figure 4.5a-4.5d. These figures show that with an increase in duration of the simulation the mesh size becomes less critical and a coarser mesh can be used to accurately represent the response of the adhesive. Based on these results the model is considered to be converged for a mesh size of 0.25 mm for time durations exceeding one day. Since the computational time for this mesh was relatively short no further changes have been made to the mesh, resulting in a final mesh as shown in Figure 4.6

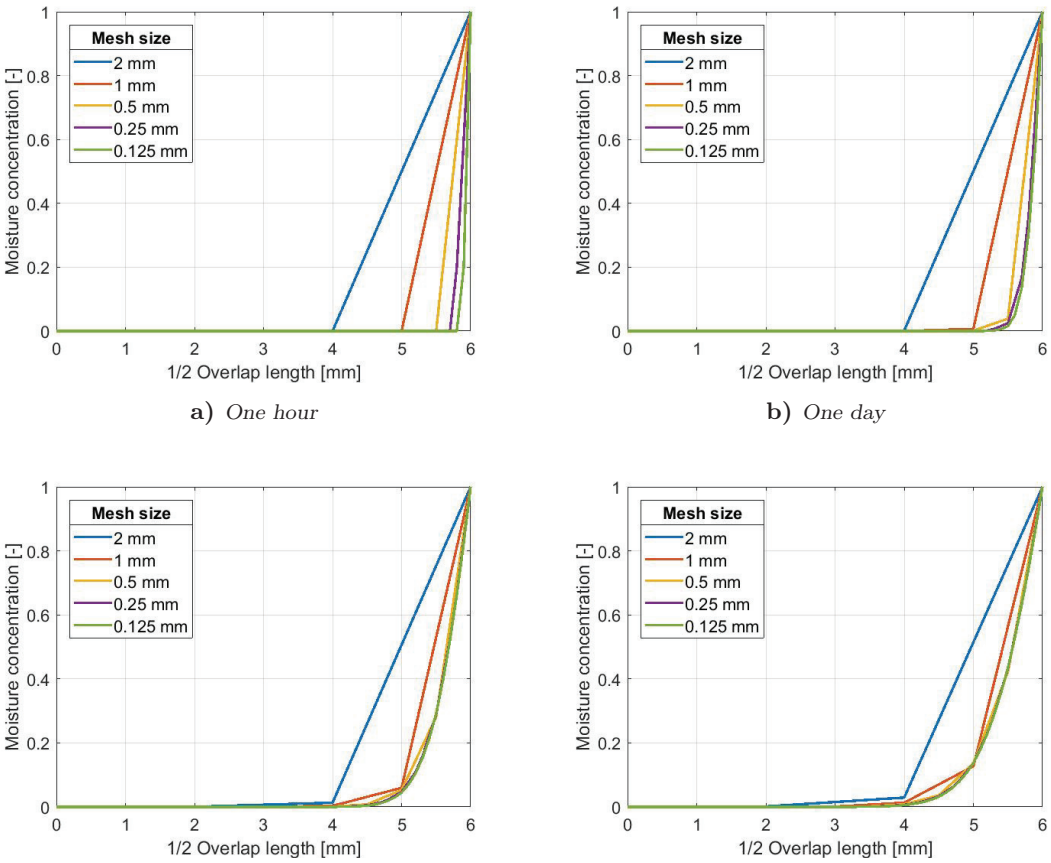

a) *One hour* **b)** *One day*

c) *One week* **d)** *Two weeks*

Figure 4.5: Water profile along half the overlap length at respectively one week (4.5c) and two weeks (4.5d).

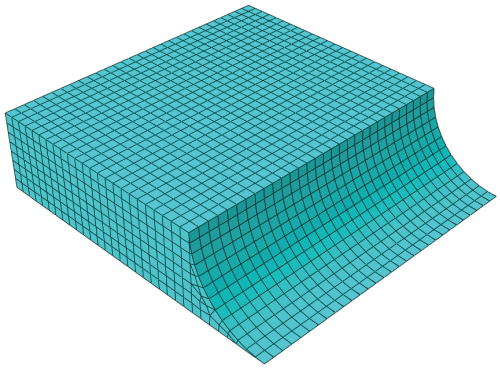

Figure 4.6: Final mesh for the modelled adhesive layer.

The first step to determining the water uptake using the output from the FEM model is to collect moisture concentration data of the top, middle and bottom surfaces (indicated by dotted lines in Figure 4.7a - 4.7c). This data is then used to create moisture concentration maps (see Figure 4.8a). The mid surface is defined as the middle of the curvature of the fillet as opposed to half the adhesive thickness. This has been done because of the gradient in moisture concentration through the thickness caused by the fillet. Taking the mid surface at the middle of the curvature of the fillet results gives the moisture concentration halfway this gradient.

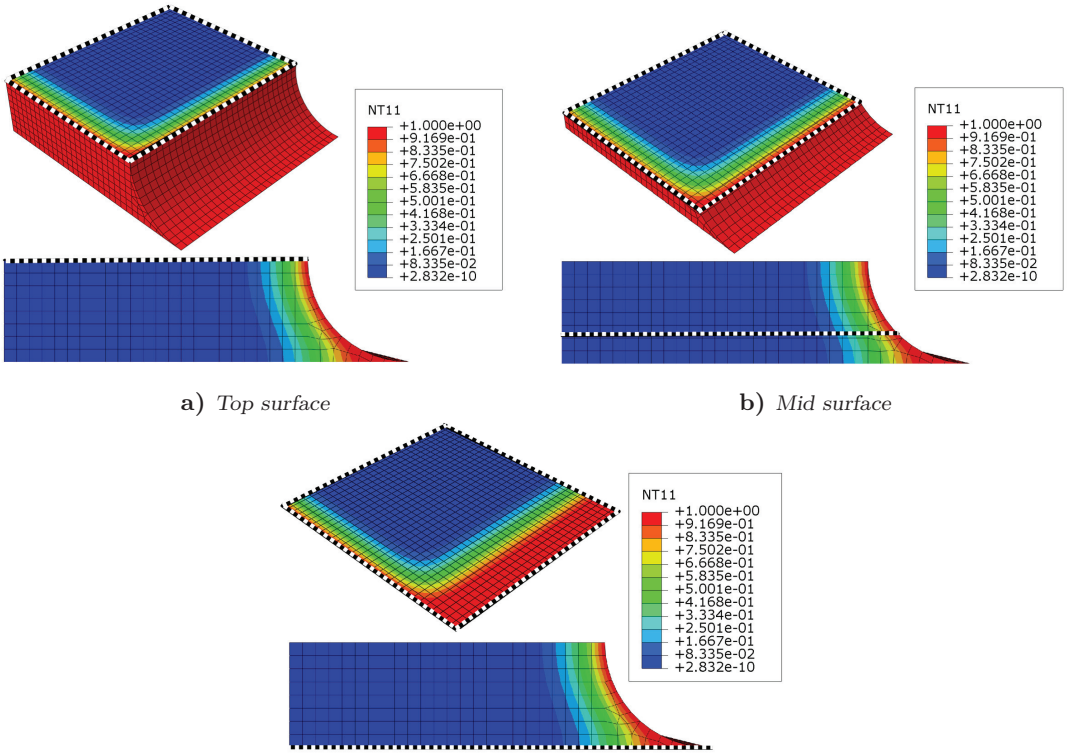

a) *Top surface*

b) *Mid surface*

c) *Bottom surface*

Figure 4.7: Data collected for moisture concentration map of top (4.7a), middle (4.7b) and bottom surface (4.7c). Shown for a mesh size of 0.25 mm at two weeks

By integrating the moisture concentration maps over the area of their respective surfaces the volume under the graph can be obtained. This volume is then divided by the volume under a fully saturated concentration map (see Figure 4.8b) to obtain the water uptake of the surface as a percentage. The water uptake percentage of the bond line as a whole is approximated by taking the average of the three surfaces. By performing these steps for different time periods it is possible to simulate the evolution in moisture concentration in the adhesive over time.

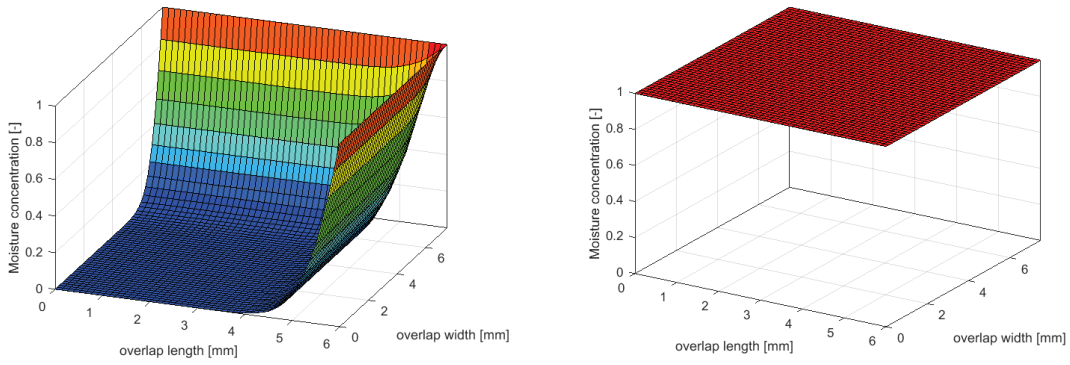

a) *Two weeks* **b)** *Fully saturated*

Figure 4.8: Moisture concentration maps of top surface after two weeks (4.8a) and when fully saturated (4.8b).

To be able to link the simulation results to the experimental results the water uptake percentage will need to be converted to a weight change in grams. Bordes et al. [26] found the weight change of saturated Araldite 2015 samples in 40^{o}C de-ionized water to be 8.4% of the initial weight. Since the density (1.4 g/cm^3 [69]) and dimensions (see Figure 3.1 in Chapter 3.1) of the adhesive are known this result can be used to determine the water uptake in grams at a certain water uptake percentage. This can be expressed in the following formula:

$$w_t = C_t \cdot 8.4\% \cdot V \cdot \rho, \tag{4-1}$$

were w_t is the water uptake in grams at time t, C_t is the moisture concentration, or water uptake percentage, at time t, V is the volume of the adhesive and ρ is the density.

Verification of the model has successfully been carried out through continuity, degeneracy and consistency testing. This is done by using respectively slight changes of input, extreme input values and different input values that should give the same result [72]. The simulation results for the continuity, degeneracy and consistency testing can be found in Table A.1-A.2 in Appendix A.2.

The model and method have been validated using results from a study by Bordes et al. [26]. In this study bulk specimens of Araldite 2015 with dimensions of 1.5 x 15 x 80 mm^3 were subjected to de-ionized water and salt water at 20, 40 and 60^{o}C. Gravimetric tests were conducted to determine the weight change of the specimens over time and create a Fickian model. The bulk specimens used in the study by Bordes et al. [26] were recreated in Abaqus using the same procedure as described above. This model was then used to simulate the water uptake of the bulk adhesive during the duration of the experiments. The water uptake w_t was determined as described above. In Figure 4.9 the numerical results have been plotted with the graph of the experimental results from Bordes et al. [26] as the background. In this graph the weight change ((w_t, the weight

at time t - initial weight, $w_0)/w_0$) as a percentage, is plotted versus $t^{1/2} \times S/V$, where t is the time in days, S the sample surface area and V the sample volume. As can be seen in the figure the numerical results were a close match to the experimental results from Bordes et al. [26]. The model and method are therefore considered to be validated.

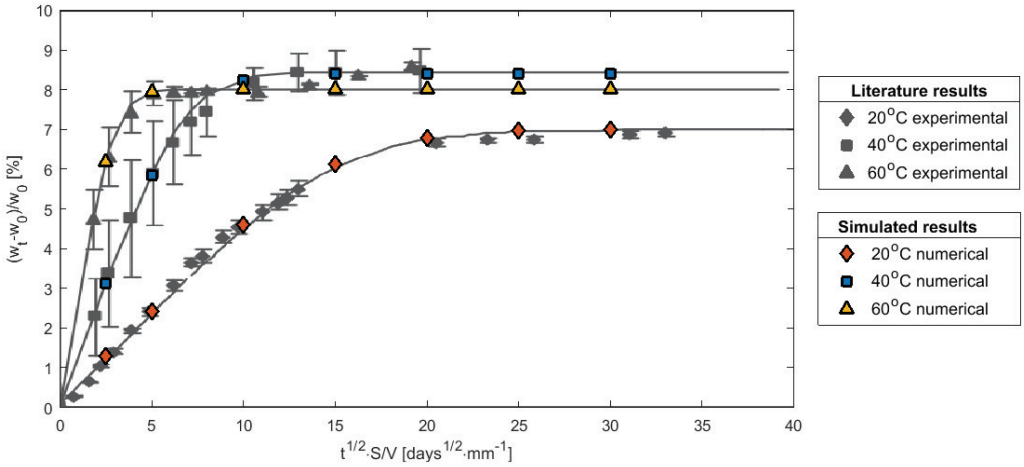

Figure 4.9: Comparison of numerical and experimental results for the water uptake of Araldite 2015 in de-ionized water. Experimental results from Bordes et al. [26]

4.1.2 Modeling results

Figure 4.10 presents the predicted moisture concentration and water uptake of the adhesive layer in the single lap joints over time for the experimental duration and until saturation. The actual values can be found in Table A.4 and Table A.5 in Appendix A.3.

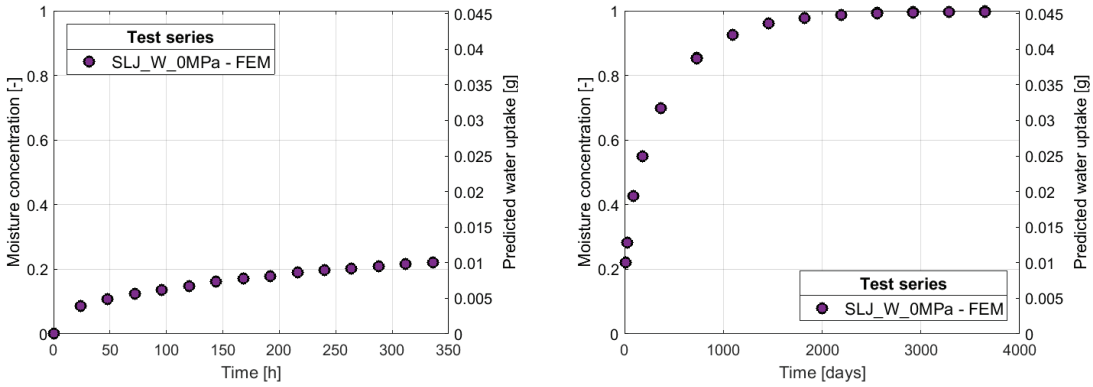

a) *Experimental duration* **b)** *Until saturation*

Figure 4.10: Moisture concentration and water uptake of the adhesive layer in 40^{o}C water over time predicted using FEM.

The figure shows that the total water uptake during the experimental period is relatively small when compared to the saturation water uptake. The water uptake is however large enough to be determined using the available scales. Based on these predictions it would not be realistic to perform experiments at full saturation for joints with this exact geometry since it would take many years for this state to be reached.

Figure 4.11 presents the predicted water uptake profiles over time for the experimental duration (Figure 4.11a) and until saturation (Figure 4.11b). These water uptake profiles show the progress of moisture absorption in the adhesive layer over time. The location that corresponds to these results is indicated by the black line in Figure 4.4a and the dotted lines in Figure 4.4b.

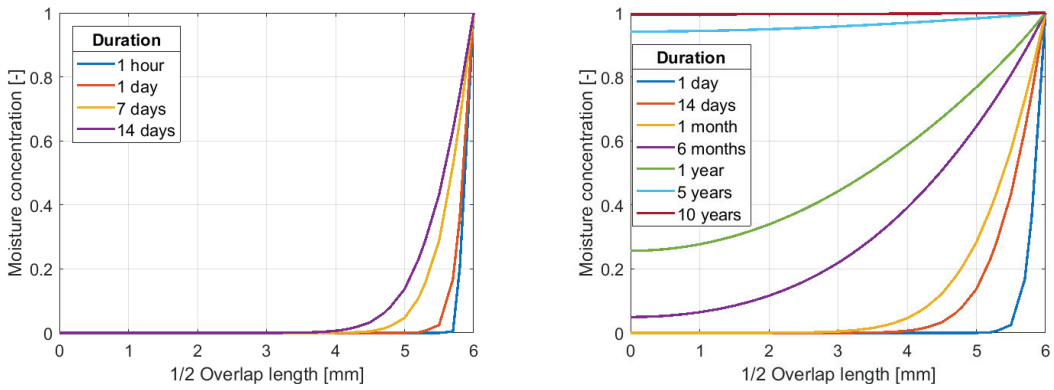

a) *Experimental duration* **b)** *Until saturation*

Figure 4.11: Water uptake profiles of the adhesive layer in 40°C water over time predicted using FEM.

Figure 4.11a shows that during the experiments most of the adhesive layer remains dry and that the water only penetrates the outer 2 mm of the adhesive. This suggests that the majority of the adhesive is unaffected by the moisture absorbed during the experimental work. Figure 4.11b shows that it takes a long time for the inner parts of the adhesive to reach saturation.

4.1.3 Experimental results

The experimental work was carried out with two sets of specimens. For the first set of specimens the adherends are coated with coating 1 while for the second coating 2 has been used. First the first set will be discussed, followed by the second.

First set of specimens

The first specimens that will be discussed are the specimens whose substrates have been coated with two layers of "Hammerite No.1 Rust Beater" - coating 1. The water uptake

of the unloaded specimens was determined immediately after specimens were removed from the water. For the loaded specimens the grips first needed to be removed. The mean ± the standard deviation of the water uptake results for the experimental duration of 14 days is presented in Figure 4.12. Table A.4 and Table A.6 in Appendix A.3 show the actual values for respectively the numerical results and the experimental results.

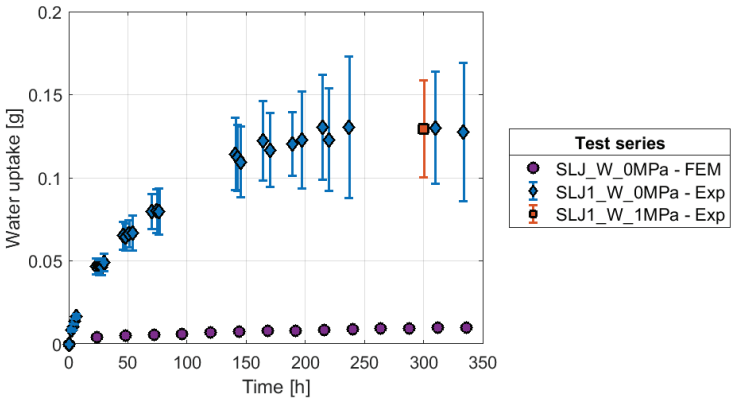

Figure 4.12: Water uptake of the single lap joints with coating 1 immersed in 40^{o}C distilled water.

Figure 4.12 shows that the simulated weight change is much lower than the measured weight change. It also shows that the specimens subjected to combined moisture and loading do not show a significant difference in water uptake when compared to the unloaded specimens. Up to a load level of 1 MPa and for a duration of 14 days the loading did therefore not seem to have an influence on the water uptake of the specimens. The experiments were however conducted with small sample sizes and the figure shows a large scatter in the water uptake measurements of both the loaded and unloaded specimens. Therefore, caution should be exercised when drawing conclusions.

Both the large experimental weight change and the scatter are attributed to the coating on the substrates. During the experiments it was found that this coating was also absorbing water, resulting in a weight increase that is not caused by the adhesive. Water bubbles were observed to be forming and growing under the coating (see Figure 4.13a) and the coating was found to detach at the edges when handling the specimens (see Figure 4.13a and Figure 4.13b). The subsequently damaged coating results in a weight loss between measurements and in rusting of the adherends. This rusting of the adherends also contaminated the distilled water. The scatter in the results is thought to come from the amount of coating not being uniform across specimens - see Table 4.2.

The water uptake of the coating is estimated by repeating the water uptake experiments under the same ageing conditions with plain steel plates with coating 1. The experimental data for these experiments is presented in Table A.7 in Appendix A.3. The mean amount of coating on the specimens (see Table 4.2) is used to predict the water uptake of coating 1 on the single lap joints. Figure 4.14a plots the mean and standard deviation

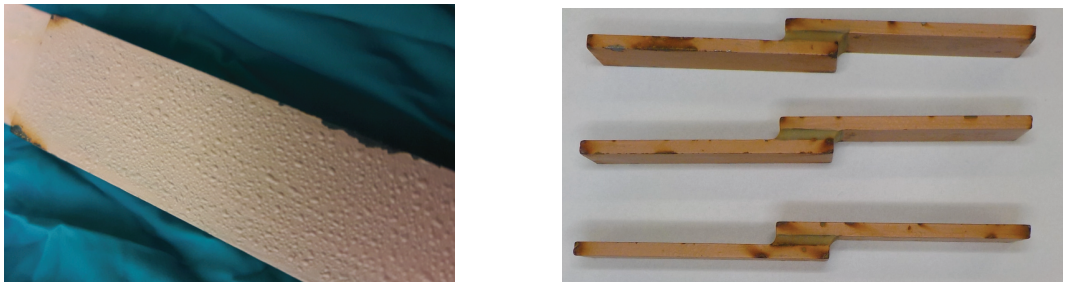

a) b)

Figure 4.13: Water bubbles, detachment of coating and rust on single lap joints with coating 1

of the predicted water uptake of coating 1 on the single lap joints with the results from Figure 4.12. The actual values for the predicted water uptake of coating 1 are listed in Table A.8 in Appendix A.3.

Specimen type	Amount of coating [g/m^2]
Single lap joint specimens	81.45 ± 17.46
Coated steel specimens	109.59 ± 2.45

Table 4.2: Amount of coating on the specimens with coating 1 in g/m^2.

Figure 4.14a shows that a large part of the measured water uptake is indeed caused by water absorption through the coating. It also shows that the gravimetric measurements for the coated plain steel specimens produced consistent results with little scatter. The "SLJ1_W_0MPa - Exp" and "Coating 1" results can be used to get a prediction for the water uptake of the adhesive layer in the single lap joints. This can be done by taking the mean of "SLJ1_W_0MPa - Exp" minus the mean of "Coating 1". Figure 4.14b compares the water uptake of the adhesive predicted using this method with the water uptake predicted using FEM. The values for the water uptake of the adhesive predicted using FEM can be found in Table A.9 in Appendix A.3.

Figure 4.14b shows that there are significant differences between the two predictions for the water uptake of the adhesive. The prediction that followed from experimental results starts with an increasing water uptake with a much larger slope. Over time the water uptake starts to slow down and around 200 hours it starts to decrease, suggesting that the adhesive is losing water. This suggestion of a weight loss after 200 hours is caused by the water uptake of "SLJ1_W_0MPa - Exp" reaching a plateau at around 200 hours while the weight of "Coating 1" is still increasing - see Figure 4.14a. The reason that "SLJ1_W_0MPa - Exp" reaches a plateau before "Coating 1" is the larger amount of coating on the coated steel specimens - see Table 4.2. With a thicker coating it will take longer until saturation, and thus a plateau, is reached.

One of the reasons for the larger slope of prediction based on the experimental work in Figure 4.14b is the diffusion coefficient that was used for the FEM model. This diffusion

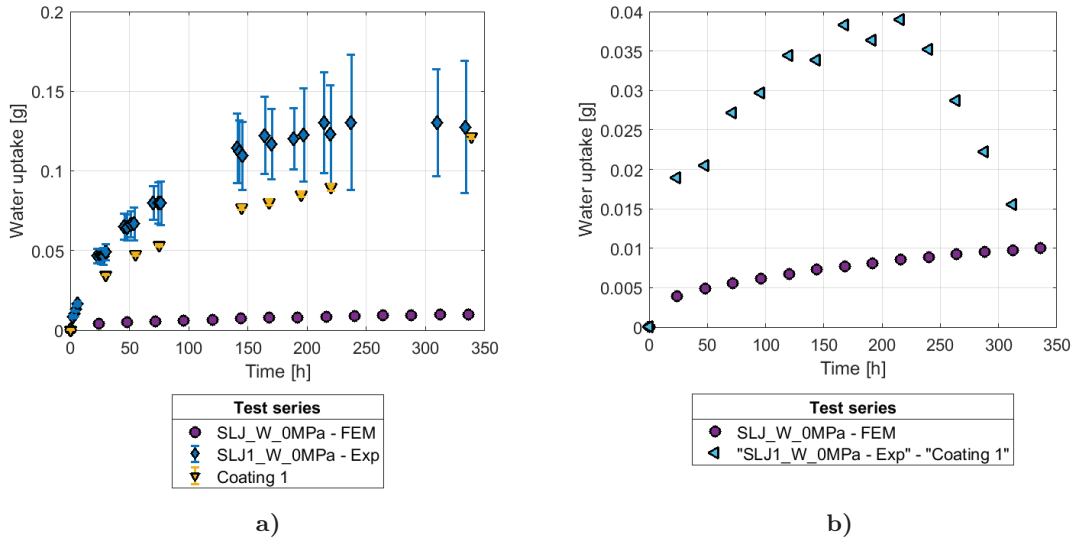

a) b)

Figure 4.14: Comparison of experimental and predicted water uptake for single lap joint specimens with coating 1. (a) Experimental results for the single lap joints with coating 1 with the predicted water uptake of coating 1. (b) Water uptake of the adhesive layer predicted using FEM and experimental results

coefficient comes form the work of Bordes et al. [26]. Figure 4.9 shows the experimental results that were used to derive the diffusion coefficient. The figure shows that there is a large amount of scatter in the gravimetric results for experiments at 40^{o}C. The diffusion coefficient is based on the mean value of the results. The diffusion coefficient of the adhesive layer in the single lap joints used for this thesis might just be large than this mean value. A second reason for the larger slope is the bubble forming on the coating of the adherends. The single lap joint specimens with coating 1 showed more and larger bubble forming than the coated steel specimens. This would mean that part of the water uptake in Figure 4.14b comes from water bubbles in the coating.

The finding that the coating of the adherends is responsible for the majority of the measured water uptake has implications for the comparison of the water uptake between the loaded and unloaded single lap joints. The clamping of the loaded single lap joints (see Figure 4.15) results in a lower amount of the coating (directly) being exposed to the environment. This could result in the water uptake of the coating on the loaded single lap joints being lower than for the unloaded specimens, resulting in a lower total water uptake. By visual inspection of the specimens it was found that the clamped areas showed signs of exposure to water. It was however not possible to quantify how the water uptake of clamped areas compared to unclamped areas. If the coating on the loaded specimens does indeed have a lower water uptake because of the clamping the comparison made in Figure 4.12 would give a distorted view of the influence of loading on water uptake.

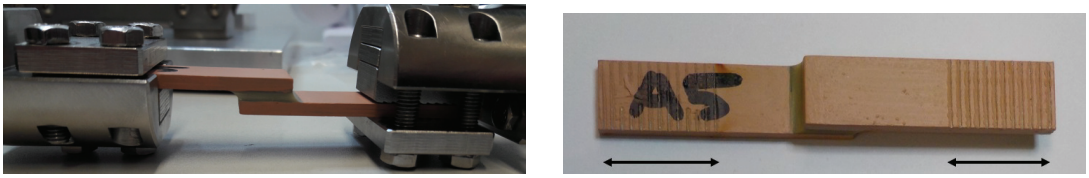

a) *Clamped specimen* **b)** *Clamped area indicated by arrow*

Figure 4.15: Clamping of single lap joints subjected to combined moisture and loading.

Second set of specimens

Due to the significant influence of the coating on the water uptake of the single lap joints, it was decided to coat the remaining specimens with an extra top coat - coating 2. This set of specimens had first been coated with two layers of "Hammerite No.1 Rust Beater", followed by four layers of "Hammerite Direct to Rust Metal Paint" - coating 2. The water uptake measurements presented for this set were all recorded at 10 minutes after removal from either the water bath or FNCT machine. Some of the unloaded specimens were only weighed at the end of the experiments instead of periodically during the experiments to give a better basis of comparison for the specimens that were subjected to combined moisture and loading. Figure 4.16 shows the mean ± standard deviation of the water uptake values measured during the experiments and predicted by the FEM. The actual values are presented in Table A.4 and Table A.10 in Appendix A.3.

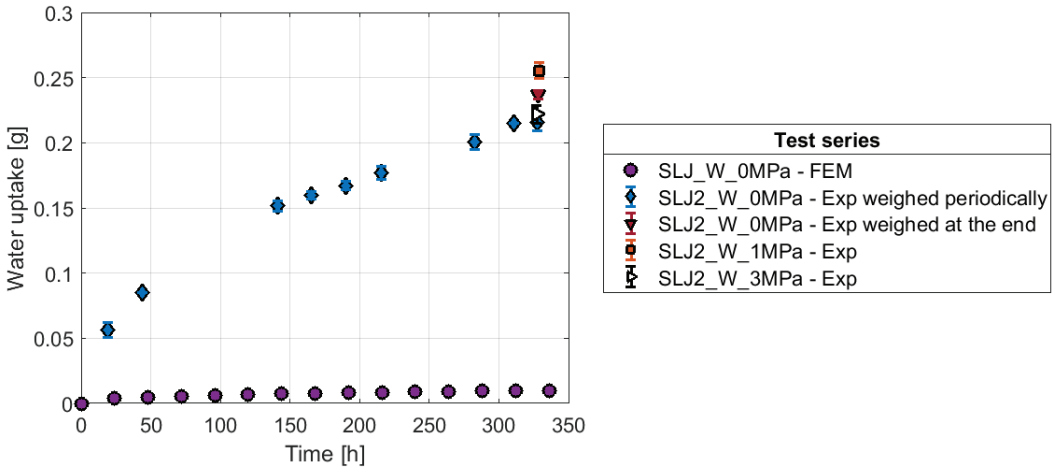

Figure 4.16: Water uptake of single lap joints with coating 2 immersed in 40^{o}C distilled water.

Figure 4.16 shows that the water uptake for the single lap joints with coating 2 is much more stable than for coating 1, with significantly lower standard deviations. The measured water uptake is however still much larger than predicted for the adhesive bond line using FEM. Table 4.3 compares the mean water uptake of the (un)loaded single lap joints with the uptake of the unloaded joints only weighed at the end as the baseline.

Test series	Water uptake [g]	Difference
SLJ1_W_0MPa - Exp weighed periodically	0.2155	-10%
SLJ1_W_0MPa - Exp weighed at the end	0.2371	-
SLJ1_W_1MPa - Exp	0.2554	+8%
SLJ1_W_3MPa - Exp	0.2219	-6%

Table 4.3: Comparison of the water uptake for loaded and unloaded single lap joints with coating 2 in 40^{o}C distilled water.

The larger water uptake of the unloaded single lap joints only weighed at the end when compared to the ones weighed periodically is as expected. This is caused by desorption of the water during the periods specimens are removed from the water. Table 4.3 also shows a larger water uptake for 1 MPa and a lower water uptake for 3 MPa. This implies that at low loading levels the water uptake is promoted while at higher load levels the loading hinders the water uptake. It should however be noted that small sample sizes were used and that problems with the coating and the clamps made the loaded single lap joints not representative, as will be discussed below.

The larger water uptake of single lap joints when compared to the simulated water uptake of the adhesive is again attributed to the coating on the adherend. Figure 4.17 shows a comparison between an unloaded specimen after the experiment is finished and a dry reference specimen. The unloaded specimen shows a significant amount of water bubbles and a slight change of colour of the coating. A significant change can be observed between the colour of the dry adhesive and the colour of the aged adhesive layer. These observations were consistent across all single lap joints with coating 2.

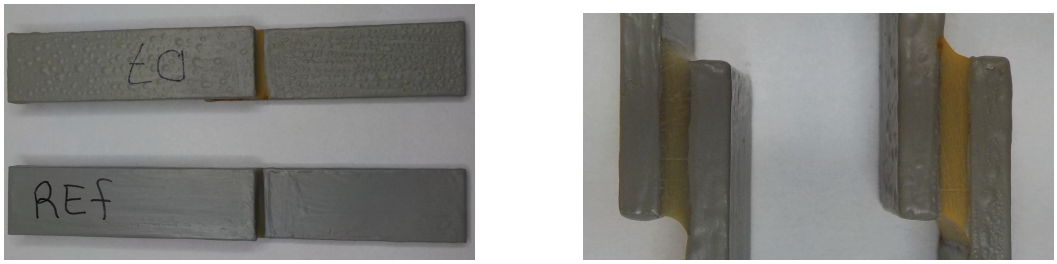

a) *Unloaded specimen (top) and reference specimen* **b)** *Reference specimen (left) and unloaded specimen*

Figure 4.17: Degradation of coating 2 on single lap joints after 14 days of exposure to 40^{o}C distilled water

The loaded single lap joints also experienced difficulties with the coating and clamping, which are thought to have contributed to these specimens not being representative for the influence of loading on the water uptake. Figure 4.18 shows that part of the coating remained stuck in the clamps upon removal of the specimen. This posed difficulties when trying to recover all loose parts of the coating and wiping every surface dry with a paper towel before weighing the joints. These two problems result in respectively an underestimate and an overestimate of the water uptake of the specimen.

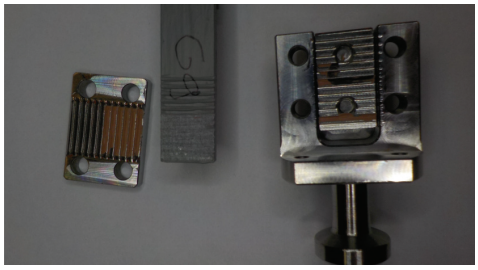

a)

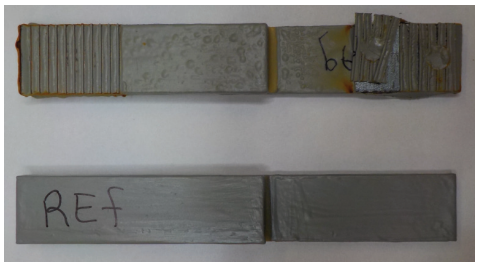

b) *Loaded specimen (top) and reference specimen*

Figure 4.18: Damaged coating on single lap joints with coating 2 caused by the clamping.

For this second series of experiments the water uptake of coating 2 on the single lap joints was predicted by coating plain steel adherends with coating 2 and immersing them in 40^{o}C distilled water for 14 days. The experimental data for these experiments is presented in Table A.8 in Appendix A.3. The water uptake of the coating on the single lap joints is again predicted by using the amount of coating on the specimens as presented in Table 4.4. The predicted water uptake of the coating is presented in Figure 4.19a. The actual values can be found in Table A.12 in Appendix A.3.

Specimen type	Amount of coating [g/m^2]
Single lap joint specimens	229.57 ± 23.41
Coated steel specimens	253.22 ± 18.76

Table 4.4: Amount of coating on the specimens with coating 2 in g/m^2.

Figure 4.19a shows that the predicted water uptake for the coating does indeed encompass a large part of the water uptake found for the single lap joint specimens. Figure 4.19b shows the simulated water uptake of the adhesive is compared the predicted water uptake of the adhesive that follows from "SLJ2_W_0MPa - Exp" minus "Coating 2". This graph is created by taking the mean of the two data sets and interpolating them so they can be subtracted. The values for the predicted water uptake of the adhesive can be found in Table A.13 in Appendix A.3.

Figure 4.19b shows that the water uptake of the adhesive predicted from the experimental work is much larger than the water uptake predicted using FEM. The results in Figure 4.19a are very consistent with little scatter and should therefore, despite the small sample sizes, give a good prediction. The difference in water uptake is thought to be caused by the diffusion coefficient that has been used. As explained above, this diffusion coefficient is based on the mean water uptake results by Bordes et al. [26]. Their water uptake data does however show a large amount of scatter. The water uptake of the adhesive layers in this thesis might simply be larger than what this mean diffusion coefficient predicts.

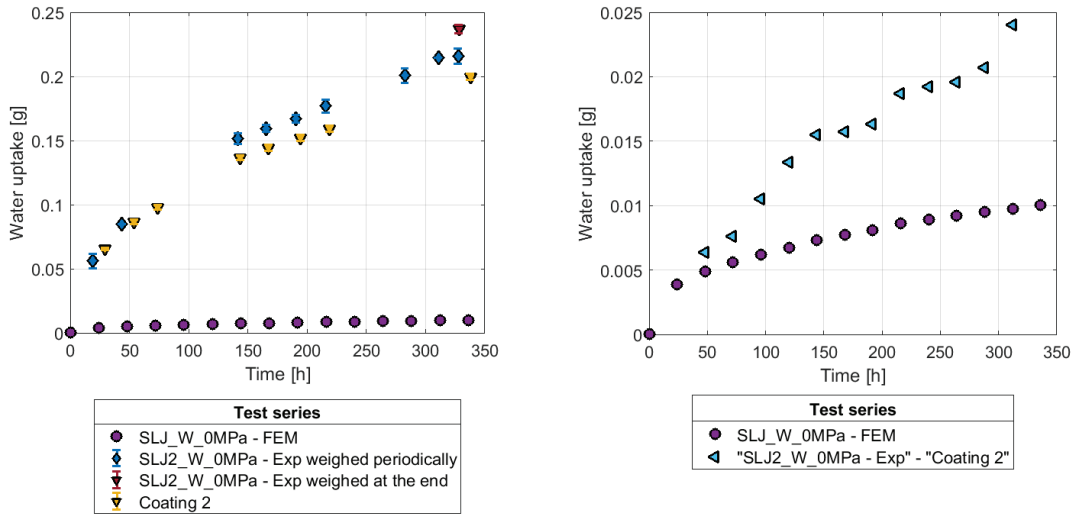

a) **b)**

Figure 4.19: Comparison of experimental and predicted water uptake for single lap joint specimens with coating 2. (a) Experimental results for the single lap joints with coating 1 with the predicted water uptake of coating 2. (b) Water uptake of the adhesive layer predicted using FEM and experimental results.

4.1.4 Conclusion and recommendations

The work carried out in this section aims to answer the following sub-research question:

> *How does the load level influence the water uptake of steel bonded joints subjected to hygrothermal and creep loadings?*

The results presented in this section were inconclusive on the effect of the load level on the water uptake. Experiments with coated steel specimens showed that the majority of the water uptake of the single lap joint specimens came from the coating. The water uptake of the adhesive was predicted using FEM and experimental results. There were however large differences between these two predictions. These differences have been attributed to the diffusion coefficient that was used for the FEM and to differences in the water uptake of the coating of the single lap joints and plain steel specimens.

It is recommended that the experiments are repeated using specimens with stainless steel adherends. This would eliminate the need for a protective coating and would mean the measured weight gain would come solely from the water uptake of the adhesive. It would be interesting to compare the water uptake in distilled water with the water uptake in seawater. For the specimens subjected to combined moisture and loading it would be desirable to use a larger sample size. If the same FNCT machine were to be used it is recommended to change the joint design so that joints can be gripped and loaded using

holes in the adherends, as per ASTM D2294 [73]. Experiments should preferably be longer than the two weeks to be able to observe a more long-term effect of the moisture and loading. For specimens tested under combined moisture and loading specimens should be tested for different time durations so it is possible to see the evolution is weigh gain/water uptake. Finally, it is recommended that gravimetric tests are performed using bulk adhesive specimens and that a new diffusion coefficient is derived to see how it compares to the one used in this study.

4.2 Creep

This section will present and discuss the experimental and modeling creep results for the ageing of single lap joint specimens at elevated temperatures in water and air with loading as described in Chapter 3. The work has been carried out to answer the following sub-research question:

> *How do load level and (hygro)thermal conditions influence the creep behaviour of loaded steel bonded joints?*

First the experimental results will be presented. This will be followed by the modeling results. Finally the sub-research question will be answered and recommendations will be given.

4.2.1 Experimental results

This section will present the experimental results for the creep experiments. The focus of the section will be on the experimental results of the single lap joints with coating 2. The single lap joints with coating 1 are not included in the analysis because the rusting of the adherends resulted in contamination of the water. The results for the single lap joints with coating 1 can be found in Section B.1 in Appendix B.

Figure 4.20 - 4.21d present the creep results for the single lap joints with coating 2 loaded at 1 MPa, 3 MPa, 6 MPa and 9 MPa. The results for SLJ2_A_9MPa and SLJ2_W_9MPa are not visible in these graphs due to the short duration of these experiments. They are however clearly depcited in Figure 4.21d. The actual creep strain values are listed in Table B.11 - B.15 in Appendix B. Whenever possible the results are presented as the mean $\pm$ the standard deviation of the experimental data. The creep strain presented in the graphs is from the moment the applied load reached the set value. This has been done because it was not possible to apply the desired load instantaneously or control the load sequence up till the desired magnitude had been reached. The strain recorded before the load reached the set value can be found in Figure B.3 - B.9 and Table B.2 - B.8 in Appendix B.

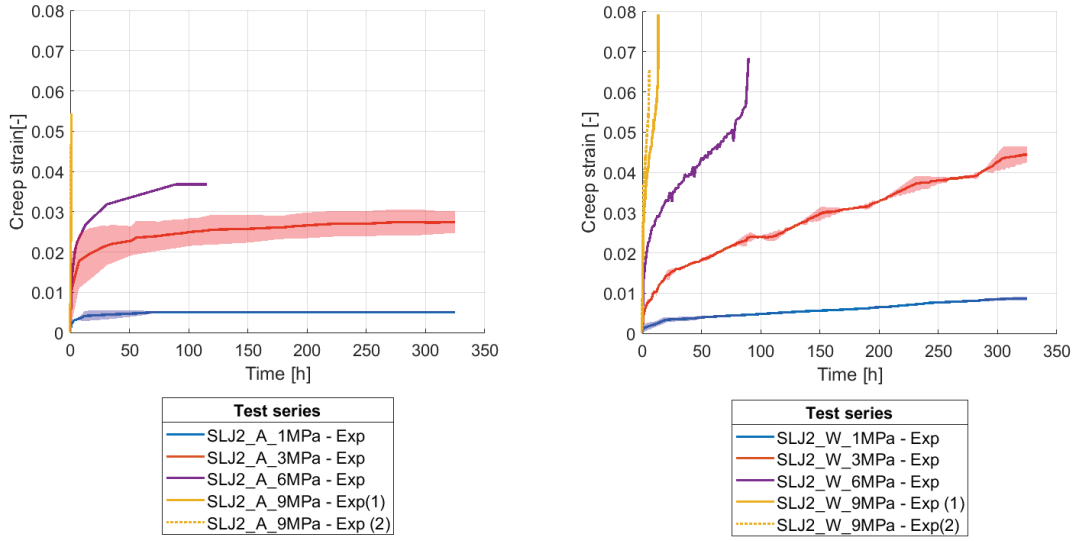

a) *Air* **b)** *Water*

Figure 4.20: Creep strain for specimens subjected to loads of 1 MPa, 3 MPa, 6 MPa and 9 MPa.

Figures 4.20a and 4.20b show that an increase in the load level results in a larger instantaneous creep strain, ε_0, and a larger strain rate, $\dot{\varepsilon}$. Table 4.5 presents the instantaneous strains and strain rates for these figures.

Test series	Instantaneous strain [-]	Strain rate [h^{-1}]
SLJ2_A_1MPa	$2.060 \pm 0.701 \times 10^{-3}$	3.175×10^{-8}
SLJ2_A_3MPa	$1.053 \pm 0.851 \times 10^{-2}$	1.452×10^{-5}
SLJ2_A_6MPa	1.150×10^{-2}	5.821×10^{-5}
SLJ2_A_9MPa	3.384×10^{-2} / 3.267×10^{-2}	-
SLJ2_W_1MPa	$1.146 \pm 1.216 \times 10^{-3}$	1.802×10^{-5}
SLJ2_W_3MPa	$4.272 \pm 0.226 \times 10^{-3}$	9.726×10^{-5}
SLJ2_W_6MPa	1.291×10^{-2}	3.394×10^{-4}
SLJ2_W_9MPa	3.267×10^{-2} / 2.070×10^{-2}	4.472×10^{-3} / 2.402×10^{-3}

Table 4.5: Instantaneous strain and strain rate for specimens loaded at 1 MPa, 3 MPa, 6 MPa and 9 MPa in air and distilled water

Table 4.5 shows that the instantaneous strain is not proportional to the load level, it does however increase with an increase in the load level. For single lap joints loaded in water the instantaneous strain is generally lower than the one for the same load level in air. The strain rates show that the water has a significant effect on the viscoelastic response. Single lap joints loaded in water experience a much larger strain rate than the ones loaded in air at the same load level. For specimens loaded at 1 MPa in air the strain rate is very low: no significant amount of secondary creep is observed.

Figures 4.21a - 4.21d compare the creep strains of specimens loaded in air and in water at the same load level. For load levels of 1 MPa and 3 MPa these figures show a larger instantaneous creep strain for the specimens loaded in air than for the specimens loaded in water. Once the creep reaches the secondary creep stage the creep of the specimens tested in water starts to become larger than the creep of the specimens tested in air. This is due to a higher strain rate $\dot{\varepsilon}$. For specimens loaded at 9 MPa specimens loaded in air failed sooner than specimens loaded in water. This suggests that the influence of moisture on the creep response is dependent on the percentage of moisture in the adhesive. At the initial stages of water absorption (low moisture percentage) creep is suppressed while at later stages (high(er) moisture percentage) creep is promoted.

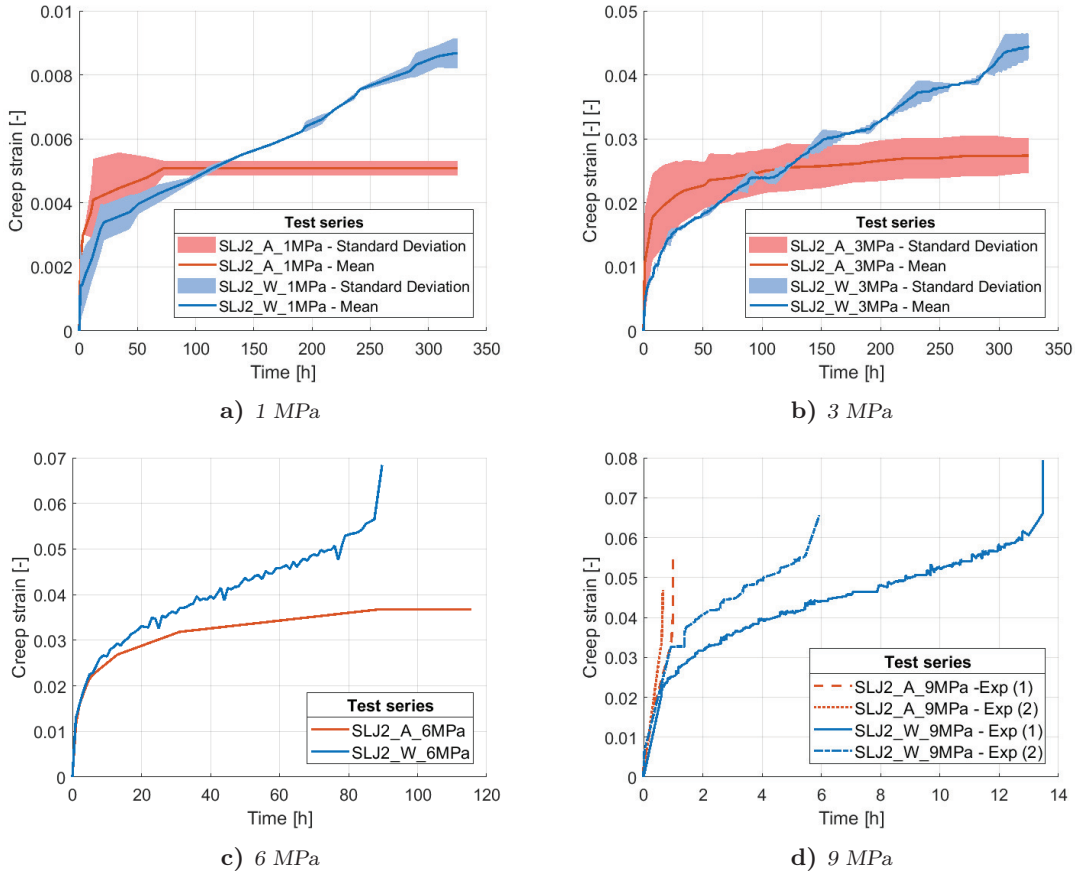

a) *1 MPa* **b)** *3 MPa*

c) *6 MPa* **d)** *9 MPa*

Figure 4.21: Creep strain for specimens loaded at 1 MPa, 3 MPa, 6 MPa and 9 MPa.

No mention of this phenomenon has been found in literature. A similar trend can however possibly be observed in some of the creep deformation of single lap joints presented by Springer & Wang [17]. Creep experiments are normally conducted on much larger time scales and the creep response might not be measured at time durations this short, as for example in Gellert & Turley [11]. On top of that, the influence of moisture on the creep response is often determined using specimens that have been subjected to moisture

for a predefined time or until saturation before testing [6, 46, 50–52], leading to testing conditions that are different than in this thesis.

Literature does however give a possible explanation for the phenomenon. Dean's [40] results suggest that there are two relaxation processes contributing to the creep deformation of their epoxy adhesive. The first of these processes is the glass-to-rubber relaxation mechanism, which contributes at long creep times. At short creep times they found that the deformation was dominated by a different mechanism. The magnitude of this mechanism might be sensitive to the moisture concentration in the adhesive [40]. Other studies have also reported the presence of a small relaxation process with a magnitude sensitive to moisture concentration, referred to as ω-relaxation [40, 74]. A third relaxation mode that can be identified is the β-relaxation mode, which is associated with the motions of small units of the macromolecular chains [74].

Discussions related to water diffusion mode and epoxy-water interactions are mainly done using the following two approaches. The first approach is based on the bonding between water molecules and macromolecules, which could reduce the molecular mobility at short distances in the epoxy resin and thereby decrease the ω- and β-relaxations. The second approach assumes that the water diffusing in the epoxy resin resides in the free volume of the material and acts as a plasticizer, thereby amplifying the ω- and β-relaxations [74]. The behaviour found in this thesis suggests that both of these processes might be at play. Initially, when the water is starting to diffuse into the adhesive the bonding of the water molecules and macromolecules decreases the relaxations, resulting in a creep deformation that is initially lower for specimens tested in water than for specimens tested in air. As the water continues to diffuse into the adhesive the plasticizing effect of the water residing in the free volume becomes stronger, resulting in a larger strain rate for specimens tested in water than for specimens tested in air.

4.2.2 Modeling results

As discussed in Section 2.3 the first step in modeling the viscoelastic behaviour is to determine whether the measured response is linear or nonlinear. To do this isochronals have been constructed from the creep curves. Figure 4.22a and Figure 4.22b show the isochronals for respectively the specimens loaded in air and water. The actual data can be found in Table B.9 and Table B.10 in Appendix B.

The isochronals show that the creep response is not linear for the range of loads used during the experiments and that a nonlinear viscoelastic model is required. The creep behaviour is modeled using the simplest model that gave a satisfactory simulation, which was the three-element solid model (see Figure 4.23). In this model the linear elements will be substituted with nonlinear elements.

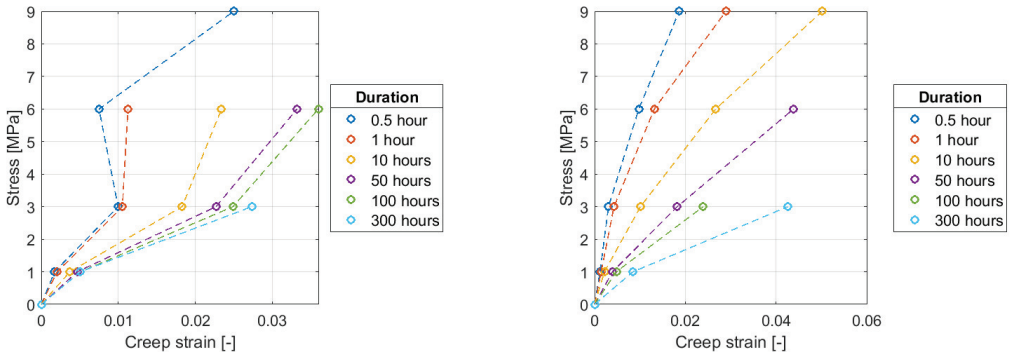

a) *Air* **b)** *Water*

Figure 4.22: Isochronous creep curves

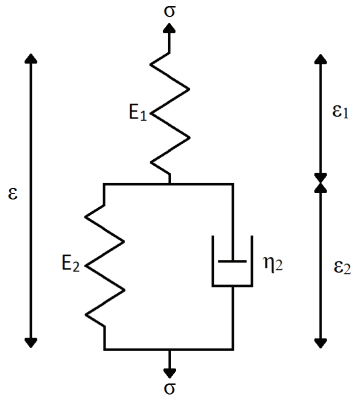

Figure 4.23: Three-element solid model

The constitutive equation for the this model can be found to be as follows using the constitutive equations of the spring ($\sigma = E \cdot \varepsilon_1$) and the Kelvin-Voigt model (2-5) (see Section 2.3) [5]:

$$\sigma + \frac{\eta_2}{E_1 + E_2}\dot{\sigma} = \frac{E_1 E_2}{E_1 + E_2}\varepsilon + \frac{E_1 \eta_2}{E_1 + E_2}\dot{\varepsilon} \tag{4-2}$$

First, non-linear regression was used to estimate the parameters E_1, E_2 and η_2 of the three-element solid model based on the experimental data. Time was assumed as an independent variable and the creep strain ϵ_c was assumed as a dependent variable. Table 4.6 presents the results for the different load levels and environment. Figure 4.24 compares the experimental results with the results obtained using the three-element-solid model with the parameters from Table 4.6. For the calculation of the parameters for 9 MPa the mean creep strain up till the moment the first specimen starts to experience tertiary creep has been used, see Table B.16 in Appendix B.

		η_2	E_1	E_2	R^2
Air	1 MPa	2.1960×10^3	558.7076	291.6049	0.9771
	3 MPa	4.8447×10^3	237.2689	191.2114	0.9845
	6 MPa	2.7302×10^3	485.7719	222.2175	0.9918
	9 MPa	181.4632	4.8243×10^3	28.1336	0.9999
Water	1 MPa	4.2580×10^4	393.6629	29.7576	0.9847
	3 MPa	1.8666×10^4	297.9413	32.6847	0.9889
	6 MPa	6.5642×10^3	342.1374	98.704	0.9814
	9 MPa	189.429	4.2468×10^3	165.6324	0.9915

Table 4.6: Parameters of the three-element-solid model for specimens with the second coating system

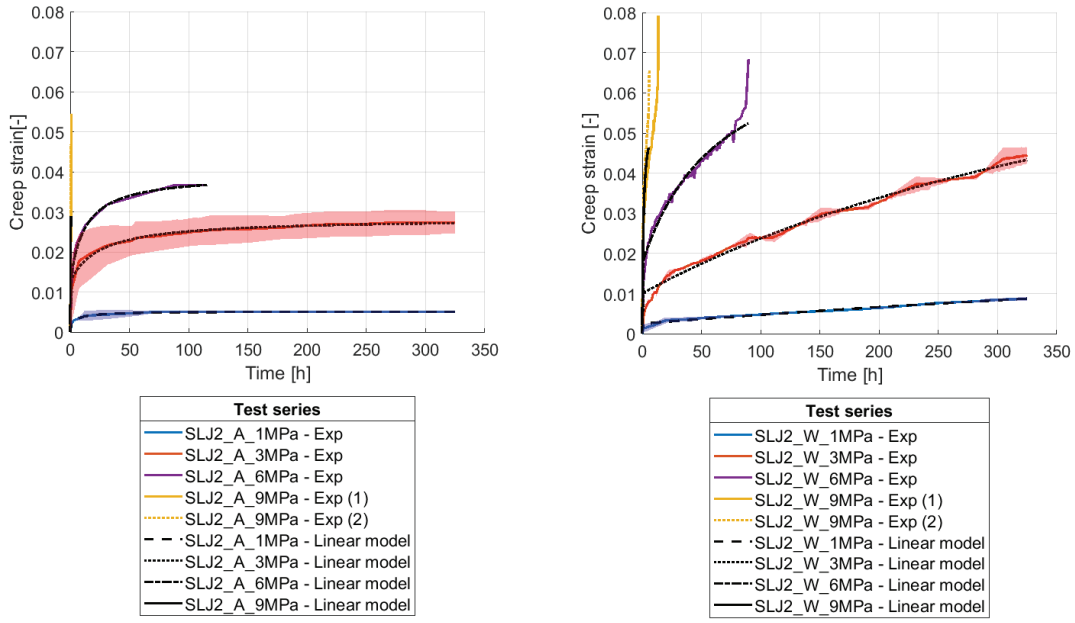

a) *Air* **b)** *Water*

Figure 4.24: Experimental creep strain and creep strain simulated using linear three element solid models for specimens subjected to loads of 1 MPa, 3 MPa, 6 MPa and 9 MPa

The next step in the model is to determine the parameters E_1, E_2 and η_2 as a function of stress. This is done by using the results in Table 4.6. The level of stress is assumed to be an independent variable and $E_1(\sigma)$, $E_2(\sigma)$ and $\eta_2(\sigma)$ are assumed to be the dependent variables. This results in equations (4-3) - (4-5) with coefficients a_i. The values for coefficients a_i for creep in air and in water are presented in respectively Table 4.7 and Table 4.8.

$$\eta_2(\sigma) = a_1\sigma^2 + a_2\sigma + a_3 \tag{4-3}$$
$$E_1(\sigma) = a_4\sigma^2 + a_5\sigma + a_6 \tag{4-4}$$
$$E_2(\sigma) = a_7\sigma^2 + a_8\sigma + a_9 \tag{4-5}$$

a_1	a_2	a_3
-166.89	1338.2	1430.5
a_4	a_5	a_6
160.46	-1108.3	1696.3
a_7	a_8	a_9
-3.2999	5.1525	263.59

Table 4.7: Coefficient values a_i for creep in air

a_1	a_2	a_3
791.84	-12955	53397
a_4	a_5	a_6
138.94	-949.47	1418.9
a_7	a_8	a_9
1.5683	2.1402	21.735

Table 4.8: Coefficient values a_i for creep in water

Figures 4.25-4.27 show the changes in the values of the parameters η_2, E_1 and E_2 as a function of stress level. The regression dependencies of the parameters is presented by the red line. The dashed lines indicate the values obtained by extrapolation.

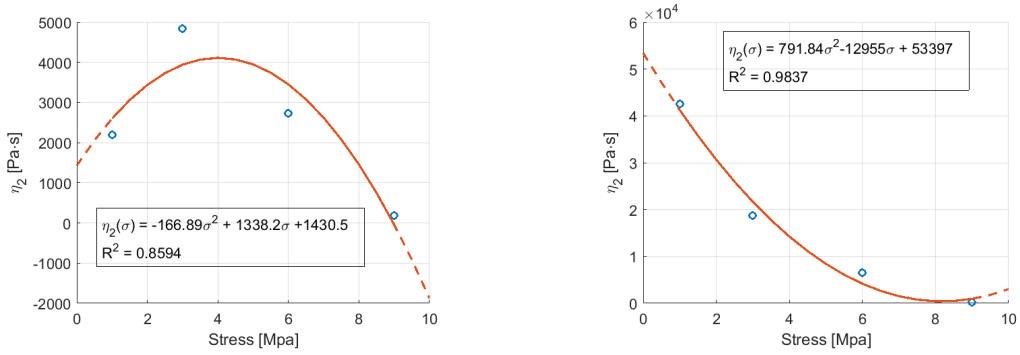

a) *Air* **b)** *Water*

Figure 4.25: Plot of regression dependency for the coefficient of viscosity $\eta_2(\sigma)$.

Figure 4.25a shows that it was not possible to achieve a good fit for $\eta_2(\sigma)$ for specimens tested in air. The current fit results in enormous relative errors, especially for the η_2 for 9 MPa. The η_2 values for 3 MPa, 6 MPa and 9 MPa in Figure 4.25a and all results in Figure 4.25b show that an increase in load results in a decrease in η_2. This is in line with what would be expected when looking at the response of the viscous dashpot to a load σ: $\varepsilon(t) = \sigma t/\eta$. A smaller value of η will result in the same value of ε being reached in a shorter amount of time. The unexpected result for the η_2 value for specimens loaded in air at 1 MPa is attributed to the load level being so low that there was no secondary creep.

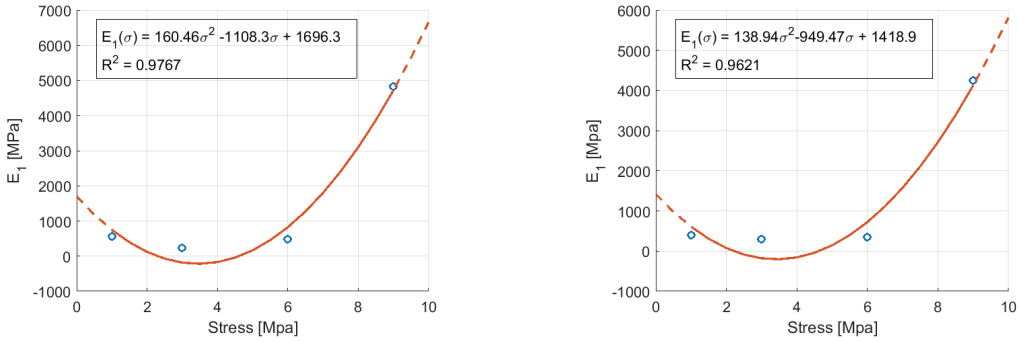

a) *Air* **b)** *Water*

Figure 4.26: Plot of regression dependency for modulus of elasticity $E_1(\sigma)$.

Figure 4.26 shows that for 1 MPa, 3 MPa and 6 MPa the values for E_1 are the same order of magnitude, for 9 MPa the values are however an order of magnitude larger. The fit that was achieved is reasonably good. The fit is however dominated by the E_1 value for 9 MPa and gives an enormous relative error for the E_1 for 3 MPa - it gives a negative value instead of a positive one. The results suggest that it might not be possible to simulate the creep behaviour for this wide range of load levels (1 MPa - 9 MPa) with one model: The response for E_1 might be too different for the load level of 9 MPa to be fitted in one function $E_1(\sigma)$. A better result would have been achieved by taking a constant value for the low levels and using an exponential one for higher load levels.

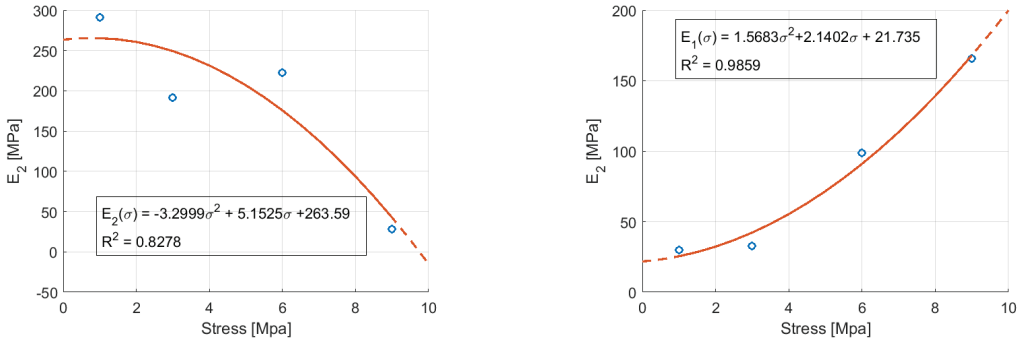

a) *Air* **b)** *Water*

Figure 4.27: Plot of regression dependency for modulus of elasticity $E_2(\sigma)$.

Figure 4.27 shows almost opposite behaviour for $E_2(\sigma)$ for air and water. For specimens tested in air an increase in load level leads to a decrease in E_2 while for specimens tested in water an increase was observed. This suggests that the water causes a fundamental change in the behaviour of the spring corresponding to E_2 in the three-element solid model. For the E_2 values of specimens tested in air in Figure 4.27a the obtained fit is not satisfactory. When looking at the downward trend it seems like the value for either

3 MPa or 6 MPa is off, making a good fit impossible. Looking back on the experimental results in Section 4.2.1 it is thought to be most likely caused by the 6 MPa results. These results showed behaviour different from the other loads and, unlike the 3 MPa results, come from only one specimen.

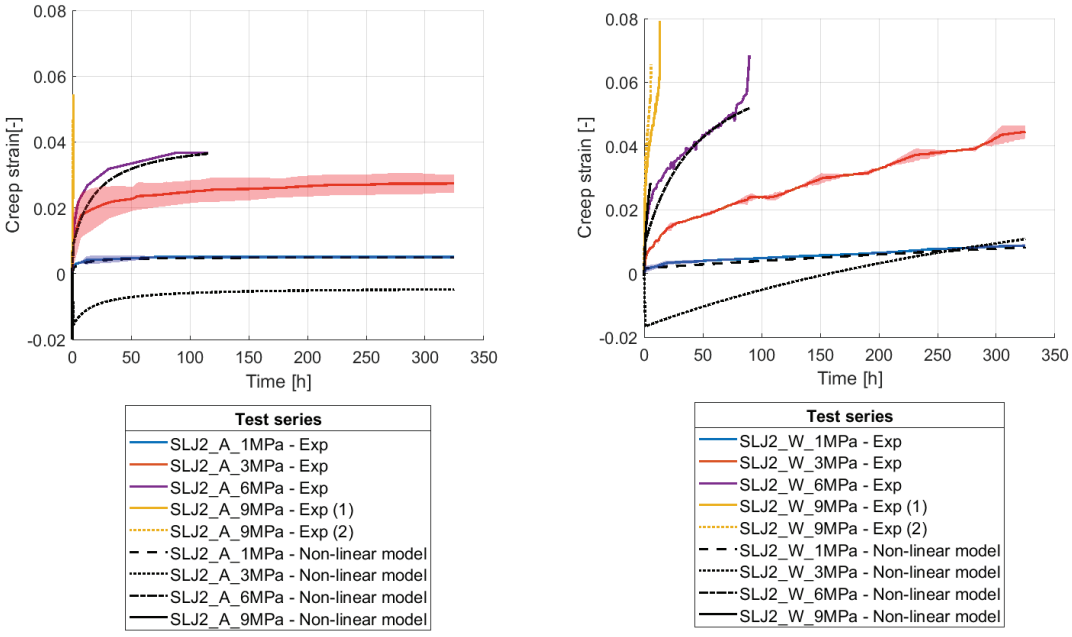

a) *Air* **b)** *Water*

Figure 4.28: Experimental creep strain and creep strain simulated using non-linear three element solid model for specimens subjected to loads of 1 MPa, 3 MPa, 6 MPa and 9 MPa

The coefficients in Table 4.7 and 4.8 have been used with Equations (4-3) - (4-5) to simulate the creep behaviour of the specimens loaded in air and in water. The results for this simulation are plotted together with the experimental results in Figure 4.28. As can be seen in this figure it was not possible to get a good representation of the experimental results across the different load levels by replacing the linear elements in the three-element-solid model with non-linear elements. The simulation of 1 MPa and 6 MPa gives a reasonable representation but for 3 MPa and 9 MPa the simulation is way off. For 3 MPa and 9 MPa in air and for 3 MPa in water the model gives a negative creep strain. For the 3 MPa results this is caused by the E_1 being negative (see Figure 4.26) while for the 9 MPa in air results the η_2 value is negative (see Figure 4.25). The fits that were used try to minimize the absolute error over the range of data points. This results in one value dominating the whole fit, leading to enormous relative errors in the other data points. Ultimately, this resulted in a non-linear model that can not accurately model the creep response. Figure 4.24 and Table 4.6 showed that it is possible to use a three-element-solid model to model the creep strain over a range of loads in air

and in water. The unsuccessful representation of the creep response by the non-linear model is therefore attributed to the creep response of the specimens being too different across the load range 1 MPa - 9 MPa to fit the behaviour in a single creep model.

4.2.3 Conclusion and recommendations

The aim of this chapter was to answer the following research question:

> *How do load level and (hygro)thermal conditions influence the creep behaviour of loaded steel bonded joints?*

It was found that both the load level and the environment have a large influence on the creep behaviour of metal-to-metal bonds. An increase in load level results in a larger elastic portion of the creep strain and a higher strain rate. For the specimens loaded in air the load levels were mostly found to be too low for the time frame under consideration, resulting in a very low amount of secondary creep. In general, the specimens loaded in water experienced a larger amount of creep than the specimens loaded in air.

When comparing the creep strain results for specimens loaded in air and in water it was found that the creep response is suppressed in the initial stages of moisture absorption while it is promoted at later stages. The suppression of the creep response is explained by the water molecules bonding to the macromolecules. This decreases the relaxations and results in a lower creep deformation. As the water continues to diffuse the plasticizing effect of the water residing in the free volume becomes stronger, resulting in a larger strain rate for specimens tested in water than for specimens tested in air.

The section showed that it was possible to use a three-element-solid model to model the creep strain over a range of loads in air and in water. The attempt to construct a nonlinear model using the non-linear regression results in Table 4.6 was however unsuccessful. This is attributed to the creep response of the specimens being too different across the load range 1 MPa - 9 MPa to fit the behaviour in a single creep model using simple relations.

It is recommended that the experiments are repeated using a joint design as described in ASTM D2294 [73]. By using holes to grip and load the specimens it is impossible for the specimens to slip during the experiments. Future experiments should preferably be longer than two weeks to observe the long term behaviour of the loaded metal-to-metal joints in water and air. It is also recommended to use a larger sample size. If it is possible to conduct long term experiments the testing temperature should be reduced so that the glass transition temperature of the adhesive is not reached in any of the testing configurations. It would be interesting to compare the creep of specimens loaded in distilled water with specimens loaded in seawater. It was not possible to control or measure the humidity in the testing environment for the joints tested in air. It would be desirable to be able to control the relative humidity to ensure the composition of the environment remains constant [76]. For future experiments it would be desirable to start

by testing the joints at a wide range of loads in the (presumably) harshest environment until failure. By doing this it is possible to test at load levels that are appropriate for the duration of the experiment, ensuring that loads are not too low (low amount of creep observed) or too high (failure of specimens before the end of experiment). By testing the joints at load levels in the same range it should be possible to successfully develop a nonlinear creep model using the approach described in this chapter.

4.3 Residual lap shear strength and stiffness

This section aims to answer the following sub-research question:

> *How do the creep and (hygro)thermal loadings influence the residual strength and stiffness of steel bonded joints?*

The section will start by presenting the initial strength of the lap shear joints. This will be followed by the residual strength results for the first and second set of specimens. Finally the sub-research question will be answered and recommendations will be given. The stiffnesses reported in this section are determined as the slope of the initial elastic region of the force-displacement curve.

4.3.1 Initial lap shear strength and stiffness

As mentioned in Chapter 3 the initial lap shear strength of the metal-to-metal bonds has been determined two times, once at DASML and once at BAM. This was followed by a retest at DASML after a few months. This section will present and discuss the fracture surfaces, lap shear strengths and stiffnesses that followed from these tensile tests.

Figure 4.29 presents typical failure modes that can be expected in metal-to-metal bonds. With adhesive failure failure occurs at the interface between adherend and adhesive, as opposed to cohesive failure where failure occurs within the adhesive. With thin-layer cohesive failure the failure occurs within the adhesive but very close to the adhesive-adherend interface. This failure mode is characterized by one substrate interface having a light dusting of adhesive while the other has a thick layer of adhesive left [75].

Figure 4.29: Typical failure modes for metal-to-metal bonds. From: [75]

The first results that will be presented are for the single lap joints in test series SLJ_Ref1. The tensile testing for this test series was conducted at the DASML. Figure 4.30 shows the fracture surfaces for these specimens. Table 4.9 presents the strength, stiffness and a

description of the failure modes for these specimens. Figure 4.33 compares the strength and stiffness of the SLJ_Ref1 specimens with the other sets of reference specimens.

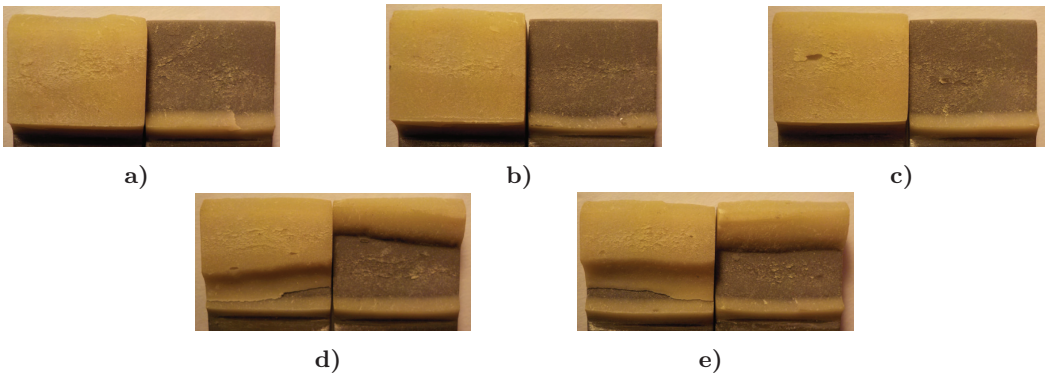

Figure 4.30: Fracture surfaces for reference specimens SLJ_Ref1 tested at DASML.

Test series	Strength [MPa]	Stiffness [N/mm]	Failure mode
SLJ_Ref1 - a	22	19 775	Thin-layer cohesive failure
SLJ_Ref1 - b	19.5	18 825	Thin-layer cohesive failure
SLJ_Ref1 - c	19.8	19 069	Thin-layer cohesive failure
SLJ_Ref1 - d	19.9	17 497	Mixed mode: Thin-layer cohesive failure with fracture jumping from one interface to the other
SLJ_Ref1 - e	19.7	19 244	Mixed mode: Thin-layer cohesive failure with fracture jumping from one interface to the other

Table 4.9: Strength, stiffness and description of failure mode for reference specimens SLJ_Ref1 tested at DASML.

Figure 4.30a - 4.30c show thin-layer cohesive failure. Cracks started to form in the middle of the fillet before quickly moving to and propagating near the interface. In Figure 4.30d and 4.30e the fracture jumped from one interface to the other shortly before failure of the specimen, resulting in a mixed failure mode. It is hypothesized that this failure behaviour has been caused by a slight misalignment resulting in the clamps being positioned parallel but either placed too far apart or to close to each other. Since these specimens failed differently they have been excluded from the determination of the reference strength of the single lap joints. With the exception of SLJ_Ref1-a the reported strengths are all relatively close to each other. There is a bit more scatter in the stiffness results but they are still considered to be in the same range.

Initially, the results from SLJ_Ref1 were used as a baseline for the initial lap shear strength and stiffness. Comparing the first test results from Section 4.3.2 tested at BAM to this baseline did however show an unexpectedly large strength/stiffness reduction. Since the testing equipment at DASML and BAM is not identical it was decided to test a second round of unconditioned specimens at the BAM to see if the results from SLJ_Ref1 could be replicated. Figure 4.31 shows the fracture surfaces for the reference specimens in test series SLJ_Ref2 tested at the BAM. Table 4.10 presents the strength,

stiffness and a description of the failure modes for these specimens. Figure 4.33 compares the strength and stiffness of the SLJ_Ref2 specimens with the other sets of reference specimens.

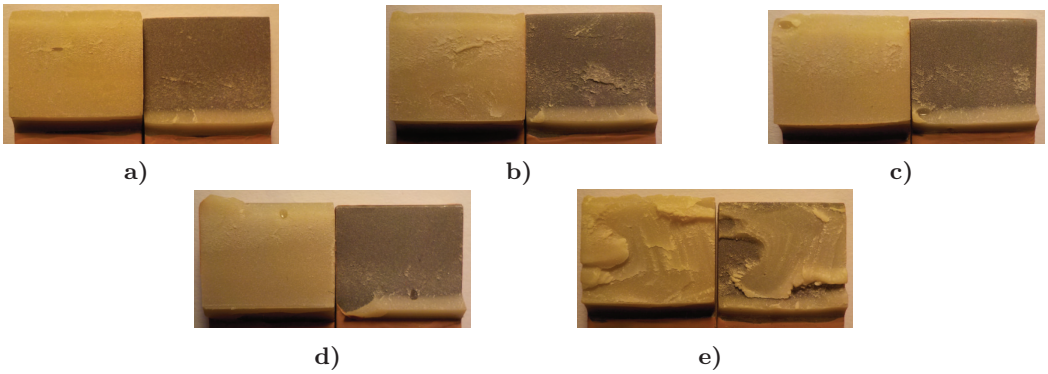

Figure 4.31: Fracture surfaces for reference specimens SLJ_Ref2 tested at BAM.

Test series	Strength [MPa]	Stiffness [N/mm]	Failure mode
SLJ_Ref2 - a	18.6	7 429	Thin-layer cohesive failure
SLJ_Ref2 - b	15.2	7 481	Thin-layer cohesive failure
SLJ_Ref2 - c	16.9	7 977	Thin-layer cohesive failure
SLJ_Ref2 - d	18.1	8 881	Thin-layer cohesive failure
SLJ_Ref2 - e	15.1	8 272	Mixed mode: (Thin-layer) cohesive failure with tearing of the adhesive layer

Table 4.10: Strength, stiffness and description of failure mode for reference specimens SLJ_Ref2 tested at BAM.

Figure 4.31a - 4.31d show thin-layer cohesive failure. The fracture surface in Figure 4.31e shows a different failure mechanism and is not included in the determination of the initial lap shear strength. This specimen shows tearing of the adhesive layer as opposed to the relatively smooth crack growth of the other specimens. The different failure behaviour is attributed to an additional force introduced by a misalignment of the clamps resulting in them not being parallel. This results in the adhesive being loaded in two directions: the desired in plane shear loading and a type of cleavage loading the adhesive layer at an angle. There is a relatively large amount of scatter in the strength and stiffness results reported for test series SLJ_Ref2.

Both the strength and stiffness results of SLJ_Ref1 and SLJ_Ref2 are distinctively different. SLJ_Ref2 consistently shows lower strengths and stiffnesses. The test series did however use different testing equipment and different durations of storage before testing. Test series SLJ_Ref1 was tested within a day after manufacturing was finished while SLJ_Ref2 was stored under ambient conditions for a month and a half. As mentioned in Chapter 2, Dean [40] found that specimens stored under ambient conditions experienced a larger creep strain than specimens stored in a desiccator. It is possible that the humidity of the air affected the adhesive layer, resulting in a lower strength and stiffness.

To test this hypothesis the tensile testing at the DASML has been repeated with test series SLJ_Ref3 which has been stored under ambient conditions for eight months.

Figure 4.32 shows the fracture surfaces for test series SLJ_Ref3. Table 4.11 presents the strength, stiffness and a description of the failure modes for these specimens. Figure 4.33 compares the strength and stiffness of the SLJ_Ref3 specimens with the other sets of reference specimens.

a) **b)**

Figure 4.32: Fracture surfaces for reference specimens SLJ_Ref2 tested at BAM.

Test series	Strength [MPa]	Stiffness [N/mm]	Failure mode
SLJ_Ref3 - a	16.9	20 057	Thin layer cohesive failure
SLJ_Ref3 - b	18.8	20 638	Thin layer cohesive failure

Table 4.11: Strength, stiffness and description of failure mode for reference specimens SLJ_Ref3 tested at BAM.

The fracture surfaces in Figure 4.32 show thin-layer cohesive failure. With two samples the sample size is low. The results do not show a consistent strength, the stiffnesses that were found are however fairly similar. The strengths that are found are in line with the strengths from SLJ_Ref2, the stiffnesses are similar to the results from SLJ_Ref1.

Figure 4.33 compares the strength and stiffness results for the three sets of reference specimens. Figure 4.33a shows that SLJ_Ref2 and SLJ_Ref3 have a comparable lap shear strength, suggesting that the difference between SLJ_Ref1 and SLJ_Ref2 might indeed have been caused by different storage times. This suggests that Araldite 2015 does indeed degrade over time under ambient conditions. The sample size is however very low and more research is necessary to determine the strength of Araldite 2015 over time under more controlled ambient conditions.

Figure 4.33b shows comparable stiffnesses for SLJ_Ref1 and SLJ_Ref3, with the stiffness for SLJ_Ref2 being significantly lower. Comparing the stiffness results with the lap shear strength results in Figure 4.33a shows that there is no direct link between the two. SLJ_Ref2 and SLJ_Ref3 do for example have similar lap shear strengths but distinctively different stiffnesses, suggesting a strong dependence of the measured stiffness on the testing equipment. Stiffness is a property that is dependent on the geometry, the material and the boundary conditions. Subjecting several identical specimens to different loadings will result in different measured stiffnesses. Since the geometry and material are consistent for all test series the difference must come from the boundary conditions, which lay in the testing equipment.

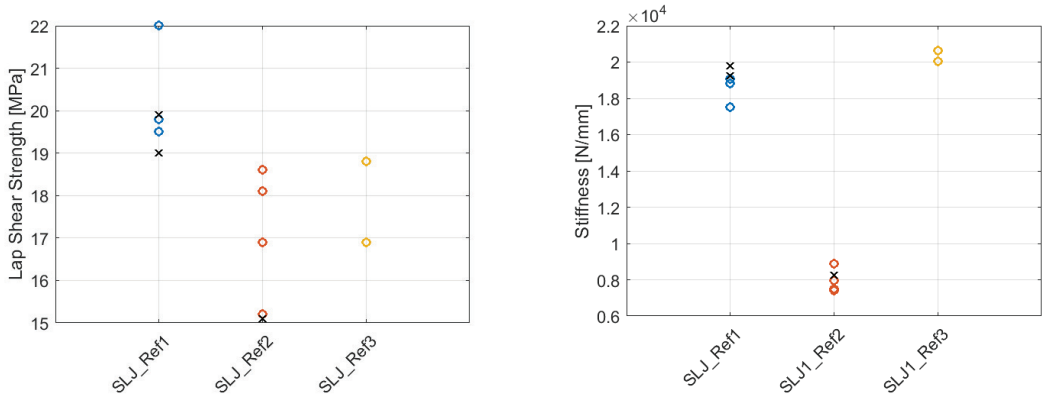

a) *Initial lap shear strength* **b)** *Initial stiffness*

Figure 4.33: Initial lap shear strength and residual stiffness for single lap joints.

All the tensile testing for the determination of the residual lap shear strength and residual stiffnesses has been done using the testing equipment at BAM. Because of this the results from SLJ_Ref2 will be used as a baseline for the initial lap shear strength and stiffness. The residual lap shear strength and stiffness results discussed in the following section will be compared to these results.

4.3.2 Residual lap shear strength and stiffness

This section will present and discuss the fracture surfaces, lap shear strengths and stiffnesses that followed from the tensile testing of aged metal-to-metal bonds. These specimens were subjected to one of three (hygro)thermal ageing conditions at different load levels, as described in Chapter 3. The section will start by presenting the tensile testing results for the individual test series. Once all results have been discussed the residual lap shear strength and stiffness will be determined. These values will be compared across the different test series.

The first results that will be discussed are the results for specimens that were subjected to condition 1 - Ageing at elevated temperatures in water without loading. For this condition two test series are available, the first with coating 1 and the second with coating 2. Figure 4.34 shows the fracture surfaces for test series SLJ1_W_0MPa (Figure 4.34a - 4.34c) and test series SLJ2_W_0MPa (Figure 4.34d - 4.34g). Table 4.12 presents the strength, stiffness and a description of the failure modes for these specimens.

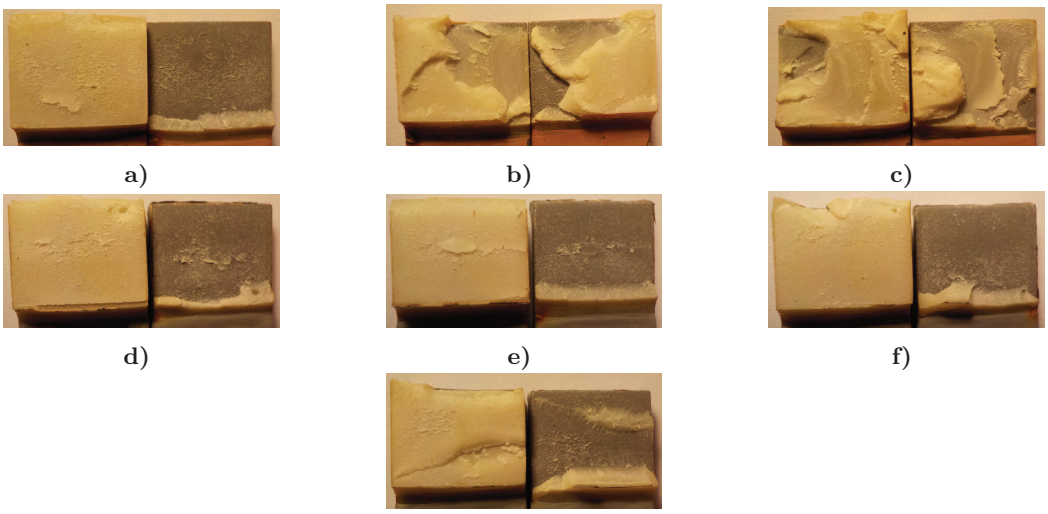

Figure 4.34: Fracture surfaces for test series SLJ1_W_0MPa and SLJ2_W_0MPa tested at BAM.

Test series	Strength [MPa]	Stiffness [N/mm]	Failure mode
SLJ1_W_0MPa - a	14.2	7 405	Cohesive failure near the interface
SLJ1_W_0MPa - b	12.9	6 874	Mixed mode: Cohesive failure (near the interface) with tearing of the adhesive layer
SLJ1_W_0MPa - c	9.43	6 050	Mixed mode: Cohesive failure (near the interface) with tearing of the adhesive layer
SLJ2_W_0MPa - d	16.5	7 366	Cohesive failure near the interface
SLJ2_W_0MPa - e	16.0	7 651	Cohesive failure near the interface
SLJ2_W_0MPa - f	16.7	7 529	Cohesive failure near the interface
SLJ2_W_0MPa - g	17.4	8 159	Mixed mode: Cohesive failure (near the interface)

Table 4.12: Strength, stiffness and description of failure mode for reference specimens SLJ1_W_0MPa and SLJ2_W_0MPa tested at BAM.

Figure 4.34a and 4.34d - 4.34f show cohesive failure near the interface. Figure 4.34b, 4.34c and 4.34g show a mixed failure mode with cohesive failure (near the interface). The fracture surfaces of Figure 4.34b, 4.34c also show tearing of the adhesive in a similar fashion as in Figure 4.31e. This is again attributed to a misalignment of the clamps resulting in an extra cleavage loading on the adhesive layer. Footage of the tensile testing of Figure 4.34g showed one of the spacers had been improperly placed, resulting in unwanted loading of the specimen. These specimens will be disregarded. With the two disregarded specimens for SLJ1_W_0MPa there is only one sample left in the set, making the results unreliable. The results can however be used to get an indication of the residual strength and stiffness. For SLJ2_W_0MPa the samples left in the set show consistent strengths and stiffnesses. This shows that the results are repeatable.

Next the results for the specimens that were subjected to condition 2 - Ageing at elevated temperatures in water with loading will be discussed. First, the results for 1 MPa will be presented followed by the ones for 3 MPa. For 1 MPa two test series are available: one with coating 1 and one with coating 2.

The results for test series SLJ1_W_1MPa and SLJ2_W_1MPa are shown in Figure 4.35 and Table 4.13. The fracture surfaces for test series SLJ1_W_1MPa are shown in Figure 4.35a and 4.35b, the ones for SLJ2_W_1MPa are depicted in Figure 4.37a and 4.37b. Table 4.13 presents the strength, stiffness and a description of the failure modes for these specimens.

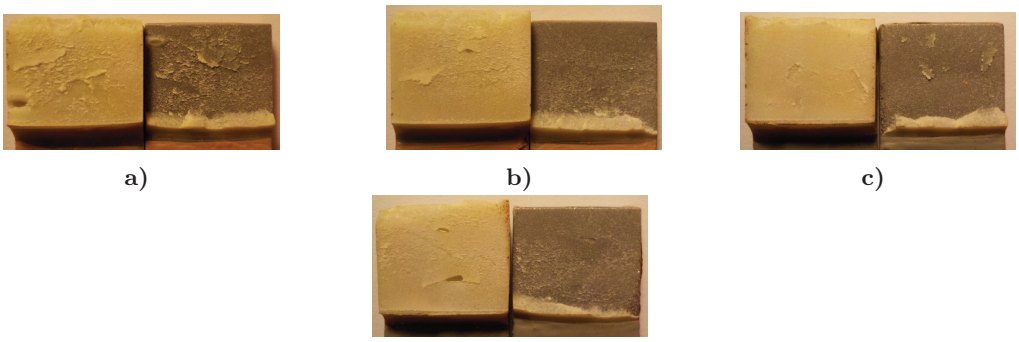

a) **b)** **c)** **d)**

Figure 4.35: Fracture surfaces for test series SLJ1_W_1MPa and SLJ2_W_1MPa tested at BAM.

Test series	Strength [MPa]	Stiffness [N/mm]	Failure mode
SLJ1_W_1MPa - a	15.1	6 394	Cohesive failure near the interface
SLJ1_W_1MPa - b	15.5	6 689	Cohesive failure near the interface
SLJ2_W_1MPa - c	16.4	6 583	Cohesive failure near the interface
SLJ2_W_1MPa - d	17.1	7 881	Cohesive failure near the interface

Table 4.13: Strength, stiffness and description of failure mode for reference specimens SLJ1_W_1MPa and SLJ2_W_1MPa tested at BAM.

Figure 4.35 shows fracture surfaces with cohesive failure near the interface. With only two samples for each set the sample sizes are small. The strength results are however consistent for both test series, which shows repeatbility. The stiffness is more consistent for the SLJ1_W_1MPa set than for the SLJ2_W_1MPa set.

Test series SLJ2_A_3MPa corresponds to single lap joints that were subjected to condition 2 with a load level of 3 MPa. Figure 4.36 shows the fracture surfaces for this test series. Table 4.14 presents the strength, stiffness and a description of the failure modes for these specimens.

a) b)

Figure 4.36: Fracture surfaces for test series SLJ2_W_3MPatested at BAM.

Test series	Strength [MPa]	Stiffness [N/mm]	Failure mode
SLJ2_W_3MPa - a	16.8	6 973	Mixed mode: Cohesive failure (near the interface)
SLJ2_W_3MPa - b	16.7	7 045	Mixed mode: Cohesive failure (near the interface) with tearing of the adhesive layer

Table 4.14: Strength, stiffness and description of failure mode for reference specimens SLJ2_W_3MPa tested at BAM.

Figure 4.36 shows fracture surfaces with mixed failure modes. For both specimens the crack did not initiate in the middle of the fillet like with the other specimens. Instead, it seems to have (mostly) started at one of the interfaces near the fillet. Another observation that can be made is the diagonal line from middle left to bottom right that can be observed for both specimens. It is hypothesised that this might have been caused by the specimens being placed under a slight angle instead of perfectly straight. The position of the specimens was checked using a small builders level. The coating on the adherends did however make this more difficult since it was not applied perfectly flat. On top of this specimen SLJ2_W_3MPa - b does again show tearing of the adhesive, which is attributed to a misalignment of the clamps leading to a type of cleavage loading. The specimens show very consistent strength and stiffness results, suggesting good repeatability. Despite this, set SLJ2_W_3MPa will be disregarded because of the fracture surfaces.

The third and last results to be presented are for condition 3 - Ageing at elevated temperatures in air with loading. For this condition two test series are available. The first test series to be presented is for specimens loaded at 1 MPa, the second for specimens loaded at 3 MPa.

Figure 4.37 shows the fracture surfaces for test series SLJ2_A_1MPa: specimens subjected to condition 3 with a load level of 1 MPa. Table 4.15 presents the strength, stiffness and a description of the failure modes for these specimens.

a) b)

Figure 4.37: Fracture surfaces for test series SLJ2_A_1MPa tested at BAM.

Test series	Strength [MPa]	Stiffness [N/mm]	Failure mode
SLJ2_A_1MPa - a	17.8	8 218	Cohesive failure near the interface
SLJ2_A_1MPa - b	17.8	7 861	Cohesive failure near the interface

Table 4.15: Strength, stiffness and description of failure mode for reference specimens SLJ2_A_1MPa tested at BAM.

Figure 4.37 shows fracture surfaces with cohesive failure near the interface. The test series has only two specimens and is therefore small, both the strength and stiffness results are however very consistent which shows repeatability.

The single lap joints in test series SLJ2_A_3MPa were subjected to condition 3 with a load level of 3 MPa. Figure 4.38 shows the fracture surfaces for this test series. Table 4.16 presents the strength, stiffness and a description of the failure modes for these specimens. Figures 4.39a and 4.39b compare the strength and stiffness of the SLJ2_A_3MPa specimens with the other sets of specimens.

a) **b)**

Figure 4.38: Fracture surfaces for test series SLJ2_A_3MPa tested at BAM.

Test series	Strength [MPa]	Stiffness [N/mm]	Failure mode
SLJ2_A_3MPa - a	15.6	6 937	Mixed mode: Cohesive failure near the interface with adhesive failure
SLJ2_A_3MPa - b	15.7	7 755	Mixed mode: Cohesive failure (near the interface)

Table 4.16: Strength, stiffness and description of failure mode for reference specimens SLJ2_A_3MPa tested at BAM.

Figure 4.38 shows fracture surfaces with predominant cohesive failure near the interface. Specimen SLJ2_A_3MPa-a shows cohesive failure near the interface with a small part of adhesive failure - see the top-middle of the fracture surface on the right. This suggests that the bond area might have been slightly contaminated before application of the adhesive. SLJ2_A_3MPa - b shows a combination of cohesive failure and cohesive failure near the interface. It is suggested that the triangular portion of the fracture surface might have been partly caused by a void creating a preferential path for the crack growth. However, no definitive explanation has been found for the occurrence of this failure pattern.

The goal of the tensile testing of the preconditioned specimens is to see how the results found for the residual lap shear strengths and stiffnesses compare to the intial values. To make this comparison more convenient a Residual Strength Index [RSI_1] and a Residual Stiffness Index [RSI_2] are introduced. This indices are defined as follows:

$$\mathrm{RSI}_1 = \frac{\sigma_t}{\sigma_0} \tag{4-6}$$

$$\mathrm{RSI}_2 = \frac{k_t}{k_0}, \tag{4-7}$$

where σ_t and k_t are defined as respectively the lap shear strength and stiffness at time t after preconditioning. σ_{t0} and k_{t0} are defined as the initial lap shear strength and stiffness at time $t = 0$, before preconditioning. This representation shows how damaging the various conditions have been to the strength and stiffness of the metal-to-metal bonds. A RSI_1 or RSI_2 of 1 indicates that there has been no damage and that the conditioning had no detrimental effects. A value larger than 1 indicates an improvement of properties while a value smaller than 1 means that the conditioning damaged the bond.

Figure 4.39 shows the RSI_1 and RSI_2 values for the test series discussed above. The presented values have been determined with respect to the mean initial lap shear strength and initial stiffness from test series SLJ_Ref2. The actual values can be found in Table C.1 in Appendix C. The black crosses denote the specimens that have been excluded from the analysis for reasons described above.

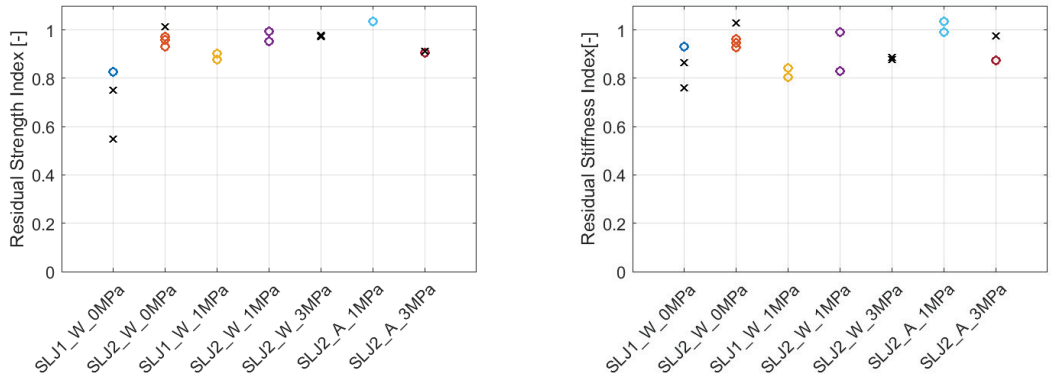

a) *Residual Strength Index* **b)** *Residual Stiffness Index*

Figure 4.39: Residual Strength Index and Residual Stiffness Index for single lap joints.

The results show that moisture has a negative effect on the residual lap shear strength and residual stiffness. Loading specimens at 1 MPa had a positive effect and resulted in a lower strength loss or even in a strength increase. This effect is not as obvious for the stiffness. For loading in air there is indeed a stiffness increase, loading in water with coating 1 did however result in a stiffness decrease compared to the unloaded case. For loading in air with coating 2 the scatter is large, making it impossible to judge the effect of the conditioning. Loading the specimens at 3 MPa resulted in a strength and stiffness loss. The strength/stiffness decrease for specimens subjected to moisture can be attributed to swelling and plasticisation of the polymer network caused by moisture absorption. The strength/stiffness increase of low load levels can be explained by the

creep deformation orienting the molecular chains of the epoxy in the direction of loading and the adhesive layer thereby experiencing some kind of strain hardening. At higher load levels the creep deformation becomes too large for it to have a positive effect on the adhesive. The differences between the results for the specimens with coating 1 and the specimens with coating 2 are attributed to the contamination of the water by the rusting the single lap joints with coating 1. It is hypothesized that this caused a harsher environment that resulted in more degradation of the adhesive layer.

4.3.3 Conclusion and recommendations

This section aimed to answer the following research question:

> *How do the creep and (hygro)thermal loadings influence the residual strength and stiffness of steel bonded joints?*

The section showed that the residual strength and stiffness of metal bonds are indeed affected by loading and environment. In some cases loading and environment were found to have opposite effects on the residual strength, with the loading increasing the residual strength and stiffness while the water decreased the residual strength/stiffness.

The tensile tests performed for the determination of the initial strength suggested that the tensile strength of Araldite 2015 might be affected by ambient humidity. The sample size was however very small and the humidity in which the specimens were stored was not constant. Further research is therefore necessary to determine the strength of Araldite 2015 over time under ambient conditions in a more controlled manner.

It is recommended that the experiments are repeated in combination with the recommendations for the water uptake and creep experiments in Sections 4.1 and 4.2. Again, a larger sample size is desired for the preconditioned specimens. The results presented in this section showed that even a slight misalignment of the clamps has large effect on the single lap joint specimens. Care should therefore be taken that every specimen is placed properly. If the grips used during the experiments have a chance of moving/turning the alignment should be checked between each tensile test. Since Araldite 2015 might be affected by ambient humidity it is recommended that specimens are stored in a desiccator before testing and that research is conducted on the effect of ambient humidity on Araldite 2015. The effect of ambient humidity on Araldite 2015 could be determined by storing specimens in a controlled environment for different durations before testing them until failure.

Chapter 5

Conclusions and future perspective

This thesis set out to answer the research question formulated in Chapter 1. In this final chapter this research question will be answered and directions for future research will be discussed.

The research question that has been formulated for this thesis is as follows:

> *RQ: How do hygrothermal and creep loadings influence the water uptake, creep and residual strength of metal-to-metal bonds?*

To answer this research question single lap shear joints have been designed and manufactured. These metal-to-metal bonds were then subjected to various environments (40^{o}C air and 40^{o}C distilled water) at different load levels (0 MPa, 1 MPa, 3 MPa, 6 MPa and 9 MPa). Experiments lasted for two weeks or until failure, whichever came first. After 14 days specimens were removed from the environment and tensile tested until failure to determine the residual lap shear strength.

The experiments were inconclusive on the effect of the load level on the water uptake. The majority of the water uptake of the single lap joint specimens was found to come from the coating that had been applied to the adherends to protect them from the environment. Due to a large amount of scatter it was not possible to determine the water uptake of the adhesive layer.

The load level and environment were found to have a large influence on the creep behaviour of the bonds. Increasing the load level resulted in a larger instantaneous creep strain and a higher strain rate. Specimens loaded in air generally experienced a lower creep strain than the specimens loaded in water. The specimens loaded in water were found to have a lower instantaneous creep strain than the specimens loaded in air. This suggests that the creep response was suppressed during the initial stages of moisture absorption. This behaviour can be explained by two different processes taking place in the water absorption process. As the water is starting to diffuse into the adhesive the water molecules bond to the macromolecules. This results in a reduction of the molecular mobility and thereby a lower creep deformation. As the water continues to diffuse into the adhesive the plasticizing effect of the water becomes stronger, resulting in a larger creep deformation for specimens tested in water than for specimens tested in air.

The residual strength was found to be affected by the load level and environment in different ways. At low load levels (1 MPa) loading the metal-to-metal bonds had a positive effect on the residual lap shear strength, which can be attributed to the creep

deformation orienting the molecular chains of the epoxy in the direction of loading. This results in the adhesive layer experiencing some kind of strain hardening. If the load level is increased to 3 MPa the lap shear strength is however decreased. At this load level the creep deformation has become too large for there to be a strain hardening effect and it damages the adhesive instead. Immersion of the specimens in water results in swelling and plasticisation of the adhesive, resulting in a reduced residual lap shear strength. The experimental results also suggest that Araldite 2015 might be affected by ambient humidity.

As mentioned in Chapter 1, this thesis aims to provide an initial step in the research on the long term behaviour of composite-to-metal bonds that are loaded under environmental conditions. In this initial step the focus was on the influence of environment and load level on the water uptake, creep and residual strength of the adhesive layer. The following recommendations are made for building further upon this initial step:

- To be able to focus on the behaviour of the adhesive layer the GFRP adherend was excluded for this thesis. The next step in the research on composite-to-metal bonds could be made by studying the influence of environment and load level on the water uptake, creep and residual strength of GFRP specimens. For these experiments the experimental procedures in Chapter 3 could be used as a general guideline.
- The current work has been carried out using a single joint configuration and can be build upon by varying this configuration. It is for example recommended that experiments are repeated using different (thick and thin) bond lines thicknesses to see if the same behaviour is observed.
- For this thesis it was not possible to extend the FEM model to include the creep behaviour. If the creep behaviour is included it would be possible to see the developments of the strains in the adhesive layer. This could for example be done by replacing the heat transfer (DC3D8) elements with coupled temperature-displacement (C3D8T) elements. A CREEP user subroutine could be used to define the creep in the adhesive. The model could be further extended by developing and implementing a damage model that can predict the residual strength based on the water uptake and creep.
- As described in Chapter 4.1 it was not possible to produce conclusive results on the effect of load level on the water uptake. This was caused by the coating that was applied to the steel adherends. Repeating the experiments using specimens with stainless steel adherends would eliminate this problem and should produce the results this thesis aimed to find. If these experiments are repeated it is recommended that the specimens tested under combined moisture and loading are tested for different time durations so that it is possible to see the evolution in water uptake. The maximum duration of the experiments should also be longer than two weeks to be able to observe a more long-term effect of the loading on the water uptake. If the same FNCT machine is to be used it is recommended that the joint design is changed so that they can be gripped and loaded using holes in the adherends, as per ASTM D2294 [73]. This would prevent the possibility for

any slippage of the joint during loading. In addition to testing in distilled water, it could be of interest to also repeat specimen in seawater and possibly at different temperatures. Finally, if possible the sample size of the specimens subjected to combined moisture and loading should be larger than in this thesis.

- During the creep experiments described in Chapter 4.2 it was found that at the initial stages of water absorption (low moisture percentage) creep is suppressed while at later stages (high(er) moisture percentage) creep is promoted. This can possibly be explained by two different processes being at play when water is absorbed. Since creep experiments are normally conducted on much larger time scales and specimens are often preconditioned before testing no description of this phenomenon has been found in literature. Future research could further investigate the influence of moisture absorption on the (short-term) creep response.
- Due to time constraints it was not possible to start by testing the creep loaded bonds until failure at different load levels. Because of this load levels were conservative to prevent the bonds from breaking before the end of the experiments. If similar creep experiments are repeated it is recommended to start by determining which load levels are appropriate for the desired time frame. Again, it is recommended to change the joint design as described in ASTM D2294 [73] if the same FNCT machine or a similar machine is used to prevent possible slippage. If joints are tested at load levels that are in the same range it should also be possible to successfully develop a nonlinear creep model using the approach as described in Chapter 4.2.
- It is recommended that the above recommendations are combined with a determination of the residual strength. One of the interesting conclusions from the current work is the strengthening of the adhesive layer at low load levels. Further research could investigate this further by studying joints at different load levels and different time periods. It would for example be interesting to see whether there is a development in the strengthening effect of the load.
- The work on the lap shear strength of the metal-to-metal bonds also suggested that Araldite 2015 might be affected by ambient humidity. Further research can build upon this investigation by storing specimens in a controlled environment for different durations before determining the residual strength.

Bibliography

[1] D. Burlović, A. Milat, M. Balunović, D. Frank, E. A. Kotsidis, I. G. Kouloukouras, and N. G. Tsouvalis, "Finite element analysis of composite-to-steel type of joint for marine industry," *Welding in the World*, pp. 1–9, apr 2016.

[2] S. W. Boyd, J. I. R. Blake, R. A. Shenoi, and J. Mawella, "Optimisation of steel-composite connections for structural marine applications," *Composites Part B: Engineering*, vol. 39, no. 5, pp. 891–906, 2008.

[3] D. R. Speth, Y. P. Yang, and G. W. Ritter, "Qualification of adhesives for marine composite-to-steel applications," *International Journal of Adhesion and Adhesives*, vol. 30, no. 2, pp. 55–62, 2010.

[4] S. W. Boyd, J. I. R. Blake, R. A. Shenoi, and A. Kapadia, "Integrity of hybrid steel-to-composite joints for marine application," *Proceedings of the Institution of Mechanical Engineers Part M: Journal of Engineering for the Maritime Environment*, vol. 218, pp. 235–246, dec 2004.

[5] G. Papanicolaou and S. Zaoutsos, "Viscoelastic constitutive modeling of creep and stress relaxation in polymers and polymer matrix composites," in *Creep and Fatigue in Polymer Matrix Composites* (R. M. Guedes, ed.), pp. 3–47, Cambridge: Woodhead Publishing Limited, 2011.

[6] G. C. Papanicolaou, A. G. Xepapadaki, and D. S. Zarouchas, "Effect of water uptake on creep behaviour of glass-epoxy composites," *Plastics, Rubber and Composites*, vol. 38, no. 2, pp. 72–79, 2009.

[7] I. Ashcroft and P. Briskham, "Designing adhesive joints for fatigue and creep load conditions," in *Advances in Structural Adhesive Bonding* (D. A. Dillard, ed.), pp. 469–515, Cambridge: Woodhead Publishing Limited, 2010.

[8] R. Fernandes, M. de Moura, and R. Moreira, "Effect of moisture on pure mode I and II fracture behaviour of composite bonded joints," *International Journal of Adhesion and Adhesives*, vol. 68, pp. 30–38, jul 2016.

[9] A. Zafar, F. Bertocco, J. Schjødt-Thomsen, and J. C. Rauhe, "Investigation of the long term effects of moisture on carbon fibre and epoxy matrix composites," *Composites Science and Technology*, vol. 72, no. 6, pp. 656–666, 2012.

[10] V. S. Chevali, D. R. Dean, and G. M. Janowski, "Effect of environmental weathering on flexural creep behavior of long fiber-reinforced thermoplastic composites," *Polymer Degradation and Stability*, vol. 95, pp. 2628–2640, dec 2010.

[11] E. Gellert and D. Turley, "Seawater immersion ageing of glass-fibre reinforced polymer laminates for marine applications," *Composites Part A: Applied Science and Manufacturing*, vol. 30, pp. 1259–1265, nov 1999.

[12] M. Eftekhari and A. Fatemi, "Tensile, creep and fatigue behaviours of short fibre reinforced polymer composites at elevated temperatures: a literature survey," *Fatigue & Fracture of Engineering Materials & Structures*, vol. 38, no. 12, pp. 1395–1418, 2015.

[13] C. Humeau, P. Davies, and F. Jacquemin, "Moisture diffusion under hydrostatic pressure in composites," *Materials & Design*, vol. 96, pp. 90–98, feb 2016.

[14] C. Alia, M. V. Biezma, P. Pinilla, J. M. Arenas, and J. C. Suárez, "Degradation in Seawater of Structural Adhesives for Hybrid Fibre-Metal Laminated Materials," *Advances in Materials Science and Engineering*, vol. 2013, pp. 1–10, 2013.

[15] H. Gu, "Behaviours of glass fibre/unsaturated polyester composites under seawater environment," *Materials and Design*, vol. 30, no. 4, pp. 1337–1340, 2009.

[16] A. Kootsookos and A. P. Mouritz, "Seawater durability of glass- and carbon-polymer composites," *Composites Science and Technology*, vol. 64, no. 10-11, pp. 1503–1511, 2004.

[17] G. S. Springer and T. K. Wang, "Creep, Strength and Moisture Absorption of Adhesive Bonded FRP Joints," *Journal of Reinforced Plastics and Composites*, vol. 4, no. 2, pp. 212–225, 1985.

[18] V. M. Karbhari and S. Zhang, "E-Glass/Vinylester Composites in Aqueous Environments âĂŞ I: Experimental Results," *Applied Composite Materials*, vol. 10, no. 1, pp. 19–48, 2003.

[19] A. M. Visco, L. Calabrese, and P. Cianciafara, "Modification of polyester resin based composites induced by seawater absorption," *Composites Part A: Applied Science and Manufacturing*, vol. 39, no. 5, pp. 805–814, 2008.

[20] I. F. Soykok, "Degradation of Single Lap Adhesively Bonded Composite Joints Due to Hot Water Ageing," *The Journal of Adhesion*, vol. 8464, no. November, p. 150812074043002, 2015.

[21] A. Lagrange, C. Melennec, and R. Jacquemet, "Influence of various stress conditions of the moisture diffusion of composites in distilled water and in natural sea-water," in *Durability of polymer based composite systems for structural applications* (A. Cardon and G. Verchery, eds.), pp. 385–392, 1991.

[22] X. Han, A. D. Crocombe, S. N. R. Anwar, P. Hu, and W. D. Li, "The Effect of a HotâĂŞWet Environment on Adhesively Bonded Joints Under a Sustained Load," *The Journal of Adhesion*, vol. 90, pp. 420–436, jun 2014.

[23] A. M. Visco, N. Campo, and P. Cianciafara, "Comparison of seawater absorption properties of thermoset resins based composites," *Composites Part A: Applied Science and Manufacturing*, vol. 42, no. 2, pp. 123–130, 2011.

[24] J. Garcia-Espinel, D. Castro-Fresno, P. Parbole Gayo, and F. Ballester-Muñoz, "Effects of sea water environment on glass fiber reinforced plastic materials used for marine civil engineering constructions," *Materials & Design*, vol. 66, pp. 46–50, 2015.

[25] P. Silva, P. Fernandes, J. Sena-Cruz, J. Xavier, F. Castro, D. Soares, and V. Carneiro, "Effects of different environmental conditions on the mechanical characteristics of a structural epoxy," *Composites Part B: Engineering*, vol. 88, pp. 55–63, 2016.

[26] M. Bordes, P. Davies, J. Y. Cognard, L. Sohier, V. Sauvant-Moynot, and J. Galy, "Prediction of long term strength of adhesively bonded steel/epoxy joints in sea water," *International Journal of Adhesion and Adhesives*, vol. 29, no. 6, pp. 595–608, 2009.

[27] B. Wei, H. Cao, and S. Song, "Degradation of basalt fibre and glass fibre/epoxy resin composites in seawater," *Corrosion Science*, vol. 53, no. 1, pp. 426–431, 2011.

[28] R. Young and P. Lovell, *Introduction to Polymers*. Boca Raton: CRC Press, 3rd ed., 2011.

[29] R. Lakes, *Viscoelastic Materials*. New York: Cambridge University Press, 2009.

[30] P. Dasappa, P. Lee-Sullivan, X. Xiao, and P. H. Foss, "Tensile creep of a long-fibre glass mat thermoplastic (GMT) composite. II. viscoelastic-viscoplastic constitutive modeling," *Polymer Composites*, vol. 30, no. 9, pp. 1204–1211, 2009.

[31] P. Majda and J. Skrodzewicz, "A modified creep model of epoxy adhesive at ambient temperature," *International Journal of Adhesion and Adhesives*, vol. 29, no. 4, pp. 396–404, 2009.

[32] J. Godzimirski and M. Rośkowicz, "Numerical analysis and experimental tests for long-term strength of adhesive bonds," *Journal of Adhesion Science and Technology*, vol. 28, no. 14-15, pp. 1334–1344, 2014.

[33] W. G. Knauss and W. Zhu, "Nonlinearly viscoelastic behavior of polycarbonate. I. Response under pure shear," *Mechanics Time-Dependent Materials*, vol. 6, no. 3, pp. 231–269, 2002.

[34] M. Zehsaz, F. Vakili-Tahami, and M.-A. Saeimi-Sadigh, "Creep analysis of adhesively bonded single lap joint using finite element method," *Journal of Mechanical Science and Technology*, vol. 28, no. 7, pp. 2743–2748, 2014.

[35] S. P. Zaoutsos and G. C. Papanicolaou, "On the influence of preloading in the nonlinear viscoelastic-viscoplastic response of carbon-epoxy composites," *Composites Science and Technology*, vol. 70, no. 6, pp. 922–929, 2010.

[36] M. Hadid, S. Rechak, and A. Zouani, "Empirical nonlinear viscoelastic model for injection molded thermoplastic composite," *Polymer Composites*, vol. 23, no. 5, pp. 771–778, 2002.

[37] G. C. Papanicolaou, A. G. Xepapadaki, S. Pavlopoulou, and S. P. Zaoutsos, "On the investigation of the stress threshold from linear to nonlinear viscoelastic behaviour of polymer-matrix particulate composites," *Mechanics of Time-Dependent Materials*, vol. 13, no. 3, pp. 261–274, 2009.

[38] K. W. Allen and M. E. R. Shanahan, "The Creep Behaviour of Structural Adhesive Joints II," *The Journal of Adhesion*, vol. 8, no. 1, pp. 43–56, 1976.

[39] X. X. Yu, A. D. Crocombe, and G. Richardson, "Material modelling for rate-dependent adhesives," *International Journal of Adhesion and Adhesives*, vol. 21, no. 3, pp. 197–210, 2001.

[40] G. Dean, "Modelling non-linear creep behaviour of an epoxy adhesive," *International Journal of Adhesion and Adhesives*, vol. 27, no. 8, pp. 636–646, 2007.

[41] M. Zehsaz, F. Vakili-Tahami, and M. A. Saeimi-Sadigh, "Parametric study of the creep failure of double lap adhesively bonded joints," *Materials and Design*, vol. 64, pp. 520–526, 2014.

[42] M. Zehsaz, F. Vakili-Tahami, and M.-A. Saeimi-Sadigh, "Modified creep constitutive equation for an epoxy-based adhesive with nonlinear viscoelastic behavior," *The Journal of Strain Analysis for Engineering Design*, vol. 50, no. 1, pp. 4–14, 2015.

[43] M. A. S. Sadigh, "Creep simulation of adhesively bonded joints using modified generalized time hardening model," *Journal of Mechanical Science and Technology*, vol. 30, pp. 1555–1561, apr 2016.

[44] A. S. M. Roseley, E. Rojo, M. P. Ansell, and D. Smedley, "Creep response of thixotropic ambient temperature cure adhesives measured by DMTA in static tension and shear," *International Journal of Adhesion and Adhesives*, vol. 31, no. 6, pp. 575–582, 2011.

[45] K. W. Allen and M. E. R. Shanahan, "The Creep Behaviour of Structural Adhesive Joints-I," *The Journal of Adhesion*, vol. 7, no. 3, pp. 161–174, 1975.

[46] C.-W. Feng, C.-W. Keong, Y.-P. Hsueh, Y.-Y. Wang, and H.-J. Sue, "Modeling of long-term creep behavior of structural epoxy adhesives," *International Journal of Adhesion and Adhesives*, vol. 25, no. 5, pp. 427–436, 2005.

[47] E. Ferrier, L. Michel, B. Jurkiewiez, and P. Hamelin, "Creep behavior of adhesives used for external FRP strengthening of RC structures," *Construction and Building Materials*, vol. 25, no. 2, pp. 461–467, 2011.

[48] M. Garrido, J. R. Correia, and T. Keller, "Effect of service temperature on the flexural creep of vacuum infused GFRP laminates used in sandwich floor panels," *Composites Part B*, vol. 90, pp. 160–171, 2016.

[49] N. Su and R. I. Mackie, "Two-dimensional creep analysis of structural adhesive joints," *International Journal of Adhesion and Adhesives*, vol. 13, no. 1, pp. 33–40, 1993.

[50] J. Yao and G. Ziegmann, "Equivalence of moisture and temperature in accelerated test method and its application in prediction of long-term properties of glass-fiber reinforced epoxy pipe specimen," *Polymer Testing*, vol. 25, no. 2, pp. 149–157, 2006.

[51] P. Mannberg, B. Nyström, L. Wallström, and R. Joffe, "Service life assessment and moisture influence on bio-based composites," *Journal of Materials Science*, vol. 49, no. 15, pp. 5265–5270, 2014.

[52] M. Farshad and A. Necola, "Effect of aqueous environment on the long-term behavior of glass fiber-reinforced plastic pipes," *Polymer Testing*, vol. 23, no. 2, pp. 163–167, 2004.

[53] R. Guedes, A. Sá, and H. Faria, "Influence of moisture absorption on creep of GRP composite pipes," *Polymer Testing*, vol. 26, pp. 595–605, aug 2007.

[54] R. M. Guedes, A. Sá, and H. Faria, "On the prediction of long-term creep-failure of GRP pipes in aqueous environment," *Polymer Composites*, vol. 31, no. 6, pp. 1047–1055, 2010.

[55] G. C. Papanicolaou, A. G. Xepapadaki, K. Karagounaki, and S. P. Zaoutsos, "Time and temperature effect on the linearâĂŞnonlinear viscoelastic transition threshold of a polymeric system," *Journal of Applied Polymer Science*, vol. 108, pp. 640–649, apr 2008.

[56] R. S. Lakes, *Viscoelastic solids*. CRC Press, 1999.

[57] N. Özkaya, M. Nordin, D. Goldsheyder, and D. Leger, *Fundamentals of biomechanics: equilibrium, motion, and deformation*. Springer Science & Business Media, 2012.

[58] M. Nciri, D. Notta-Cuvier, F. Lauro, F. Chaari, B. Zouari, Y. Maalej, and Y. Maalej, "A viscoelastic-viscoplastic model for short-fibre reinforced polymers with complex fibre orientations," in *EPJ Web of Conferences* (E. Cadoni, ed.), vol. 94, p. 04008, EDP Sciences, 2015.

[59] N. Zobeiry, S. Malek, R. Vaziri, and A. Poursartip, "A differential approach to finite element modelling of isotropic and transversely isotropic viscoelastic materials," *Mechanics of Materials*, vol. 97, pp. 76–91, 2016.

[60] A. S. Wineman and K. Rajagopal, "Constitutive Equations for One-Dimensional Response of Viscoelastic Materials: Mechanical Analogs," in *Mechanical Response of Polymers: An Introduction*, ch. Constituti, pp. 28–53, Cambridge: Cambridge University Press, 2000.

[61] H. Groth, "Viscoelastic and viscoplastic stress analysis of adhesive joints," *International Journal of Adhesion and Adhesives*, vol. 10, no. 3, pp. 207–213, 1990.

[62] M. Shishesaz and A. Reza, "The Effect of Viscoelasticity of Polymeric Adhesives on Shear Stress Distribution in a Single-Lap Joint," *The Journal of Adhesion*, vol. 89, pp. 859–880, nov 2013.

[63] S. Sahellie and H. Pasternak, "Expectancy of the lifetime of bonded steel joints due to long-term shear loading," *Archives of Civil and Mechanical Engineering*, vol. 15, no. 4, pp. 1061–1069, 2015.

[64] Raahe Steel Works, "Test Report S700MC," 2016.

[65] M. L. Abel, R. D. Allington, R. P. Digby, N. Porritt, S. J. Shaw, and J. F. Watts, "Understanding the relationship between silane application conditions, bond durability and locus of failure," *International Journal of Adhesion and Adhesives*, vol. 26, no. 1-2, pp. 2–15, 2006.

[66] W.-S. Kim and J.-J. Lee, "Adhesion strength and fatigue life improvement of co-cured composite/metal lap joints by silane-based interphase formation," *Journal of Adhesion Science and Technology*, vol. 21, no. June 2014, pp. 125–140, 2007.

[67] J. J. Mazza, J. B. Avram, and R. J. Kuhbandar, "Grit-Blast/Silane (GBS) Aluminum Surface Preparation for Structural Adhesive Bonding," 2003.

[68] R. A. Gledhill, S. J. Shaw, and D. A. Tod, "Durability of adhesive-bonded joints employing organosilane coupling agents," *International Journal of Adhesion and Adhesives*, vol. 10, pp. 192–198, jul 1990.

[69] Huntsman, "Araldite ® 2015 - Technical Data Sheet," 2015.

[70] R. D. S. G. Campilho, *Strength Prediction of Adhesively-Bonded Joints*. 2017.

[71] S. Yoon, B. Han, and Z. Wang, "On Moisture Diffusion Modeling Using Thermal-Moisture Analogy," *Journal of Electronic Packaging*, vol. 129, p. 421, dec 2007.

[72] M. S. Obaidat and N. A. Boudriga, *Fundamentals of Performance Evaluation of Computer and Telecommunications Systems*. John Wiley & Sons, 2010.

[73] ASTM, "ASTM D2294âĹŠ96 (Reapproved 2016) - Standard Test Method for Creep Properties of Adhesives in Shear by Tension Loading," 1996.

[74] D. Colombini, J. J. Martinez-Vega, and G. Merle, "Influence of hydrothermal ageing and thermal treatments on the viscoelastic behavior of DGEBA-MCDEA epoxy resin," *Polymer Bulletin*, vol. 48, pp. 75–82, 2002.

[75] ASTM, "ASTM D5573 - 99 (Reapproved 2012) - Standard practice for classifying failure modes in fibre-reinforced-plastic (FRP) joints.," vol. D5573, pp. 3–5, 1999.

[76] D. Liu and S. Park, "A Note on the Normalized Approach to Simulating Moisture Diffusion in a Multimaterial System Under Transient Thermal Conditions Using ANSYS 14 and 14.5," *Journal of Electronic Packaging*, vol. 136, no. 3, p. 034501, 2014.

Appendix A

Water uptake data

A.1 Heat transfer analogy

The water uptake of the lap shear joints is modeled by using the similarity between the governing equations for heat transfer (Equations (A-1) and (A-2) and moisture diffusion (Equation (A-3)).

The diffusion equation for heat transfer is as follows [76]:

$$\rho c_p \dot{T} = k\nabla^2 T, \tag{A-1}$$

where ρ is de density ($\mathrm{kg{\cdot}m^{-3}}$) and c_p is the specific heat ($\mathrm{J{\cdot}kg^{-1}{\cdot}K^{-1}}$). $\dot{T}$ and T are respectively the heat flux ($\mathrm{W{\cdot}m^{-2}}$) and the temperature (K). k is the thermal conductivity ($\mathrm{W{\cdot}m^{-1}{\cdot}K^{-1}}$), which is dependent on temperature and negligible in most cases. Assuming the thermal conductivity is uniform Equation (A-1) can be rewritten as [71]:

$$\dot{T} = \alpha\nabla^2 T, \tag{A-2}$$

where α is the thermal diffusivity ($\mathrm{m^2{\cdot}s^{-1}}$), defined as $\alpha = \mathrm{k}/(\rho{\cdot}\ c_p)$ [71]. The diffusion equation used for moisture diffusion, Fick's second law, is as follows [76]:

$$\dot{C} = D\nabla^2 C, \tag{A-3}$$

where C and $\dot{C}$ are the moisture concentration ($\mathrm{kg{\cdot}m^{-3}}$) and mass flux ($\mathrm{kg{\cdot}m^{-2}{\cdot}s^{-1}}$) respectively. D is the moisture diffusivity coefficient ($\mathrm{m^2{\cdot}s^{-1}}$) and is generally a function of temperature as well as concentration [71].

By comparing Equations (A-2) and (A-3) it is possible to establish a direct analogy between the two diffusion equations. This analogy can be expressed as [71]:

Field variable: $T = C$
Diffusion coefficient: $\alpha = D$.

Since Equations (A-2) and (A-3) are based on the assumption of uniform conductivity and diffusivity it is only possible to use this analogy if the diffusing medium is homogeneous and the temperature field is uniform at a given time [71].

A.2 Simulation results for verification

Continuity testing

Diffusion Coefficient [m^2s^{-1}]	Duration	Water uptake [g]
2.19×10^{-13}	5 days	6.62×10^{-3}
2.20×10^{-13}	5 days	6.63×10^{-3}
2.21×10^{-13}	5 days	6.64×10^{-3}
2.20×10^{-13}	4.5 days	6.39×10^{-3}
2.20×10^{-13}	5.5 days	6.85×10^{-3}

Table A.1: Simulation results for continuity testing

Degeneracy testing

Diffusion Coefficient [m^2s^{-1}]	Duration	Water uptake [g]
1.15×10^{-12}	1 second	1.53×10^{-3}
8.02×10^{-14}	1 second	1.53×10^{-3}
1.15×10^{-12}	1000 days	4.53×10^{-2}
8.02×10^{-14}	1000 days	3.17×10^{-2}

Table A.2: Simulation results for degeneracy testing

Consistency testing

Diffusion Coefficient [m^2s^{-1}]	Duration [days]	Water uptake [g]
4.40×10^{-13}	2.5	6.63×10^{-3}
2.20×10^{-13}	5	6.63×10^{-3}
1.10×10^{-13}	10	6.63×10^{-3}

Table A.3: Simulation results for consistency testing

A.3 Numerical and experimental data - Water uptake

Time [h]	Normalised moisture concentration [-]	Water uptake [g]
24	0.0855	0.0039
48	0.1071	0.0049
72	0.1232	0.0056
96	0.1366	0.0062
120	0.1477	0.0067
144	0.1617	0.0073
168	0.1704	0.0077
192	0.1784	0.0081
216	0.1894	0.0086
240	0.1964	0.0089
264	0.2033	0.0092
288	0.2095	0.0095
312	0.2154	0.0098
336	0.2211	0.0100

Table A.4: Numerical results for the water uptake of the adhesive layer in 40^{o}C distilled water for the experimental period.

Time [days]	Normalised moisture concentration [-]	Water uptake [g]
14	0.2211	0.0100
30	0.2822	0.0128
90	0.4262	0.0193
180	0.5493	0.0249
365	0.6997	0.0317
730	0.8540	0.0387
1095	0.9266	0.0420
1460	0.9612	0.0436
1825	0.9781	0.0444
2190	0.9876	0.0448
2555	0.9931	0.0451
2920	0.9953	0.0452
3285	0.9972	0.0452
3650	0.9982	0.0453

Table A.5: Numerical results for the water uptake of the adhesive layer in 40^{o}C distilled water until saturation.

Time [h]	Water uptake [g]	
	Unloaded	1 MPa
2.22	0.0083 ± 0.0010	-
3.42	0.0102 ± 0.0019	-
4.82	0.0134 ± 0.0018	-
6.20	0.0167 ± 0.0013	-
23.04	0.0467 ± 0.0046	-
25.29	0.0471 ± 0.0040	-
26.07	0.0461 ± 0.0044	-
28.14	0.0464 ± 0.0052	-
29.92	0.0490 ± 0.0051	-
45.75	0.0651 ± 0.0082	-
47.86	0.0645 ± 0.0081	-
51.02	0.0664 ± 0.0081	-
53.99	0.0667 ± 0.0104	-
70.17	0.0796 ± 0.0106	-
74.26	0.0799 ± 0.0131	-
76.53	0.0797 ± 0.0138	-
140.86	0.1143 ± 0.0218	-
142.62	0.1120 ± 0.0199	-
145.21	0.1094 ± 0.0213	-
164.10	0.1223 ± 0.0241	-
170.08	0.1167 ± 0.0221	-
188.82	0.1202 ± 0.0193	-
197.01	0.1226 ± 0.0291	-
214.32	0.1303 ± 0.0317	-
219.75	0.1228 ± 0.0308	-
237.11	0.1303 ± 0.0425	-
300	-	0.1295 ± 0.0294
310.03	0.1300 ± 0.0336	-
333.85	0.1275 ± 0.0415	-

Table A.6: Experimental results for the water uptake of the single lap joints with coating 1 in 40°C distilled water.

Time [h]	Water uptake [g]
30	0.0469 ± 0.0001
54.93	0.0642 ± 0.0015
74.89	0.0718 ± 0.0010
144.63	0.1035 ± 0.0020
168.07	0.1081 ± 0.0025
194.76	0.1148 ± 0.0022
220.02	0.1208 ± 0.0030
338.59	0.1633 ± 0.0013

Table A.7: Experimental results for the water uptake of steel specimens coated with coating 1 in 40^{o}C distilled water.

Time [h]	Water uptake [g]
30	0.0348 ± 0.0000
54.93	0.0477 ± 0.0011
74.89	0.0534 ± 0.0007
144.63	0.0769 ± 0.0015
168.07	0.0804 ± 0.0019
194.76	0.0853 ± 0.0016
220.02	0.0898 ± 0.0022
338.59	0.1213 ± 0.0010

Table A.8: Predicted water uptake for coating 1 on the first set of single lap joints in 40^{o}C distilled water.

Time [h]	Water uptake [g]
24.0000	0.0190
48.0000	0.0205
72.0000	0.0272
96.0000	0.0297
120.0000	0.0345
144.0000	0.0339
168.0000	0.0383
192.0000	0.0363
216.0000	0.0389
240.0000	0.0352
264.0000	0.0287
288.0000	0.0222
312.0000	0.0156

Table A.9: Predicted water uptake of the adhesive in single lap joints with coating 1 in 40^{o}C distilled water. Determined as the difference between the results from Table A.6 and Table A.8

Time [h]	Water uptake [g]			
	Unloaded		1 MPa	3 MPa
	Weighed periodically	Weighed at the end		
19.25	0.0561 ± 0.0057	-	-	-
43.72	0.0850	-	-	-
141.47	0.1515 ± 0.0042	-	-	-
165.48	0.1595 ± 0.0028	-	-	-
190.37	0.1671 ± 0.0030	-	-	-
215.40	0.1768 ± 0.0052	-	-	-
282.86	0.2006 ± 0.0054	-	-	-
310.85	0.2146	-	-	-
327.18	-	-	-	0.2219 ± 0.0069
327.75	0.2155 ± 0.0060	-	-	-
328.50	-	0.2371 ± 0.0033	-	-
328.95	-	-	0.2554 ± 0.0059	-

Table A.10: Experimental results for the water uptake of the single lap joints with coating 2 in 40^{o}C distilled water.

Time [h]	Water uptake [g]
29.18	0.0723 ± 0.0009
54.13	0.0956 ± 0.0019
74.02	0.1078 ± 0.0020
143.59	0.1508 ± 0.0021
167.17	0.1591 ± 0.0025
194.48	0.1679 ± 0.0024
218.96	0.1756 ± 0.0024
338.33	0.2201 ± 0.0028

Table A.11: Experimental results for the water uptake of the coated steel specimens with coating 2 in 40^{o}C distilled water.

Time [h]	Water uptake [g]
29.18	0.0656 ± 0.0008
54.13	0.0867 ± 0.0017
74.02	0.0977 ± 0.0018
143.59	0.1367 ± 0.0019
167.17	0.1443 ± 0.0023
194.48	0.1522 ± 0.0022
218.96	0.1592 ± 0.0022
338.33	0.1996 ± 0.0025

Table A.12: Predicted water uptake for coating 2 on the single lap joint specimens in 40^{o}C distilled water.

Time [h]	Water uptake [g]
48.0000	0.0064
72.0000	0.0076
96.0000	0.0105
120.0000	0.0134
144.0000	0.0155
168.0000	0.0157
192.0000	0.0163
216.0000	0.0187
240.0000	0.0192
264.0000	0.0196
288.0000	0.0207
312.0000	0.0240

Table A.13: Predicted water uptake of the adhesive in single lap joints with coating 2 in 40^{o}C distilled water. Determined as the difference between the results from Table A.10 and Table A.12

Appendix B

Creep testing data

B.1 First coating system

The creep results for specimens loaded at 1 MPa with the first coating system are presented numerically in Table **??** and graphically in Figure B.1. The results are presented as the mean ± the standard deviation of the experimental data. The results up till the moment the applied load had the desired magnitude can be found in Figure B.2 and Table B.1.

Figure B.1 shows that the specimens experienced both primary and secondary creep before the experiment was terminated. It was not possible to record the recovery of the specimens upon removal of the load.

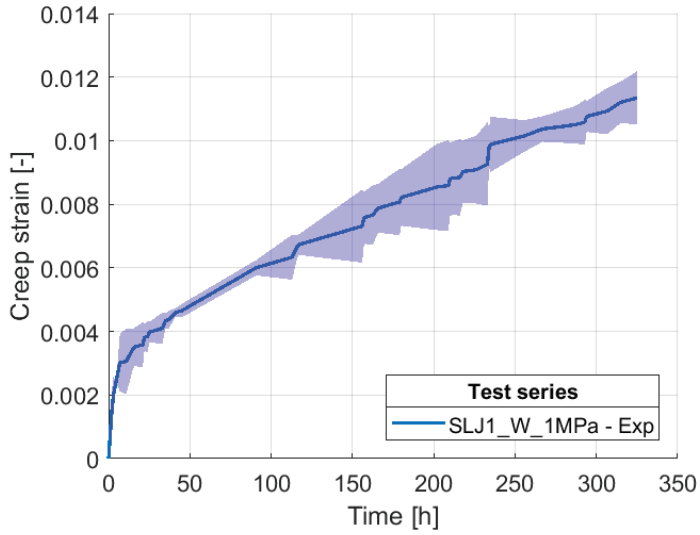

Figure B.1: Creep strain results for specimens with the first coating system loaded at 1 MPa

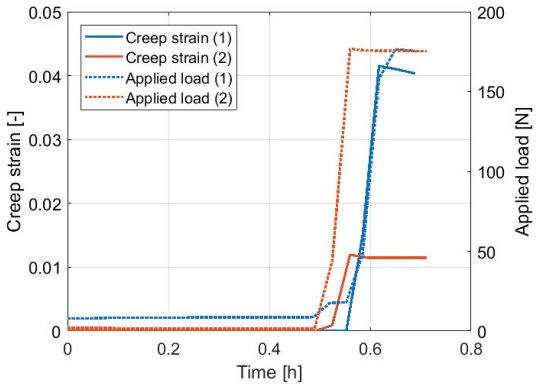

Figure B.2: Initial creep strain and applied load for specimens with the first coating system loaded at 1 MPa in water

Time [h]	Applied Load [N]	Creep Strain [-]	Time [h]	Applied Load [N]	Creep Strain [-]
0	8.0000	0	0	2.0000	0
0.0325	7.9847	0	0.0350	1.9000	0
0.0650	8.1000	0	0.0700	1.9000	0
0.0975	8.4519	0	0.1050	1.8000	0
0.1300	8.5000	0	0.1400	1.7000	0
0.1625	8.5000	0	0.1750	1.7000	0
0.1950	8.5000	0	0.2100	1.6000	0
0.2275	8.5000	0	0.2450	1.6000	0
0.2600	8.6000	0	0.2800	1.6000	0
0.2925	8.6000	0	0.3150	1.6000	0
0.3250	8.6000	0	0.3500	1.6000	0
0.3575	8.6000	0	0.3850	1.6000	0
0.3900	8.6000	0	0.4200	1.6000	0
0.4225	8.6000	0	0.4550	1.6000	0
0.4550	8.6388	0	0.4900	1.7000	0
0.4875	8.7000	0	0.5250	44.3171	0.0009
0.5200	17.6000	0	0.5600	176.7834	0.0119
0.5525	17.9000	0	0.5950	175.7347	0.0115
0.5850	48.2634	0.0149	0.6300	175.6000	0.0115
0.6175	158.0862	0.0415	0.6650	175.5731	0.0115
0.6500	176.5228	0.0410	0.7000	175.4442	0.0115
0.6892	175.5000	0.0403	0.7120	175.4000	0.0115

Table B.1: Initial creep strain and applied load for specimens with the first coating system loaded at 1 MPa in water

B.2 Second coating system

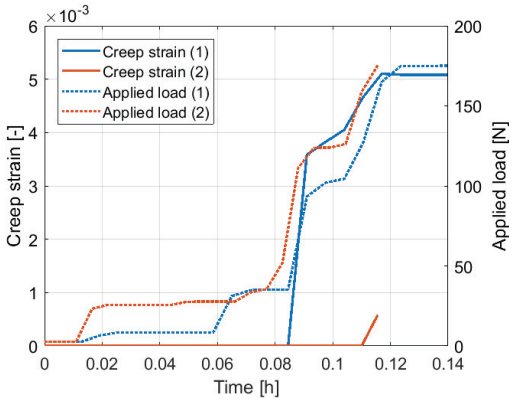

Figure B.3: Initial creep strain and applied load for specimens with the second coating system loaded at 1 MPa in air

Time [h]	Applied Load [N]	Creep Strain [-]
0	2.7000	0
0.0065	2.7000	0
0.0130	2.7000	0
0.0195	6.7191	0
0.0260	8.5000	0
0.0325	8.4684	0
0.0390	8.4000	0
0.0455	8.4000	0
0.0520	8.4000	0
0.0585	8.4000	0
0.0650	31.1662	0
0.0715	34.8209	0
0.0780	35.3000	0
0.0845	35.3000	0
0.0910	93.3282	0.0036
0.0975	102.0224	0.0038
0.1040	104.4462	0.0041
0.1105	126.8722	0.0047
0.1170	165.0450	0.0051
0.1235	174.7677	0.0051
0.1300	174.9014	0.0051
0.1397	175.1000	0.0051

Time [h]	Applied Load [N]	Creep Strain [-]
0	2.7000	0
0.0055	2.7000	0
0.0110	2.7000	0
0.0165	23.2593	0
0.0220	25.7000	0
0.0275	25.6801	0
0.0330	25.6434	0
0.0385	25.6066	0
0.0440	25.6000	0
0.0495	27.6475	0
0.0550	27.7000	0
0.0605	27.7000	0
0.0660	27.7000	0
0.0715	33.4148	0
0.0770	35.4520	0
0.0825	51.7294	0
0.0880	111.2411	0
0.0935	123.8275	0
0.0990	123.9206	0
0.1045	126.2462	0
0.1100	158.7291	0
0.1156	175.4000	0.0006

Table B.2: Initial creep strain and applied load for specimens with the second coating system loaded at 1 MPa in air

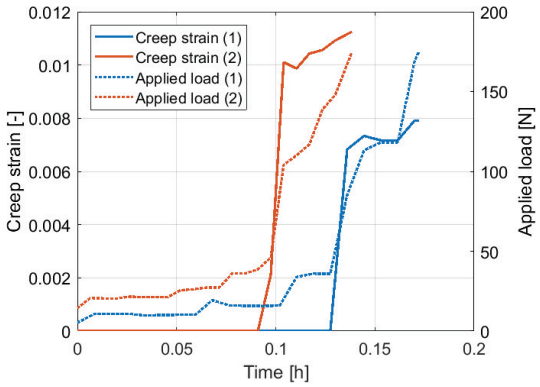

Figure B.4: Initial creep strain and applied load for specimens with the second coating system loaded at 1 MPa in water

Time [h]	Applied Load [N]	Creep Strain [-]	Time [h]	Applied Load [N]	Creep Strain [-]
0	5.2000	0	0	14.3000	0
0.0085	10.7000	0	0.0065	20.6840	0
0.0170	10.6383	0	0.0130	20.4865	0
0.0255	10.9008	0	0.0195	20.3468	0
0.0340	9.7672	0	0.0260	21.5000	0
0.0425	10.0929	0	0.0325	21.3789	0
0.0510	10.1379	0	0.0390	21.3000	0
0.0595	10.1990	0	0.0455	21.2371	0
0.0680	19.3674	0	0.0520	25.6170	0
0.0765	16.0272	0	0.0585	26.2000	0
0.0850	15.8052	0	0.0650	27.2000	0
0.0935	15.7014	0	0.0715	27.2000	0
0.1020	15.9711	0	0.0780	36.0853	0
0.1105	33.8338	0	0.0845	35.9826	0
0.1190	35.9780	0	0.0910	38.7124	0
0.1275	35.8446	0	0.0975	46.0379	0.0021
0.1360	85.1911	0.0068	0.1040	104.1459	0.0101
0.1445	113.2343	0.0073	0.1105	110.1380	0.0099
0.1530	118.2000	0.0072	0.1170	116.9164	0.0104
0.1615	118.2000	0.0072	0.1235	138.7141	0.0106
0.1700	168.9958	0.0079	0.1300	147.9543	0.0109
0.1721	174.9000	0.0079	0.1384	174.7000	0.0113

Table B.3: Initial creep strain and applied load for specimens with the second coating system loaded at 1 MPa in water

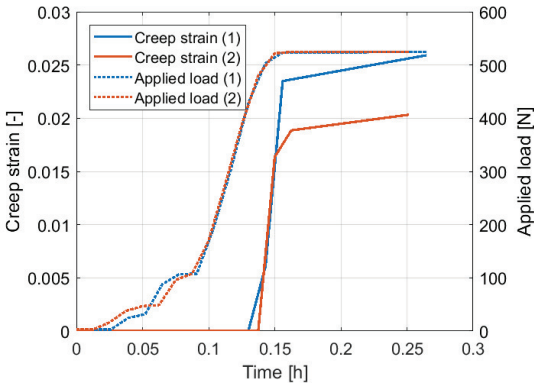

Figure B.5: Initial creep strain and applied load for specimens with the second coating system loaded at 3 MPa in air

Time [h]	Applied Load [N]	Creep Strain [-]
0	2.8000	0
0.0130	2.8000	0
0.0260	2.8000	0
0.0390	24.4000	0
0.0520	31.7304	0
0.0650	88.0211	0
0.0780	107.3124	0
0.0910	107.4994	0
0.1040	195.3115	0
0.1170	305.1864	0
0.1300	428.5313	0
0.1430	503.5744	0.0061
0.1560	523.3867	0.0235
0.1690	523.5436	0.0238
0.1820	523.7004	0.0241
0.1950	523.8573	0.0244
0.2080	524.0142	0.0247
0.2210	524.1711	0.0249
0.2340	524.3280	0.0252
0.2470	524.4849	0.0255
0.2600	524.6418	0.0258
0.2648	524.7000	0.0259

Time [h]	Applied Load [N]	Creep Strain [-]
0	2.7000	0
0.0125	2.7000	0
0.0250	16.3000	0
0.0375	37.8448	0
0.0500	46.9000	0
0.0625	49.0061	0
0.0750	95.8854	0
0.0875	107.8470	0
0.1000	170.3990	0
0.1125	275.4956	0
0.1250	387.5686	0
0.1375	480.2159	0
0.1500	521.8621	0.0164
0.1625	524.7346	0.0189
0.1750	524.7718	0.0191
0.1875	524.8090	0.0193
0.2000	524.8462	0.0195
0.2125	524.8835	0.0197
0.2250	524.9207	0.0199
0.2375	524.9579	0.0201
0.2500	524.9951	0.0203
0.2516	525.0000	0.0203

Table B.4: Initial creep strain and applied load for specimens with the second coating system loaded at 3 MPa in air

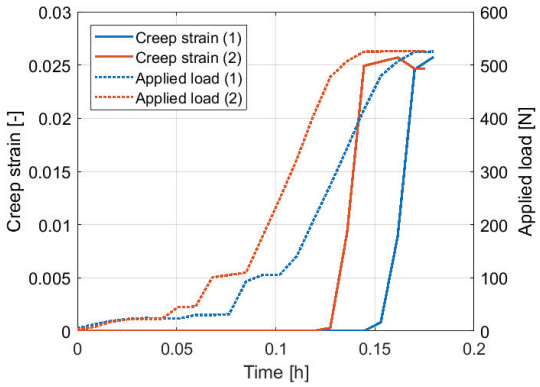

Figure B.6: Initial creep strain and applied load for specimens with the second coating system loaded at 3 MPa in water

Time [h]	Applied Load [N]	Creep Strain [-]
0	5.1000	0
0.0085	12.7447	0
0.0170	19.0415	0
0.0255	22.8041	0
0.0340	24.4000	0
0.0425	23.5000	0
0.0510	23.5000	0
0.0595	30.1009	0
0.0680	30.0000	0
0.0765	31.7020	0
0.0850	93.1678	0
0.0935	105.8162	0
0.1020	105.9956	0
0.1105	140.0313	0
0.1190	207.9375	0
0.1275	273.9685	0
0.1360	344.1222	0
0.1445	416.3086	0
0.1530	479.8479	0.0008
0.1615	506.8937	0.0089
0.1700	524.4887	0.0246
0.1796	525.3000	0.0257

Time [h]	Applied Load [N]	Creep Strain [-]
0	2.5000	0
0.0085	7.8572	0
0.0170	17.5615	0
0.0255	21.9890	0
0.0340	21.8222	0
0.0425	22.8000	0
0.0510	45.4131	0
0.0595	45.8000	0
0.0680	100.7861	0
0.0765	105.4000	0
0.0850	110.0307	0
0.0935	179.0164	0
0.1020	248.6658	0
0.1105	321.5475	0
0.1190	404.8958	0
0.1275	477.4432	0.0003
0.1360	507.3549	0.0093
0.1445	525.0450	0.0249
0.1530	525.5897	0.0253
0.1615	526.1345	0.0257
0.1700	525.7447	0.0247
0.1755	525.7000	0.0247

Table B.5: Initial creep strain and applied load for specimens with the second coating system loaded at 3 MPa in water

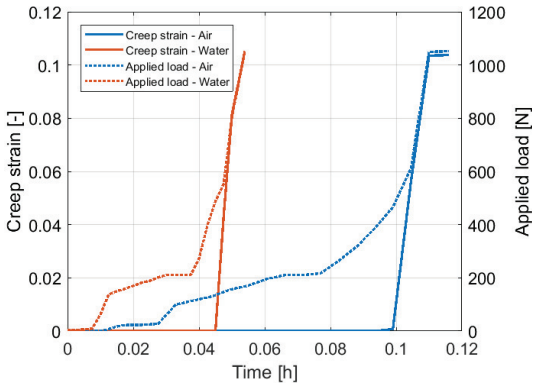

Figure B.7: Initial creep strain and applied load for specimens with the second coating system loaded at 6 MPa

Time [h]	Applied Load [N]	Creep Strain [-]
0	2	0
0.0055	2	0
0.0110	2.1	0
0.0165	22.3	0
0.0220	22.9	0
0.0275	27.1	0
0.0330	99.9	0
0.0385	115.2	0
0.0440	130.4	0
0.0495	155.9	0
0.0550	171	0
0.0605	195.4	0
0.0660	210.1	0
0.0715	210.6	0
0.0770	217	0
0.0825	263.7	0
0.0880	317.8	0
0.0935	386.3	0
0.0990	465.6	0.0007
0.1045	612.1	0.0562
0.1100	1049.6	0.1035
0.1161	1051.8	0.1038

Time [h]	Applied Load [N]	Creep Strain [-]
0	4.7	0
0.0025	4.6	0
0.0050	5.6	0
0.0075	9.3	0
0.0100	62.4	0
0.0125	137.2	0
0.0150	149.8	0
0.0175	159.2	0
0.0200	170	0
0.0225	181.5	0
0.0250	188.8	0
0.0275	201.4	0
0.0300	210.8	0
0.0325	211.1	0
0.0350	211.3	0
0.0375	211.5	0
0.0400	271.7	0
0.0425	394.9	0
0.0450	487.6	0
0.0475	552.4	0.0432
0.0500	802.1	0.0812
0.0539	1050.8	0.1053

Table B.6: Initial creep strain and applied load for specimens with the second coating system loaded at 6 MPa

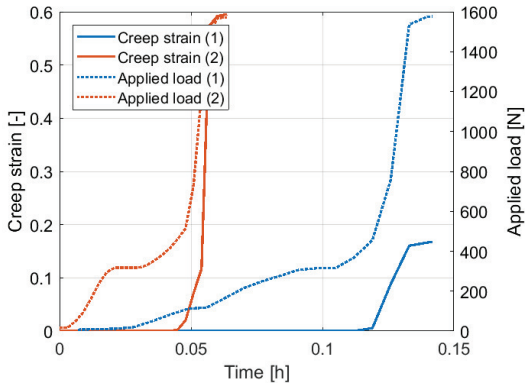

Figure B.8: Initial creep strain and applied load for specimens with the second coating system loaded at 9 MPa in air

Time [h]	Applied Load [N]	Creep Strain [-]
0	0	0
0.0070	6.8	0
0.0140	9.3	0
0.0210	11.4	0
0.0280	19.4	0
0.0350	48.1	0
0.0420	82.1	0
0.0490	112.2	0
0.0560	117.8	0
0.0630	165.8	0
0.0700	214.7	0
0.0770	249.4	0
0.0840	277.1	0
0.0910	307.2	0
0.0980	315.2	0
0.1050	315.4	0
0.1120	368.5	0
0.1190	455.8	0.0055
0.1260	759.7	0.0887
0.1330	1536.5	0.1603
0.1400	1575.6	0.1665
0.1418	1577.2	0.1674

Time [h]	Applied Load [N]	Creep Strain [-]
0	16.1	0
0.0030	16.2	0
0.0060	48.2	0
0.0090	93.7	0
0.0120	163.0	0
0.0150	239.7	0
0.0180	295.7	0
0.0210	317.6	0
0.0240	317.8	0
0.0270	318.0	0
0.0300	318.2	0
0.0330	328.1	0
0.0360	353.2	0
0.0390	380.6	0
0.0420	415.9	0
0.0450	462.0	0.0029
0.0480	515.7	0.0207
0.0510	735.1	0.0717
0.0540	1187.8	0.1168
0.0570	1487.9	0.5737
0.0600	1568.4	0.5919
0.0638	1572.2	0.5955

Table B.7: Initial creep strain and applied load for specimens with the second coating system loaded at 9 MPa in air

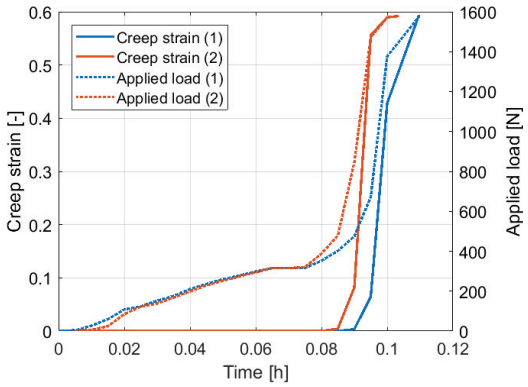

Figure B.9: Initial creep strain and applied load for specimens with the second coating system loaded at 9 MPa in water

Time [h]	Applied Load [N]	Creep [mm]
0	2.5	0
0.0050	3.4	0
0.0100	26.4	0
0.0150	59.5	0
0.0200	108.5	0
0.0250	123.9	0
0.0300	152.1	0
0.0350	175.8	0
0.0400	210.3	0
0.0450	236.3	0
0.0500	259.4	0
0.0550	278.0	0
0.0600	298.8	0
0.0650	315.8	0
0.0700	316.0	0
0.0750	316.1	0
0.0800	352.2	0
0.0850	402.0	0
0.0900	475.2	0.0035
0.0950	672.2	0.0644
0.1000	1376.8	0.4282
0.1097	1575.5	0.5941

Time [h]	Applied Load [N]	Creep [mm]
0	0	0
0.0050	2.1	0
0.0100	6.0	0
0.0150	23.9	0
0.0200	84.3	0
0.0250	122.4	0
0.0300	137.7	0
0.0350	167.5	0
0.0400	198.8	0
0.0450	228.8	0
0.0500	251.8	0
0.0550	273.8	0
0.0600	295.1	0
0.0650	315.0	0
0.0700	315.2	0
0.0750	320.5	0
0.0800	388.3	0
0.0850	479.0	0.0043
0.0900	845.5	0.0821
0.0950	1471.7	0.5562
0.1000	1572.3	0.5894
0.1036	1578.8	0.5925

Table B.8: Initial creep strain and applied load for specimens with the second coating system loaded at 9 MPa in water

	Creep strain [-]					
	0.5 h	1 h	10 h	50 h	100 h	300 h
0 MPa	0	0	0	0	0	0
1 MPa	0.0017	0.0021	0.0036	0.0047	0.0051	0.0051
3 MPa	0.0100	0.0105	0.0181	0.0227	0.0248	0.0273
6 MPa	0.0033	0.0059	0.0162	0.0266	0.0300	-
9 MPa	0.0250	-	-	-	-	-

Table B.9: Stresses and strains at different times for specimens loaded in air

	Creep strain [-]					
	0.5 h	1 h	10 h	50 h	100 h	300 h
0 MPa	0	0	0	0	0	0
1 MPa	0.0012	0.0015	0.0021	0.0039	0.0048	0.0085
3 MPa	0.0031	0.0043	0.0098	0.0181	0.0240	0.0424
6 MPa	0.0052	0.0088	0.0213	0.0367	-	-
9 MPa	0.0186	0.0289	0.0502	-	-	-

Table B.10: Stresses and strains at different times for specimens loaded in water

Time [h]	Creep strain [-]	
	Air	Water
0	0	0
10	0.0037 ± 0.0008	0.0022 ± 0.0007
20	0.0042 ± 0.0012	0.0033 ± 0.0007
30	0.0044 ± 0.0011	0.0035 ± 0.0005
40	0.0045 ± 0.0010	0.0037 ± 0.0005
50	0.0047 ± 0.0008	0.0039 ± 0.0003
60	0.0048 ± 0.0006	0.0041 ± 0.0003
70	0.0050 ± 0.0003	0.0043 ± 0.0003
80	0.0051 ± 0.0002	0.0045 ± 0.0002
90	0.0051 ± 0.0002	0.0046 ± 0.0001
100	0.0051 ± 0.0002	0.0048 ± 0.0001
110	0.0051 ± 0.0002	0.0050 ± 0.0001
120	0.0051 ± 0.0002	0.0052 ± 0.0001
130	0.0051 ± 0.0002	0.0053 ± 0.0001
140	0.0051 ± 0.0002	0.0055 ± 0.0000
150	0.0051 ± 0.0002	0.0056 ± 0.0000
160	0.0051 ± 0.0002	0.0058 ± 0.0000
170	0.0051 ± 0.0002	0.0059 ± 0.0000
180	0.0051 ± 0.0002	0.0061 ± 0.0000
190	0.0051 ± 0.0002	0.0062 ± 0.0000
200	0.0051 ± 0.0002	0.0065 ± 0.0002
210	0.0051 ± 0.0002	0.0067 ± 0.0001
220	0.0051 ± 0.0002	0.0069 ± 0.0000
230	0.0051 ± 0.0002	0.0072 ± 0.0001
240	0.0051 ± 0.0002	0.0075 ± 0.0000
250	0.0051 ± 0.0002	0.0077 ± 0.0001
260	0.0051 ± 0.0002	0.0078 ± 0.0001
270	0.0051 ± 0.0002	0.0079 ± 0.0002
280	0.0051 ± 0.0002	0.0081 ± 0.0002
290	0.0051 ± 0.0002	0.0083 ± 0.0004
300	0.0051 ± 0.0002	0.0085 ± 0.0004
310	0.0051 ± 0.0002	0.0086 ± 0.0004
320	0.0051 ± 0.0002	0.0087 ±0.0005

Table B.11: Creep strain results for specimens with the second coating system loaded at 1 MPa

Time [h]	Creep strain [-]	
	Air	Water
0	0	0
10	0.01834 ± 0.0067	0.0101 ± 0.0005
20	0.0200 ± 0.0061	0.0142 ± 0.0008
30	0.0215 ± 0.0050	0.0160 ± 0.0003
40	0.0222 ± 0.0044	0.0171 ± 0.0001
50	0.0227 ± 0.0037	0.0182 ± 0.0004
60	0.0236 ± 0.0040	0.0194 ± 0.0003
70	0.0238 ± 0.0038	0.0209 ± 0.0000
80	0.0242 ± 0.0037	0.0224 ± 0.0005
90	0.0246 ± 0.0036	0.0238 ± 0.0011
100	0.0249 ± 0.0035	0.0239 ± 0.0002
110	0.0251 ± 0.0035	0.0240 ± 0.0010
120	0.0255 ± 0.0037	0.0254 ± 0.0007
130	0.0256 ± 0.0036	0.0268 ± 0.0000
140	0.0257 ± 0.0035	0.0284 ± 0.0006
150	0.0257 ± 0.0034	0.0297 ± 0.0016
160	0.0259 ± 0.0032	0.0303 ± 0.0010
170	0.0260 ± 0.0031	0.0308 ± 0.0002
180	0.0261 ± 0.0029	0.0312 ± 0.0003
190	0.0264 ± 0.0031	0.0315 ± 0.0007
200	0.0266 ± 0.0032	0.0328 ± 0.0000
210	0.0268 ± 0.0032	0.0342 ± 0.0006
220	0.0269 ± 0.0032	0.0357 ± 0.0012
230	0.0270 ± 0.0032	0.0370 ± 0.0020
240	0.0270 ± 0.0032	0.0374 ± 0.0016
250	0.0270 ± 0.0032	0.0380 ± 0.0009
260	0.0272 ± 0.0032	0.0385 ± 0.0002
270	0.0273 ± 0.0032	0.0387 ± 0.0001
280	0.0273 ± 0.0032	0.0390 ± 0.0005
290	0.0273 ± 0.0032	0.0407 ± 0.0005
300	0.0273 ± 0.0031	0.0426 ± 0.0021
310	0.0273 ± 0.0029	0.0437 ± 0.0028
320	0.0274 ± 0.0028	0.0442 ± 0.0023

Table B.12: Creep strain results for specimens with the second coating system loaded at 3 MPa

Time [h]	Creep strain [-]	Time [h]	Creep strain [-]
	Air		Water
0	0	0	
5.7500	0.0224	4.2500	0.0215
11.5000	0.0259	8.5000	0.0265
17.2500	0.0280	12.7500	0.0289
23.0000	0.0296	17.0000	0.0313
28.7500	0.0312	21.2500	0.0329
34.5000	0.0321	25.5000	0.0345
40.2500	0.0326	29.7500	0.0378
46.0000	0.0331	34.0000	0.0378
51.7500	0.0336	38.2500	0.0388
57.5000	0.0341	42.5000	0.0395
63.2500	0.0346	46.7500	0.0411
69.0000	0.0351	51.0000	0.0430
74.7500	0.0356	55.2500	0.0440
80.5000	0.0361	59.5000	0.0454
86.2500	0.0365	63.7500	0.0472
92.0000	0.0367	68.0000	0.0474
97.7500	0.0367	72.2500	0.0502
103.5000	0.0367	76.5000	0.0506
109.2500	0.0367	80.7500	0.0527
115.0000	0.0367	85.0000	0.0555
115.6565	0.0367	87.4698	0.0565
-	-	89.7168	0.0684

Table B.13: Creep strain results for specimens with the second coating system loaded at 6 MPa

Time [h]	Creep strain [-]	Time [h]	Creep strain [-]
Air (1)		Air (2)	
0	0	0	0
0.0475	0.0049	0.0325	0.0028
0.0950	0.0068	0.0650	0.0046
0.1425	0.0086	0.0975	0.0064
0.1900	0.0105	0.1300	0.0081
0.2375	0.0123	0.1625	0.0099
0.2850	0.0142	0.1950	0.0117
0.3325	0.0160	0.2275	0.0134
0.3800	0.0179	0.2600	0.0152
0.4275	0.0196	0.2925	0.0169
0.4750	0.0209	0.3250	0.0187
0.5225	0.0222	0.3575	0.0205
0.5700	0.0234	0.3900	0.0222
0.6175	0.0248	0.4225	0.0240
0.6650	0.0262	0.4550	0.0258
0.7125	0.0273	0.4875	0.0275
0.7600	0.0287	0.5200	0.0293
0.8075	0.0301	0.5525	0.0311
0.8550	0.0314	0.5850	0.0328
0.9025	0.0328	0.6175	0.0356
0.9500	0.0352	0.6500	0.0468
0.9990	0.0413	0.6510	0.0469
0.9993	0.0545	-	-

Table B.14: Creep strain results for specimens with the second coating system loaded at 9 MPa in air

Time [h]	Creep strain [-]	Time [h]	Creep strain [-]
Air (1)		Air (2)	
0	0	0	0
0.6500	0.0228	0.2750	0.0137
1.3000	0.0280	0.5500	0.0218
1.9500	0.0317	0.8250	0.0298
2.6000	0.0334	1.1000	0.0327
3.2500	0.0365	1.3750	0.0327
3.9000	0.0395	1.6500	0.0385
4.5500	0.0403	1.9250	0.0403
5.2000	0.0415	2.2000	0.0416
5.8500	0.0441	2.4750	0.0419
6.5000	0.0449	2.7500	0.0444
7.1500	0.0464	3.0250	0.0447
7.8000	0.0464	3.3000	0.0460
8.4500	0.0488	3.5750	0.0482
9.1000	0.0501	3.8500	0.0493
9.7500	0.0523	4.1250	0.0503
10.4000	0.0527	4.4000	0.0509
11.0500	0.0540	4.6750	0.0525
11.7000	0.0567	4.9500	0.0532
12.3500	0.0583	5.2250	0.0540
13.0000	0.0607	5.5000	0.0564
13.4730	0.0661	5.9225	0.0654
13.4750	0.0793	5.9227	0.0656

Table B.15: Creep strain results for specimens with the second coating system loaded at 9 MPa in water

Time [h]	Creep strain [-]	Time [h]	Creep strain [-]
Air (1)		Air (2)	
0	0	0	0
0.0325	0.0036	0.2750	0.0115
0.0650	0.0051	0.5500	0.0202
0.0975	0.0066	0.8250	0.0273
0.1300	0.0081	1.1000	0.0297
0.1625	0.0096	1.3750	0.0305
0.1950	0.0112	1.6500	0.0342
0.2275	0.0127	1.9250	0.0360
0.2600	0.0142	2.2000	0.0374
0.2925	0.0157	2.4750	0.0376
0.3250	0.0172	2.7500	0.0395
0.3575	0.0187	3.0250	0.0403
0.3900	0.0202	3.3000	0.0413
0.4225	0.0217	3.5750	0.0428
0.4550	0.0231	3.8500	0.0438
0.4875	0.0244	4.1250	0.0448
0.5200	0.0257	4.4000	0.0454
0.5525	0.0271	4.6750	0.0466
0.5850	0.0284	4.9500	0.0473
0.6175	0.0302	5.2250	0.0478
0.6500	0.0362	5.5000	0.0497

Table B.16: Mean creep strain results for specimens with the second coating system loaded at 9 MPa

Appendix C

Tensile testing data

Test series	RSI_1 [-]	RSI_2 [-]
SLJ1_W_0MPa - a	0.8256	0.9324
SLJ1_W_0MPa - b	0.7500	0.8655
SLJ1_W_0MPa - c	0.5483	0.7618
SLJ2_W_0MPa - d	0.9593	0.9275
SLJ2_W_0MPa - e	0.9302	0.9634
SLJ2_W_0MPa - f	0.9709	0.9480
SLJ2_W_0MPa - g	1.0116	1.0273
SLJ1_W_1MPa - a	0.8779	0.8051
SLJ1_W_1MPa - b	0.9012	0.8422
SLJ2_W_1MPa - c	0.9535	0.8289
SLJ2_W_1MPa - d	0.9942	0.9923
SLJ2_W_3MPa - a	0.9767	0.8780
SLJ2_W_3MPa - b	0.9709	0.8871
SLJ2_A_1MPa - a	1.0349	1.0348
SLJ2_A_1MPa - b	1.0349	0.9898
SLJ2_A_3MPa - a	0.9070	0.8735
SLJ2_A_3MPa - b	0.9128	0.9765

Table C.1: Values for the Initial Strength Index and Initial Stiffness Index